Acid catalysis using zirconia-supported Keggin heteropoly acids

A thesis submitted to the

UNIVERSITY OF PUNE

for the degree of

DOCTOR OF PHILOSOPHY

(in Chemistry)

BY

Biju M. Devassy

CATALYSIS DIVISION
NATIONAL CHEMICAL LABORATORY
PUNE- 411008
INDIA

September 2005

CERTIFICATE

Certified that the work incorporated in the thesis, **"Acid catalysis using zirconia-supported Keggin heteropoly acids"** submitted by **Mr. Biju M. Devassy**, for the Degree of **Doctor of Philosophy**, was carried out by the candidate under my supervision in the Catalysis Division, National Chemical Laboratory, Pune - 411008, India. Materials obtained from other sources have been duly acknowledged in the thesis.

Dr. S. B. Halligudi

(Research Supervisor)

Dedicated to…

My Parents and Brothers

ACKNOWLEDGEMENTS

It is my great pleasure to express my heartfelt gratitude to my research supervisor, Dr. S. B. Halligudi, for his unending support and invaluable guidance throughout the period of this investigation. I sincerely thank him for the care and affection that I received from him in the entire period.

I am very much grateful to Dr. Rajiv Kumar, Head, Catalysis and Inorganic Chemistry Division, NCL, who is very kind and generous towards me and his help is gratefully acknowledged.

I am also grateful to Dr. S. Sivasanker and Dr. A. V. Ramaswamy, former Heads of the Division for their support and help during the period of my research work.

I acknowledge the friendly and cooperative attitude of all scientific staff of our Division. I would like to thank Dr. S. G. Hegde, Dr. A. J. Chandwadkar, Dr. Veda Ramaswamy, Dr. A. P. Singh, Dr. M. K. Dongare, Dr. D. Srinivas, Dr. C. V. V. Satyanarayana, Dr. C. S. Gopinath, Dr. S. P. Mirajkar, Dr. R. A. Shaikh, Dr. P. Manikandan, Dr. S. A. Pardhy, Dr. Seema Deshpande, Dr. Belhekar, Dr. Awate, Dr. T. Raja, Dr. Selvaraj, Dr. S. Umbarkar, Dr. A. K. Kinage, Mr. V. V. Bokade, Ms. Violet Samuel, Mrs. Nalini Jacob, Ms. Agashe, Mr. S. C. Jha, and Mr. Purushothaman for their valuable help and cooperation in completing my research work successfully.

I also thank Dr. C. Gopinathan, Dr. Sarada Gopinathan, Dr. P. A. Joy and Dr. Vijayamohanan for their help on various occasions. I would like to acknowledge the help received from Mr. Madhu, Mr. Kashinathan, Mr. Milind and Mr. Katti.

I sincerely thank my labmates Dr. Tressa (and family), Dhanashri, Shanbhag, Ankur, Suman, Nevin, Suresh and Nicola Toma for their friendly help and kind cooperation during the period of my work. I also thank all my friends in the division and in NCL for their help and support in one way or other, which made my work much easier.

My special thanks are due to Mr. Rajeeve Antony, Dr. K. Sreekumar, and Dr. T. M. Jyothi for their whole-hearted help.

I would like to thank my friends Dr. Shiju, Dr. Thomas, Shylesh, Surendran, Dr. Jolly, Dr. Sreejith, Dr. Sureshan, Rajesh, Dr. Shivasankar, Dr. Pradeep Pallan, Rajsankar, Sajeev, Santhosh, Hari, Dr. Muthu, Jainy, Sebastian, Dr. Kala and family for their all kind of help extended to me. Their company provided me joyful moments during the stay in Pune.

I would like to thank all my teachers in various classes for the love and encouragement that I received from them. I take this occasion to thank all my classmates till M.Tech course, whose cooperative attitude helped me very much. Also, I thank all well-wishers and friends, whose names are not mentioned here.

I would like to thank Dr. S. Sivaram, Director, NCL and Dr. P. Ratnasamy (former Director, NCL) for allowing me to carryout the research work at NCL and CSIR, New Delhi, India, for the financial support in the form of senior research fellowship.

(Biju M. Devassy)

Contents

1. Introduction

ABSTRACT

Heteropoly acids (HPAs) are a unique class of materials active in both acid and redox catalysis. These are polyoxometallates made up of heteropoly anions having metal-oxygen octahedra as the basic structural unit. HPAs can be used either directly as a bulk material or in supported form. The use in supported form is preferable because of its high surface area compared to the bulk material (5-8 m^2g^{-1}) and better accessibility of reactants to the active sites. Acidic or neutral solids, which interact weakly with HPAs such as silica, active carbon and acidic ion-exchange resin, have been reported to be suitable as HPA supports. However, heteropoly acids on these conventional supports are not highly stable in polar reaction media and part of the reaction can occur due to homogeneous catalysis. Serious problems associated with this type of materials are their susceptibility to deactivation during organic reactions due to the formation of carbonaceous deposit (coke) on the catalyst surface. The thermal stability of HPAs is not high enough to carry out conventional regeneration by burning coke at 500-550 ^oC, as routinely used in the case of zeolites and aluminosilicates. Thus the preparation of an active and stable HPA in supported form is essential in order to utilize fully the potential of these materials as catalysts.

This thesis describes the preparation, characterization and catalytic evaluation of zirconia-supported Keggin heteropoly acids such as silicotungstic acid, phosphotungstic acid and phosphomolybdic acid. The present work showed that heteropoly tungstic acids such as silicotungstic acid and phosphotungstic acid supported on zirconia acts as efficient and stable solid acid catalysts, while heteropoly molybdic acid such as phosphomolybdic acid supported on zirconia leaches to the reaction medium in presence of polar reactants.

Key words**:** Zirconia; Heteropoly acids; Silicotungstic acid; Phosphotungstic acid; Phosphomolybdic acid; Acid catalysis; Alkylation; Acylation

Chapter 1

Introduction

1.1. Introduction

Heteropolyacids (HPAs) are hydrogen forms of heteropolyanions produced by the condensation of more than two kinds of oxoanions. HPAs have several advantages as catalysts, which make them economically and environmentally attractive. On the one hand, HPAs have a very strong Brönsted acidity; on the other, they are efficient oxidants under rather mild conditions. HPAs have a very high solubility in polar solvents and fairly high thermal stability in the solid state. These properties render HPAs potentially promising acid, redox, and bifunctional catalysts in homogeneous as well as in heterogeneous systems. HPAs are widely used as model systems for fundamental research, providing unique opportunities for mechanistic studies on the molecular level. The catalytic function of heteropoly compounds has attracted much attention in recent years and design of the catalyst is possible at atomic or molecular level. Using heteropoly compounds, it is possible to establish the following relationships at the atomic/molecular levels (Scheme 1.1) [1].

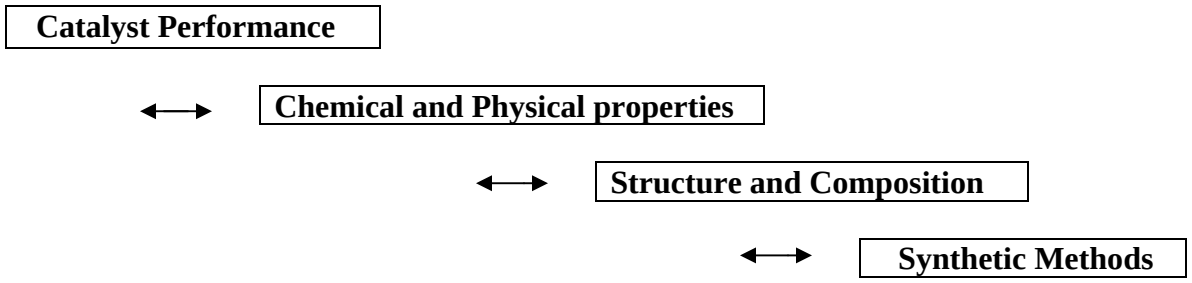

Scheme 1.1

The elucidation of catalytic processes is also possible at the atomic/molecular level due to their molecular nature. The reason why heteropoly acid catalysts are attractive is their variety and high potential as catalyst. The characteristic advantages of HPA catalysts [2] are listed in Table 1.1.

Table 1.1: Advantages of heteropoly catalysts

1.	**Catalyst design at atomic/molecular levels based on the following:**
1-1.	Acidic and redox properties These two important properties of catalysis can be controlled by choosing appropriate constituent elements (type of polyanion, addenda atom, hetero atom, counter cation etc.).
1-2.	Multifunctionality Acid-redox, acid-base, multi-electron transfer, photosensitivity, etc
1-3.	Tertiary structure, bulk-type behavior, etc., for solid state These are well controlled by countercations
2.	**Molecularity-Metal oxide cluster**
2-1.	Molecular design of the catalysts
2-2.	Cluster models of mixed oxide catalysts and relationships between solid and solution catalysts
2-3.	Description of catalytic properties at atomic/molecular levels Spectroscopic study and stoichiometry are realistic
3.	**Unique reaction field**
3-1.	Bulk type catalysis “Pseudoliquid” and bulk type II behavior provide unique three-dimensional reaction environments for catalysis
3-2.	Pseudoliquid behavior This makes spectroscopic stoichiometric studies feasible and realistic

3-3. Phase-transfer catalysis

3-4. Shape selectivity

4. **Unique basicity of polyanion**

4-1. Selective coordination and stabilization of reaction intermediates in solution and in pseudoliquid phase, and possibility also on the surface

4-2. Ligands and supports for metals and organometallics

1.2. Structure of heteropoly compounds in the solid state

In solid state, HPAs show hierarchic structure [2, 3]. The structure divided into three levels – primary, secondary and tertiary as exemplified in Fig. 1.1.

1.2.1. Primary structure

The structure of a heteropolyanion or polyoxoanion molecule itself is called a primary structure [4]. In solution, heteropolyanions are present in the unit of the primary structure, being coordinated with solvent molecules and/or protonated. Based on primary structure, different polyoxoanion structures exist.

a. Keggin structure *[5-11]:* Keggin structures are anionic metal-oxygen cluster compounds having the molecular formula $XM_{12}O_{40}$, where "X" is a central, tetrahedrally coordinated atom connecting twelve peripheral, octahedrally coordinated "M" metal atoms. Berzelius synthesized the first Keggin structure (ammonium 12-molybdophosphate) in 1826, Marignac determined the analytical composition in 1862, and Keggin correctly deduced its geometry based on powder X-ray diffraction patterns in 1933. The acid and salt forms of the structure have proven to be industrially important: as ion-exchange materials; as analytical reagents for the determination of environmental contaminant concentrations; as protein precipitants; and as catalysts.

The ideal Keggin structure of the α type has T_d symmetry and consists of a central XO_4 tetrahedron (X = heteroatoms or central atom, most commonly Si^{IV}, P^{V}, or Ge^{IV}) surrounded by twelve MO_6 octahedra (M = addenda atom, most commonly Mo or W). The twelve MO_6 octahedra comprise four groups of three edge-shared octahedra, the M_3O_{13} triplet, which have a common oxygen vertex connected to the central heteroatom. The oxygen atoms in this structure fall into four classes of symmetry-equivalent oxygens:

$X\text{-}O_a\text{-}(M)_3$, $X\text{-}O_b\text{-}M$, connecting two M_3O_{13} units by corner sharing; $X\text{-}O_c\text{-}M$, connecting two M_3O_{13} units by edge sharing; and $O_d\text{-}M$, where M is the addenda atom and X is the heteroatom. This Keggin structure is called a α isomer (Fig. 1.2A).

b. *Lacunary Keggin anion* *[6, 12]*: This is a defect derivative of a Keggin structure. In solution, several species are present in equilibrium, the composition depending on the pH. In the case of $PW_{12}O_{40}^{3-}$, the lacunary $PW_{11}O_{39}^{7-}$ is formed at pH = 2. The degradation of $PW_{11}O_{39}^{7-}$ to give $PW_9O_{34}^{9-}$ occurs at pH > 8.

c. *Dawson structure* *[13, 14]*: The Dawson structure, $M_2X_{18}O_{62}^{6-}$ is formed by the fusion of two $PW_9O_{31}^{3-}$ units, "lacunary Keggin anions," (Fig. 1.2B).

d. *Anderson structure*: This structure comprises seven edge-shared octahedra (Fig. 1.2C) [9, 10, 15].

HPAs with Keggin-structure are the most important in catalysis and this is due to several reasons, one of which is a simple synthesis procedure of Keggin-structure HPAs compared with HPAs of other structures. Besides, in contrast to HPAs with Keggin-structure, heteropolyacids of other types are thermally less stable and not capable of dehydrating at 150-200 ^oC and thus cannot be employed for reactions, which are conducted above 150 ^oC [16].

1.2.2. Secondary structure

Heteropoly compounds in the solid state are ionic crystals (sometimes amorphous) consisting of large polyanions, cations, water of crystallization, and other molecules. This three-dimensional arrangement is called the "secondary structure". The secondary structure is variable for the group A salts. For example, $H_3PW_{12}O_{40}.\ nH_2O$, is cubic for n = 0-6 and orthorhombic for n = 21. The crystal structures of Cs and NH_4 salts are the same as the cubic $H_3PW_{12}O_{40}.\ 6H_2O$, with cations at the sites of $H^+(H_2O)_2$ sites.

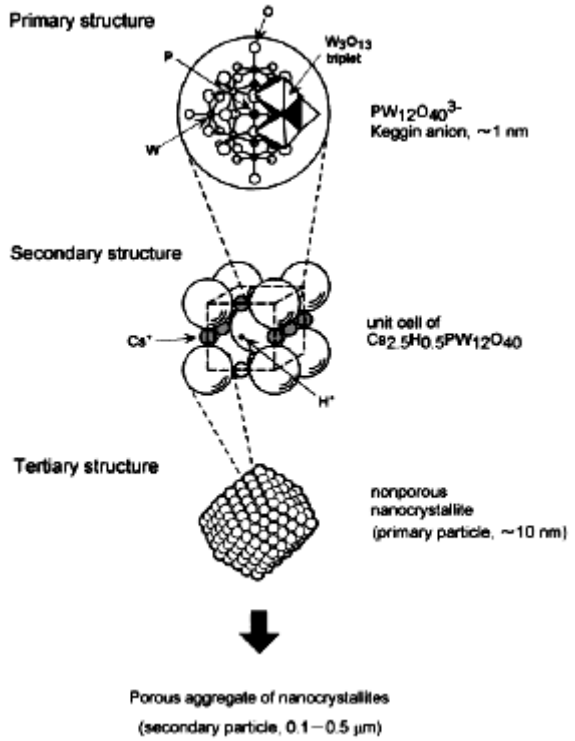

Fig. 1.1: Primary, secondary and tertiary structures; hierarchical structure of heteropoly compounds (HPAs) in the solid state [1].

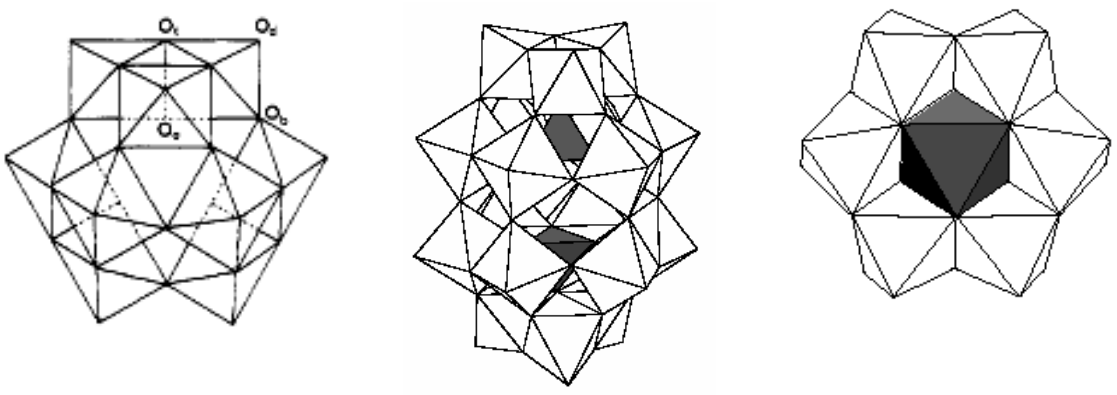

Fig. 1.2: Primary structure of heteropoly anions. (A) Keggin structure, α-$XM_{12}O_{40}^{n-}$; (B) Dawson structure, $X_2M_{18}O_{62}^{n-}$; (C) Anderson structure, $XM_6O_{24}^{n-}$.

Proton structure

The states and dynamics of protons and water in HPAs have been studied using solid-state ^{1}H, ^{31}P and ^{17}O MAS NMR spectroscopies [17]. Acidic protons are present in three forms; (a) proton attached to polyanions, (b) H_3O^+ (hydronium ion monomer) or H_2O strongly interacting with acidic protons, and (c) $H_5O_2^+$ (hydronium ion dimer). H_3O^+ and $H_5O_2^+$ weakly interact with polyanions by hydrogen bonding (Fig. 1.3).

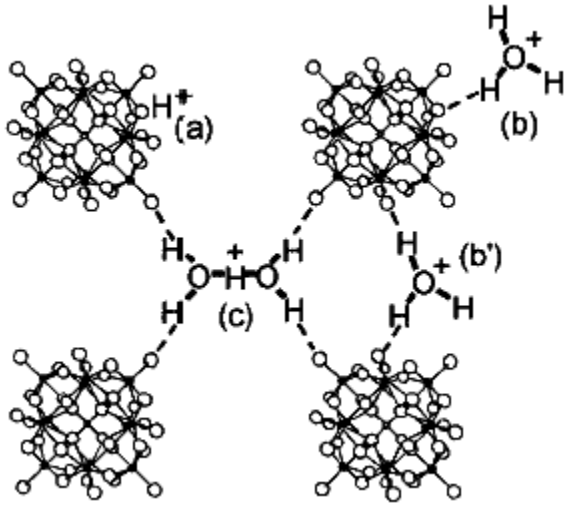

Fig. 1.3: Models proposed [1] for the states of acidic protons and water in solid $H_3PW_{12}O_{40}\cdot nH_2O$ ($0 < n < 6$); two possible positions are shown for H_3O^+.

1.2.3. Tertiary structure

Tertiary structure is the structure of solid heteropoly compounds as assembled. The size of the primary and secondary particles, pore structure, distribution of protons and cations, etc. is the elements of the tertiary structure. Countercations greatly influence the tertiary structure of HPAs. The surface area of the crystalline heteropolyacids is small (3-8 $m^2\ g^{-1}$), but some of their salts with appropriately large cations such as ammonium, cesium and rubidium show surface areas of the order of 100 to 200 $m^2\ g^{-1}$. Heteropolyacids and salts having low surface areas exhibit several common properties that are in contrast with the properties of salts with high surface areas, hence, a distinction is made in the literature: low surface area heteropolyacids and salts are termed "group A", and high surface area salts are termed "group B". Group A species are soluble in water, whereas, group B species are not; group A species decompose in the temperature range from 250 ^{o}C to 600 ^{o}C, whereas, group B species are typically stable

up to 700°C and above; and group A species exhibit interesting properties ascribed to a "pseudo-liquid" phase, whereas, group B species do not.

1.3. Synthesis

The simplest way to prepare heteropolyanions involves the acidification of an aqueous solution containing the oxoanions and the heteroatom [5, 18-22].

$$12\ WO_4^{2-} + HPO_4^{2-} + 23\ H^+ \longrightarrow [PW_{12}O_{40}]^{3-} + 12\ H_2O$$

Control of the pH and X/M (central atom/addenda atom) ratio is necessary in order to obtain the desired structure, i.e., the Keggin HPA, the Wells-Dawson HPA, the Anderson HPA, a lacunary compound or the desired specific isomer. Free acids are synthesized primarily by following two methods: (1) by extraction with ether from acidified aqueous solutions and (2) by ion exchange from salts of heteropoly acids.

1.4. Stability of heteropoly acids

Two important types of stabilities associated with heteropolyacids are: thermal stability and hydrolytic stability in solution [2, 4]. The solution stability of HPA depends on pH of the solution [23]. The thermal stability is measured mainly by X-ray diffraction (XRD), thermal gravimetric analysis, and differential thermal analysis (TG-DTA) experiments, where the exothermic peak in DTA estimates the decomposition temperature. Results from TG and DTA shows the presence of two types of water in heteropoly compounds, i.e., water of crystallization and "constitutional water molecules" [24]. Loss of former occurs at temperature below 200 ^oC. The constitutional water molecules (acidic protons bound to the oxygen of the polyanion) are lost at temperature exceeding 270 ^oC for $H_3PMo_{12}O_{40}$ or 350 ^oC for $H_3PW_{12}O_{40}$. The thermal stability of hydrogen forms of HPAs changes with heteroatom, polyatom, and polyanion structure as follows: $H_3PW_{12}O_{40} > H_4SiW_{12}O_{40} > H_3PMo_{12}O_{40} > H_4SiMo_{12}O_{40}$, while hydrolytic stability follow the order: $H_4SiW_{12}O_{40} > H_3PW_{12}O_{40} > H_4SiMo_{12}O_{40} > H_3PMo_{12}O_{40}$ [5, 25, 26]. The decomposition of HPAs causes the loss of their acidity. However, thermally decomposed molybdenum HPAs becomes reconstructed under exposure to water [27].

1.5. Characterization

The most important techniques used for characterizing heteropolyacids and the informations obtained are:

1.5.1. Infrared spectroscopy: This is the most convenient method for the characterization of heteropolyanions. Their characteristic bands can distinguish Keggin, Dawson, and lacunary heteropolyanions. The IR bands of most important Keggin heteropolyacids are given in Table 1.2 [28-32].

1.5.2. Raman spectroscopy: Vibrational frequencies in the Raman spectra of $XM_{12}O_{40}$ (X = Si, P; M = W, Mo) are summarized in Table 1.3 [33-35]. The X-O vibration in T_d symmetry of XO_4 is Raman-inactive. Among M-O bonds, M-O_d is Raman active. The states of hydrates of heteropolyacids are best distinguished by Raman spectroscopy, since Raman spectra give better-resolved OH stretching bands than IR spectra.

1.5.3. NMR spectroscopy: a) ^{31}P NMR spectroscopy. The ^{31}P chemical shift provides important information concerning the structure, composition, and electronic states of these materials. The chemical shift in aqueous solution is correlated with the P-O_a bond strength [36]. The ^{31}P NMR chemical shift is greatly depends on water of hydration in heteropolyacids [17, 37]. In $H_3PW_{12}O_{40}$. $n$$H_2O$, the values being –15.1 to –15.6 ppm for n = 6 and –11.1 to –10.5 ppm for n = 0. This is because, in the former protonated water $H(H_2O)_2^+$, is connected with the heteropolyanion by hydrogen bonding at terminal oxygens, and in the latter, protons are directly attached to oxygen atoms of the polyanion.

b) ^{183}W NMR Spectroscopy. ^{183}W Chemical shifts are sensitive to the heteroatom [38], being –103.8 ppm for $SiW_{12}O_{40}^{4-}$, and –98.8 ppm for $PW_{12}O_{40}^{3-}$. This spectroscopy is used to distinguish the structure of positional isomers. α- and β-$SiW^{12}O_{40}^{4-}$ can be distinguished by ^{183}W NMR spectroscopy; α- $SiW_{12}O_{40}^{4-}$ gives one singlet (12 equivalent atoms), and β-$SiW_{12}O_{40}^{4-}$ three resonances in the ratio 1:2:1 [39].

Other NMR techniques such as ^{1}H, ^{17}O, ^{95}Mo and ^{29}Si NMR spectroscopies were also used to characterize heteropolyacids [2].

Table 1.2: Infrared absorption bands of heteropolyacids, (M = W and Mo)(cm^{-1})

$H_3PW_{12}O_{40}$	$H_4SiW_{12}O_{40}$	$H_3PMo_{12}O_{40}$	$H_4SiMo_{12}O_{40}$	**Modes of vibration**
1080	926	1070	910	ν_{as}(X-O)
982	980	965	958	ν_{as}(M=O)
893	878	870	860	ν_{as}(M-O-M)
812	779	790	780	ν_{as}(M-O-M)

Table 1.3: Raman vibrational frequencies of Keggin anions (aqueous solutions), cm^{-1}

$PW_{12}O_{40}^{3-}$	$SiW_{12}O_{40}^{4-}$	$PMo_{12}O_{40}^{3-}$	$SiMo_{12}O_{40}^{4-}$	**Modes of vibration**
1011	998	997	982	$p\nu_{as}$(M-O_d)[a]
996	981	981	962	ν_{as}(M-O_d)

[a] $p\nu_{as}$(M-O_d) shows polarized vibration.

1.5.4. Electronic spectroscopy: Electronic absorption spectra give information about the electronic states of heteropolyanions [6].

1.6. Homogeneous reactions

HPAs catalyze a wide variety of reactions in homogeneous liquid-phase offering strong options for more efficient and cleaner processing compared to conventional mineral acids [26, 40-42]. HPAs have significantly higher catalytic activity than mineral acids and particularly in organic media, the molar catalytic activity of HPA is often 100-1000 times higher than that of H_2SO_4 [2, 43]. This makes it possible to carry out the catalytic process at a lower catalyst concentration and/or at a lower temperature. Important characteristics accounting for the high catalytic activities are the acid strength, softness of the heteropolyanion, catalyst concentration, and nature of the solvent [2]. Softness of the polyanion is important in bringing about unique activity because the intermediates like oxonium ions or carbenium ions are stabilized on the surfaces of heteropolyanion, by the virtue of softness [44]. The effect of softness becomes significant

for reactions in aqueous solutions, in which the influence of the difference in the acid strength is small, since most of the heropolyacids are completely dissociated. Further, HPA catalysis lacks side reactions such as sulfonation, chlorination, nitration, etc., which occur with mineral acids [43]. As stable, relatively nontoxic crystalline substances, HPAs are also preferable with regard to safety and ease of handling. The relative activity of Keggin HPAs primarily depends on their acid strength. Other properties, such as the oxidation potential, which determine the reducibility of HPA by reaction medium, as well as the thermal and hydrolytic stability, are also important. Typical examples for HPA catalyzed homogeneous reactions are:

1.6.1. Hydration of olefins

The HPA-catalyzed hydration of C_3-C_4 olefins is an industrially important reaction, the hydration of propene to isopropyl alcohol being the first commercial process based on HPA catalysis [45]. The hydration of isobutene to *tert*-butyl alcohol is used for the separation of isobutene from a mixture of C_4 hydrocarbon stream by the use of concentrated solution of heteropolyacids [2, 26]. Compared to the mineral acid HNO_3, $H_3PW_{12}O_{40}$ is 10 times more active and isobutene in the mixture selectively hydrated in the concentrated solution, minimizing side reactions such as isobutene olegomerization.

1.6.2. Biphasic reactions

Separation of products and recovery and recycling of a catalyst becomes easier if a homogeneously catalyzed reaction can be performed in a biphasic system consisting of two immiscible liquid phases - a catalyst phase and a product/reactant phases - with intense mass transfer between them. HPAs due to their special solubility properties, i.e., high solubility in polar solvents and insolubility in nonpolar solvents, are suitable catalysts for operating under phase-transfer conditions. The reaction predominantly proceeds in the catalyst phase, and the product formed is transferred to the less polar product phase. Typical examples for biphasic catalysis are polymerization of tetrahydrofuran (THF) to polyoxotetramethylene glycol (PTMG) [46] and synthesis of diphenyl methane by the reaction of benzene with aqueous formaldehyde [47, 48].

1.7. Heterogeneous catalysis

There are three types of catalysis of solid HPAs; (1) surface, (2) bulk type I (pseudoliquid), and (3) bulk type II catalysis (Fig. 1.4), as given in Table 1.4.

1.7.1. Surface-type catalysis

Surface-type catalysis is the ordinary heterogeneous catalysis, where the reactions take place on the two-dimensional surface (outer surface and pore wall) of solid catalysts. The reaction rate is proportional to the surface area in principle. Rates of double-bond isomerization of olefins are proportional to the surface area of $H_3PMo_{12}O_{40}$ [49].

1.7.2. Bulk-type (I) catalysis

In the bulk-type (I) catalysis, e.g., acid-catalyzed reactions of polar molecules over the hydrogen forms and group A salts at relatively low temperatures, the reactant molecules are absorbed in the interpolyanion space of the ionic crystal (not intrapolyanion) and react there, and then the products desorb from the solid [4, 50, 51]. Because of the flexible and hydrophilic nature of the secondary structures of the acid form and group A salts, polar molecules like alcohols and amines are readily absorbed into the solid bulk by substituting for water molecules and/or by expanding the distance between polyanions. The number of absorbed molecules is 10-100 times greater than the amount of monolayer adsorption estimated from N_2 adsorption. The solid behaves like a solution and the reaction field becomes three-dimensional. This is known as "pseudoliquid" catalysis first proposed in 1979 [52-54]. The reaction rate is proportional to the volume of catalyst in the ideal case; for example, the rate of acid-catalyzed reaction is governed by the bulk acidity. In the pseudoliquid phase, such catalysts appear as solids, but, behaves like liquids (solvent). As the active sites in the solid bulk *e.g.* protons, take part in catalysis, very high catalytic activities are often observed in the bulk phase.

Table 1.4: Three types of heterogeneous catalysis over solid HPA

Types	Remarks	Examples
surface type	ordinary type reactions take place on the surface rate ∝ surface area	oxidation of aldehydes and CO
bulk type (I)	"pseudoliquid phase" reactants are absorbed in solid bulk and react; rate ∝ volume (weight)	dehydration of alcohols at low temperatures
bulk type (II)	main reactions occur on the surface, but by diffusion of redox carriers, whole bulk takes part; rate ∝ volume (weight)	oxidative dehydrogenation and oxidation of H_2

1.7.3. Bulk-type (II) catalysis

This has been found to be relevant for oxidation reactions at high temperatures. Certain oxidation reactions like oxidative dehydrogenation and oxidation of hydrogen at high temperatures exhibit bulk-type (II) catalysis [55, 56]. If the rates of *bulk-type oxidation* (*e.g.* oxidative dehydrogenation) are plotted against the surface redox property, very poor correlations are found, but, the rates exhibit good correlations with *bulk* redox property. In contrast, the rate of *surface-type* oxidation correlates very well with the *surface redox property*. In this type of catalytic oxidation, although the principal reaction may proceed on the surface, the whole solid bulk takes part in redox catalysis owing to the rapid migration of redox carriers such as protons and electrons. The rate is proportional to the volume of catalyst in the ideal bulk-type (II) catalysis [3].

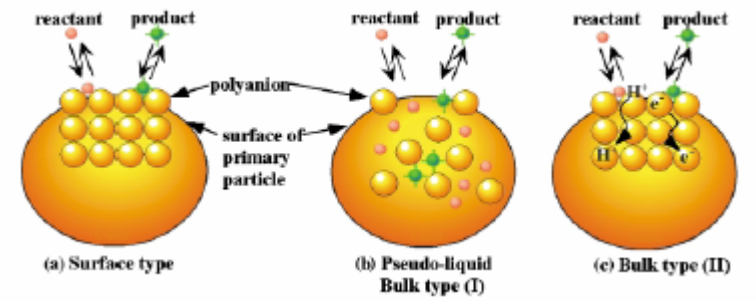

Fig. 1.4: Three types of catalysis for solid heteropoly compounds: (a) surface type, (b) pseudoliquid: bulk type (I), (c) bulk type (II) [1].

1.8. Acid and redox properties

1.8.1. Acidic properties

Acidic properties of heteropoly compounds in the solid state are sensitive to countercations, constituent elements of polyanions, and tertiary structure. Typical heteropolyacids having the Keggin structures, such as, $H_3PW_{12}O_{40}$ and $H_4SiW_{12}O_{40}$, are strong acids; protons are dissociated completely from the structures in aqueous solution. Heteropolyacids are much stronger acids than H_2SO_4, HBr, HCl, HNO_3, and $HClO_4$. The greater acid strength of heteropolyacids than that of mineral acids is explained as follows [2]. Since, in heteroplyanions the negative charge of similar value is spread over much larger anions than those formed from mineral acids, the electrostatic interaction between proton and anion is much less for heteropolyacids than for mineral acids. An additional important factor is the dynamic delocalizability of the charge or electron. The change in the electronic charge caused by deprotonation may be spread over the entire polyanion unit. In acetone, heteropolyacids show the following order of acidity: $H_3PW_{12}O_{40}$ > $H_4SiW_{12}O_{40}$ ≈ $H_3PMo_{12}O_{40}$ > $H_3PMo_{11}VO_{40}$ > $H_4SiMo_{12}O_{40}$ [43]. Solid HPAs, such as $H_3PW_{12}O_{40}$ and $H_3PMo_{12}O_{40}$ are pure Brönsted acids and stronger than the conventional solid acids, such as SiO_2-Al_2O_3, H_3PO_4/SiO_2, and HX and HY zeolites [57].

1.8.2. Redox properties

HPAs in solid state act as good oxidation catalysts and shows two types of oxidation catalysis: bulk type and surface type (Fig. 1.5). The reduction of $H_3PM_{12}O_{40}$ (M = Mo, W) and its Na salts by hydrogen proceeds in the following three steps [3, 58]:

$$x\mathrm{H_2(gas)} + \mathrm{PM_{12}O_{40}^{3-}(surface)} \rightleftharpoons 2x\mathrm{H^+(bulk)} + \mathrm{PM_{12}O_{40}^{(3+2x)-}(bulk)} \quad (1)$$

$$2x\mathrm{H^+(bulk)} + \mathrm{PM_{12}O_{40}^{(3+2x)-}(bulk)} \longrightarrow \mathrm{PM_{12}O_{40-x}^{3-}(bulk)} + x\mathrm{H_2O\ (bulk)} \quad (2)$$

$$x\mathrm{H_2O\ (bulk)} \longrightarrow x\mathrm{H_2O\ (gas)} \quad (3)$$

The first step is $H_2 \rightarrow 2H^+$ (present between polyanions) + 2e (present in polyanion), without formation of water. In the second step, the protons formed in the first step react with the oxygen of polyanion to form water, which evolves in step 3 into the gas phase. The diffusion of protons and electrons in the solid state of $H_3PM_{12}O_{40}$ (M =

Mo, W) is very rapid as compared with the rate of reduction. Since, the reduction of $H_3PM_{12}O_{40}$ (M = Mo, W) by hydrogen proceeds in the solid bulk by the rapid migration of protons and electrons, the rate is proportional to the number of polyanion in the bulk (bulk-type II catalysis).

In contrast, the rates of reduction by CO of $H_3PMo_{12}O_{40}$ and its alkali salts under the dry conditions are proportional to the specific surface areas as in the case of ordinary heterogeneous catalysis (surface type catalysis). Hence, due to the slow diffusion of oxide ion, the reduction mostly proceeds near the surface [59]. Oxidation potential of different HPAs are in the order: $H_3PMo_{12}O_{40} > H_4SiMo_{12}O_{40} >> H_3PW_{12}O_{40} > H_4SiW_{12}O_{40}$ [26].

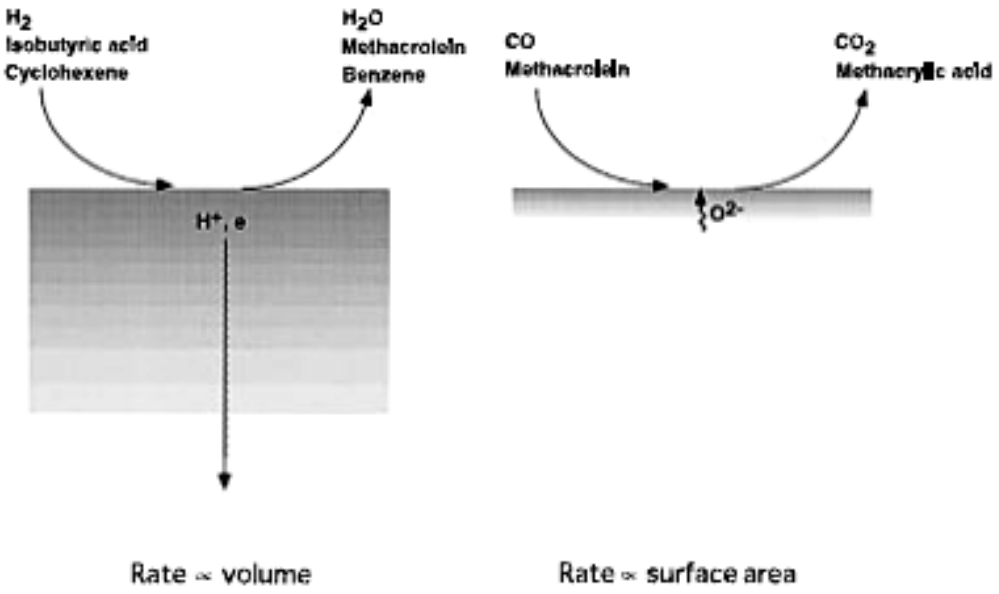

Fig. 1.5: Schematic illustration of bulk-type (II) and surface-type catalysis: (a) bulk type and (b) surface type [3].

1.9. Supported heteropolyacids

The major problem, limiting the utility of homogeneously catalyzed processes, is the well-known difficulty in catalyst recovery and recycling. As the cost of HPAs is higher than mineral acids, the recycling of HPA catalysts is the key issue to their application. A more efficient way to overcome the separation problem is the use of biphasic systems or solid HPA catalysts [26]. In heterogeneous as well as in homogeneous systems, HPAs are generally more efficient than conventional catalysts, such as SiO_2-Al_2O_3, zeolites, etc., which is in line with their relative acid strengths.

Obvious advantage of heterogeneous systems over homogeneous is easy separation of a catalyst from reaction products.

A serious problem with the solid HPA catalysts is their deactivation during organic reactions due to the formation of carbonaceous deposit (coke) on the catalyst surface. Conventional regeneration by burning coke at 500-550 °C, which is routinely used in the case of aluminosilicates and zeolites, is not applicable to HPAs because their thermal stability is not high enough to do so. Supporting HPA on a carrier inhibits the formation of coke, while bulk HPAs, having very strong acid sites and low surface area, coke forms more rapidly [60].

Hydrogen forms (or free acids) of HPAs usually have low surface areas (1-10 m^2 g^{-1}). Supporting heteropolyacids on solids with high surface areas is a useful method for improving catalytic performance, where the stability of the HPA and firm fixation are the key issues [1]. Acidic or neutral materials such as SiO_2, carbon, acidic ion-exchange resin, etc., are suitable as supports. Basic solids such as MgO and Al_2O_3, tend to decompose HPAs [61-64].

The thermal stability of HPA on SiO_2 is comparable to or slightly lower than that of the parent HPA. The interactions between $H_3PW_{12}O_{40}$ and the surface OH groups of SiO_2 have been detected at low loading levels by ^1H and ^{31}P MAS NMR and Raman spectroscopies [65-69]. HPAs supported on certain activated carbons are considered to be promising fixed-bed acid catalysts for liquid-phase reactions because of their stability towards HPA leaching from the carrier. However, the acid strength of $H_3PW_{12}O_{40}$ is reduced after loading on activated carbon or silica. Enhanced catalytic activity of HPAs was found, when they were supported on a strongly acidic ion exchange resin, Amberlyst-15 [70]. The activity was much higher than those of Amberlyst-15 and of the acids supported on active carbon. The higher activity was explained by the synergism due to the interaction of the heteropolyanions and protons of the ion exchanger.

1.10. Heterogeneous acid-catalyzed reactions

Acidity, basicity, and pseudoliquid behavior are the most important factors governing the acid catalysis of solid HPAs. The acidic properties are mainly controlled by (i) the structure and composition of the heteropolyanion itself, (ii) the countercations,

and (iii) the dispersion on supports. The secondary and tertiary structures are affected by these three factors. In addition to the acidic properties, the absorption properties for polar molecules are critical in determining the catalytic function in the case of "pseudoliquid" catalysis. Soft basicity of the heteropolyanion itself sometimes plays an important role for high catalytic activity. The soft basicity of polyanion follow the order of $SiW_{12}O_{40}^{4-}$ > $GeW_{12}O_{40}^{4-}$ > $PW_{12}O_{40}^{3-}$ > $SiMo_{12}O_{40}^{4-}$ > $SO4^{2-}$. The acidity of HPAs in the solid state reflects in general the acidity in solution; the acid strength decreases when Mo replaces W and when the central P atom is replaced by Si for Keggin HPAs, which are stronger acids than Dawson HPAs [71].

The group B heteropolyacids salt $Cs_{2.5}H_{0.5}PW_{12}O_{40}$ has strong acid sites, high surface area (100-200 m^2 g^{-1}) and acts as an efficient solid acid catalyst for a variety of organic reactions [1-4]. But, these materials, tends to become a milky suspension during liquid-phase reactions, which makes it difficult to separate the catalyst after the reaction is completed [1].

The catalyst deactivation is usually observed during the catalytic reaction, and the deactivation is sensitive to the kind of reactant, product, solvent, and reaction temperature. There are several possible causes for the catalyst deactivation, e.g., coke formation, adsorption of products, catalyst reduction, catalyst decomposition, and catalyst dissolution. HPAs containing Mo and V are susceptible for deactivation by reduction, while HPAs of W are more resistant towards deactivation by reduction. The coke formation or strong adsorption of polymerized products often causes deactivation as in the case of other solid acid catalysts. Therefore, the suppression of the deactivation and the method of regeneration are the important problems in the acid catalysis of HPAs [3].

1.11. Oxidation reactions

Keggin-type heteropoly compounds having Mo and V as addenda atoms are usually used for oxidation reactions. Two most important heterogeneous oxidation reactions catalyzed by solid HPAs are oxidation of methacrolein to methacrylic acid and oxidation of ethylene to acetic acid in presence of water and O_2. The acidity and oxidizing ability work cooperatively in methacrolein oxidation. The heteropoly catalysts of composition $H_{3-x}Cs_xPMo_{12-y}V_yO_{40}$ ($2 < x < 3$; $0 < y < 2$) are used industrially for this reaction. Acidic Cs salts that are nearly stoichiometric are used because Cs salts markedly increase the surface area and thermal stability of the catalysts [2, 3].

For the one-stage process of acetic acid production from a mixture of ethylene, water, and O_2 by the direct oxidation of ethylene, Pd-$H_4SiW_{12}O_{40}$ promoted by Se or Te was highly efficient. The combination of metallic Pd and heteropolyacid is indispensable for the reaction. The presence of small amount of Se or Te enhances the acetic acid selectivity by effectively reducing the formation of CO_2. The reaction proceeds in two steps: (1) hydration of ethylene to ethanol catalyzed by the heteropolyacid (acid catalysis) and (2) oxidation of ethanol to acetic acid on the Pd site [72].

The liquid-phase oxidation of organic substances catalyzed by heteropolyacids proceeds in homogeneous or biphasic systems, with dioxygen, hydrogen peroxide, alkylperoxides, etc., as oxidants [26]. Keggin-type mixed-addenda heteropolyanions $PMo_{12-n}V_nO_{40}^{(3+n)-}$ (HPA-n) catalytic system, discovered by Matveev et al. [73, 74] in the 1970s, is the most efficient and versatile catalyst for oxidation by O_2. As the catalysts, either one-component or two- and multicomponent systems are used. The most important two-component system includes HPA-n and Pd(II) for the oxidation of ethylene to acetaldehyde [2, 26].

Venturello [75-77] and Ishii [78-87] developed the most important hydrogen peroxide based oxidation reaction (olefin epoxidation). The reaction is usually performed under biphasic conditions in presence of Keggin type HPA (catalyst precursor) and a phase transfer reagent such as cetyl pyridinium chloride. The reaction takes place preferentially in the organic phase via the oxygen atom transfer from the peroxo polyoxometallate to the substrate. The phase-transfer reagent transfer the active peroxo polyoxometallate formed in the aqueous phase by the interaction of heteropolyanion with

hydrogen peroxide into the organic phase. The Keggin type HPA; $H_3PW_{12}O_{40}$ is the most active precursor in this type of reaction. Catalyst deactivation and the use of chlorinated hydrocarbons as solvents are the major drawbacks of Venturello-Ishi process [88].

1.12. Zirconia as a catalyst and a catalyst support

Zirconium dioxide (zirconia) is an oxide with a high melting point about (2700 ^oC), and shows low thermal conductivity, and high resistance for corrosion, which has been used for refractories, pigments, piezoelectric devices, ceramic condensers, and oxygen sensors. The partially stabilized zirconia with high mechanical strength and high tenacity is used in fine ceramics. It is quite insoluble at low and high pH.

Zirconia is usually obtained by the calcination of its hydroxide/oxyhydroxide, which is prepared by hydrolysis of zirconium salts. Mainly three crystalline modifications of zirconia are known; the monoclinic which is stable up to 1200 ^oC, the tetragonal which is stable up to 1900 ^oC, and the cubic which is stable above 1900 ^oC. However, tetragonal zirconia can be prepared at low temperatures (in the range of 550-750 ^oC) in the form of metastable phase.

Temperature ranges where the above-mentioned crystal forms are stabilized are depending upon the presence of impurities or additives. Transformation of the metastable tetragonal to the monoclinic form is sensitive to the existence of impurities or additives and they usually stabilize the metastable tetragonal form at higher temperatures [89].

ZrO_2 is stable under oxidizing and reducing atmosphere and possesses both acid and base properties. The acid site (Zr^{4+}) and base site (O^{2-}) present in ZrO_2 is very weak. In solution, acidic and basic sites are neutralized immediately, however, they may exist independently at the surface. Thus acidic and basic sites on the surface of oxides work both independently and cooperatively and hence ZrO_2 act as an acid-base bifunctional oxide and hence show *acid-base bifunctional catalysis*. The existence of both acidic and basic properties is evidenced by the adsorption of CO_2 and NH_3 [89, 90].

Zirconium oxyhydroxide adsorbs both cations and anions in an aqueous solution. In acidic solution, it adsorb anions such as SO_4^{2-} ions, while in basic solution, cations are preferentially adsorbed. The acidic and basic sites (OH) on the surface of ZrO_2 calcined at relatively low temperature are very weak. Based on ZrO_2, three processes are industrialized such as synthesis of α-olefin, ketones, and aromatic aldehydes. The high

activities of ZrO_2 in these reactions are due to the *acid-base bifunctional catalysis*. For the bifunctional catalysis, the orientation of acid-base pair sites is vitally important. The orientation can largely changed by the preparation method, the pretreatment condition, and the addition of small amounts of the other metal oxides [90].

1.13. Zirconia based solid acids

The most important zirconia based solid acids are 1) sulfated zirconia and 2) tungstated zirconia

1.13.1. Sulfated zirconia: Holm and Bailey in 1962, disclosed for the first time that sulfated zirconia modified with platinum as an active catalyst for isomerization of *n*-pentane at low temperature [91]. Later in 1970's Arata et al. observed that the sulfate treated metal oxides, ZrO_2 or Fe_2O_3, are able to isomerize *n*-butane at low temperature (room temperature), like superacids (SbF_5-HF and SbF_5-FSO_3H) [92, 93]. Zirconia, when modified with anions, such as sulfate ions, forms a highly acidic catalyst that exhibits superior catalytic activity in many reactions. The catalytic performance of sulfated zirconia is significantly dependent on the preparation methods and on the activation procedure prior to reaction. Sulfated zirconia is usually prepared by two-step procedure. In the first step, the zirconium oxyhydroxide is precipitated by the addition of aqueous ammonia to a zirconium salt, such as $ZrOCl_2$ or $ZrO(NO_3)_2$. The hydroxide obtained by the precipitation after washing and drying, impregnated with a solution of H_2SO_4 or $(NH_4)_2SO_4$ in the second step [94]. After impregnation, the resulting solid is dried and calcined at 550-650 ^oC. The calcination is a crucial step for the generation of strong acidity of sulfated zirconia. Active catalyst is prepared by the calcination of sulfated zirconia precursor at 550-650 ^oC for several hours in air [95]. Sulfated zirconia prepared by the conventional method is mainly exists in metastable tetragonal phase. However, monoclinic sulfated zirconia prepared by sulfating crystalline monoclinic sulfated zirconia is also found to be active for *n*-butane isomerization but, compared to the tetragonal one, monoclinic sulfated zirconia had low activity, which indicates that tetragonal phase favors *n*-butane isomerization [96]. Calcination at higher temperature leads to an inactive catalyst with low sulfur content. One of the functions of calcination step is to transform the inactive amorphous zirconium oxyhydroxide into active tetragonal zirconia by dehydration and serving the sulfate groups to bind the zirconia

surface to form the active sites. Another important function of the calcination is to create strong Lewis acidity (coordinatively unsaturated Zr(IV)). Sulfated zirconia is considered as a super acid initially, but later studies confirmed that acidity is similar to that of sulfuric acid. Depending on the level of surface hydration/dehydration, sulfated zirconia shows Brönsted and Lewis acidity. The acidity and surface area strongly depend on the preparation procedure, and the exact nature of acid sites as well as the structure sulfate groups remains the object of debate [97-104].

Sulfated zirconia has attracted considerable interest as a potential replacement for liquid catalysts in such processes as isomerization, hydrocracking, alkylation, acylation, etc [105-113]. However, their poor stability, and their tendency to form volatile sulfur compounds during catalysis and regeneration limits their applicability [114, 115].

1.13.2. Tungstated zirconia: Tungstated zirconia (zirconia-supported tungsten oxide, WO_x/ZrO_2-WZ) is found to be better catalyst than sulfated zirconia in terms of its easy preparation method, slow deactivation and superior stability under both reducing and oxidizing conditions. WZ catalysts were first reported to be strongly acidic by Hino and Arata [116]. They reported low temperature *n*-butane and *n*-pentane isomerization activity on WZ catalysts prepared by impregnating zirconium oxyhydroxide with aqueous ammonium metatungstate (13 wt.% W) and subsequent high temperature oxidation (800 ^oC). *n*-Pentane isomerization rates decreased markedly when metatungstate solutions were impregnated on crystalline ZrO_2 supports instead of amorphous zirconium oxyhydroxide support, suggesting that hydrated WO_x species combine with zirconium oxyhydroxide surface sites and such sites are not available after crystalline tetragonal or monoclinic ZrO_2 structures are formed. The initial formation of dispersed tungstate species occurs via anion exchange or condensation reactions of hydrated aqueous tungstate anions with surface OH species in zirconium oxyhydroxide. The resulting high dispersion of WO_x species inhibits the crystallization and sintering of the ZrO_2 support crystallites leads to the formation of WO_x clusters of varying size and catalytic properties. The catalyst with the tungsten loading slightly exceeding the theoretical monolayer coverage was found to be the most active. Under these conditions tungsten oxide species exist as three-dimensional polyoxotungstate clusters on the surface of zirconia [117-119]. The tungsten atoms in these polyoxotungstate clusters are located in a distorted

octahedral environment, which are grafted to the support through W-O-Zr bridges. The structure and the size of these clusters, as well as their specific interactions with the zirconia support, largely determine the acidic, redox, and catalytic properties of these catalysts. In WZ catalysts, WO_x clusters of intermediate size (polyoxotungstate clusters) delocalize a net negative charge caused by the slight reduction of W^{6+} centers in reactant environments containing H_2 or hydrocarbons. This temporary charge imbalance leads to the formation of Brönsted acid $(WO_3)_m\{W_{6-n}O_3\}\{n\text{-}H^+\}$ centers on the zirconia support. These Brönsted acid sites on WZ appear to form via a mechanism similar to that on heteropolytungstate clusters, but in this case, the charge imbalance is not permanent; it is reversible and created *in-situ* by the reducing environment of the acid-catalyzed reaction [120, 121].

1.14. Scope of the thesis

This thesis describes the preparation, characterization and catalytic activity studies of zirconia-supported Keggin heteropolyacids. The heteropolyacids under study include 12-tungstosilicic acid (silicotungstic acid, STA), 12-tungstophosphoric acid (phosphotungstic acid, PTA), and 12-molybdophosphoric acid (phosphomolybdic acid, PMA). The thermal stability of heteropolyacids supported on conventional supports like silica, carbon, ion exchange resin etc. are not high enough to carry out regeneration by calcination. Moreover, heteropolyacids supported on conventional supports can leach into the reaction medium in presence of polar reactants and hence catalyze the reaction homogeneously. One of the objectives of the work described in this thesis is to explore the possibility of the preparation of stable supported heteropolyacid catalysts. The thesis intends to investigate the relationship between surface properties of the catalysts with observed catalytic properties.

The thesis has been divided into six chapters.

Chapter 1 gives a general introduction to heteropoly acids (HPAs), its structure, classification, and catalytic properties. It also gives an introduction to supported-heteropoly acids and the conventional supports used for the preparation of supported-heteropoly acids. Further, this chapter gives an introduction to zirconia, its properties, and zirconia based solid acids. Finally, the scope of the thesis is outlined.

Chapter 2 describes the preparation and characterization of zirconia-supported heteropoly acid catalysts and its characterization by different techniques. Catalysts with different HPA loading (wt.%) and calcination temperature (^{o}C) were prepared. These catalysts were characterized by different techniques such as surface area (N_2 adsorption), XRD, Raman spectroscopy, TG-DTA, NH_3-TPD, FTIR pyridine adsorption, and ^{31}P MAS NMR spectroscopy. For each technique, its theory and experimental procedures are described briefly.

Chapter 3 describes the characterization results of zirconia-supported silicotungstic acid catalysts with different STA loading and calcination temperature by surface area, XRD, Raman spectroscopy, XPS, NH_3-TPD, FTIR pyridine adsorption, and DRUV-vis spectroscopy and the results are discussed.

The catalysts were used in the liquid-phase benzoylation of veratrole with benzoic anhydride and alkylation of phenol with *tert*-butanol in a fixed-bed down flow reactor. The effect of parameters like STA loading and calcination temperature on catalytic activity is studied and the relation between catalytic activities and surface properties are discussed. The most active catalyst has been used to study different reaction parameters like temperature, molar ratio, catalyst weight, effect of time/space velocity and time on stream on conversion and product selectivity.

Chapter 4 describes the characterization results of zirconia-supported phosphotungstic acid catalysts by surface area, XRD, TG-DTA, NH_3-TPD, FTIR pyridine adsorption and ^{31}P MAS NMR spectroscopy. In order to understand the role of the solvent used for the catalyst preparation, the catalyst with optimum PTA loading and calcination temperature was prepared using different solvents and characterized by ^{31}P MAS NMR spectroscopy and the results are discussed.

These catalysts were used in the liquid-phase synthesis of linear alkyl benzene by the alkylation of benzene with higher linear olefins like 1-octene and 1-dodecene and

acylation of 2-methoxy naphthalene with acetic anhydride. The effect of parameters like PTA loading and calcination temperature on catalytic activity is studied and relation between catalytic activities and surface properties are discussed. The catalysts with optimum PTA loading and calcination temperature prepared under different solvents were used in liquid-phase alkylation of benzene with 1-octene and a discussion is made on the difference in catalytic activity between the catalysts prepared in different solvents. The most active catalyst has been used to study different reaction parameters like temperature, molar ratio, catalyst weight and effect of time on conversion and product selectivity.

Chapter 5 describes the characterization results of zirconia-supported phosphomolybdic acid catalysts with different PMA loading and calcination temperature by XRD and ^{31}P MAS NMR spectroscopy. The nature of acidic sites present in the most active catalyst is probed by FTIR pyridine adsorption.

These catalysts were used in liquid-phase synthesis of linear alkyl benzenes by the alkylation of benzene with higher linear olefins like 1-octene and 1-dodecene and alkylation of phenol with *tert*-butanol in a fixed-bed down flow reactor. The effect of parameters like PMA loading and calcination temperature on catalytic activity is studied. The most active catalyst has been used to study the reaction parameters like temperature, catalyst weight, molar ratio, space velocity and time on stream on conversion and product selectivity.

Chapter 6 gives the summary and conclusions reached in this thesis.

1.15. References

1. M. Misono, Chem. Commun. (2001) 1141.
2. T. Okuhara, N. Mizuno, M. Misono, Adv. Catal. 41 (1996) 113.
3. N. Mizuno, M. Misono, Chem. Rev. 98 (1998) 199.
4. M. Misono, Catal. Rev. Sci. Eng. 29 (1987) 269; 30 (1988) 339.
5. G.A. Tsigdinos, Top. Curr. Chem. 76 (1978) 1.
6. M.T. Pope, "Heteropoly and Isopoly Oxometalates". Springer-Verlag, Berlin, 1983.
7. M.T. Pope, A. Muller, Angew. Chem. Int. Ed. Engl. 30 (1991) 34.
8. "Polyoxometallates: From Platonic Solids to Anti-Retroviral Activity." (M.T Pope and A. Muller, Eds.). Kluwer, Dordrecht, 1994.
9. Y. Jeannin, G. Herve, A. Proust, Inorg. Chim. Acta 189 (1992) 319.
10. T.J.R. Weakly, Struct. Bonding 18 (1974) 131.
11. J.F. Keggin, Nature (London) 131 (1933) 908.
12. L. Pettersson, I. Anderson, L.O. Ohman, Inorg. Chem. 25 (1986) 4726.
13. B. Dawson, Acta Crystallogr. 6 (1953) 113.
14. H. D'Amour, Acta Crystallogr. B32 (1976) 729.
15. J.S. Anderson, Nature 140 (1937) 850.
16. M.N. Timofeeva, Appl. Catal. A 256 (2003) 19.
17. S. Uchida, K. Inumaru, M. Misono, J. Phys. Chem. B 104 (2000) 8108.
18. G.A. Tsigdinos, Ind. Eng. Chem. Prod. Res. Dev. 13 (1974) 267.
19. B. Gruttner, and G. Jander, in "Handbook of Preparative Inorganic Chemistry," 2nd Ed. (G. Brauer, Ed.), Academic Press, New York, 1976, Vol. 2, p. 1716.
20. J.C. Bailar, Inorg. Synth. 1 (1939) 132.
21. H. Hu, J. Biol. Chem. 43 (1920) 189.
22. R.D. Hall, J. Am. Chem. Soc. 24 (1907) 780.
23. F. Cavani, Catal. Today 41 (1998) 73.
24. C. Rocchiccioli-Deltcheff, Inorg. Chem. 22 (1983) 207.
25. M. Fournier, C. F-Jantou, C. Rabia, G. Herve, S. Launary, J. Mater. Chem. 2 (1992) 971.
26. I.V. Kozhevnikov, Chem. Rev. 98 (1998) 171.

27. I.V. Kozhevnikov, Appl. Catal. A 256 (2003) 3.
28. C. Rocchiccioli-Deltcheff, R. Thouvent, R. Franck, Spectrochim. Acta 32A (1976) 587.
29. D.H. Brown, Spectrochim. Acta 19 (1963) 583.
30. C. Hu, M. Hashimoto, T. Okuhara, M. Misono, J. Catal. 143 (1993) 437.
31. T. Okuhara, C. Hu, M. Hashimoto, M. Misono, Bull. Chem. Soc. Jpn. 67 (1994) 1186.
32. F. Boeschen, B. Brus, B. Krebs, Acta Crystallogr. B30 (1974) 48.
33. C. Rocchiccioli, M. Fournier, R. Franck, R. Thouvent, Inorg. Chem. 22 (1983) 207.
34. C. Rocchiccioli-Deltcheff, R. Thouvent, J. Chem. Res. (S) (1977) 46; (M) (1977) 546.
35. T. Fukumoto, K. Murata, S. Ikeda, Anal. Chem. 56 (1984) 929.
36. C. Rocchiccioli, R. Thouvenot, Spectrosc. Lett. 12 (2) (1979) 127.
37. Y. Kanada, Y. Lee, S. Nakata, S. Asaoka, M. Misono, Chem. Lett. (1988) 139.
38. R. Acerete, C.F. Hammer, L.C.W. Baker, J. Am. Chem. Soc. 101 (1979) 267.
39. J. Lefevre, F. Chauveau, P. Doppelt, J. Am. Chem. Soc. 103 (1981) 4581.
40. I. V. Kozhevnikov, K.I. Matveev, Appl. Catal. 5 (1983) 135.
41. I. V. Kozhevnikov, Stud. Surf. Sci. Catal. 90 (1994) 21.
42. I. V. Kozhevnikov, Catal. Rev. Sci. Eng. 37 (1995) 311.
43. I. V. Kozhevnikov, Russ. Chem. Rev., 56 (1987) 811.
44. K. Urabe, K. Fukita, Y. Izumi, Shokubai (Catalyst) 22 (1983) 223.
45. M. Misono, N. Nojiri, Appl. Catal. 64 (1990) 1.
46. A. Aoshima, S. Tonomura, S. Yamamatsu, Polym. Adv. Tech. 2 (1990) 127.
47. Z. Hou, T. Okuhara, J. Chem. Soc., Chem. Commun. (2001) 1686.
48. Z. Hou, T. Okuhara, J. Mol. Catal. A 206 (2003) 121.
49. M. Misono, Y. Konishi, M. Furuta, Y. Yoneda, Chem. Lett. (1978) 709.
50. M. Misono, N. Mizuno, K. Katamura, A. Kasai, Y. Konishi, K. Sakata, T. Okuhara, Y. Yoneda, Bull. Chem. Soc. Jpn. 55 (1982) 400.
51. T. Okuhara, S. Tatematsu, K.Y. Lee, M. Misono, Bull. Chem. Soc. Jpn. 62 (1989) 717.
52. M. Misono, K. Sakata, Y. Yoneda, W.Y. Lee, in “Proc. 7th Int. Congr. Catal.

Tokyo, 1980," Kodansha, Tokyo, Elsevier, Amsterdam, 1981; p. 1047.
53. K. Sakata, M. Furuta, M. Misono, Y. Yoneda, ACS/CSJ Chemical Congr. Honolulu, April, 1979.
54. M. Misono, 1st Japan-France Catal. Seminar, July (1979).
55. T. Komaya, M. Misono, Chem. Lett. (1983) 1177.
56. M. Misono, N. Mizuno, T. Komaya, In Proc. 8th Int. Congr. Catal. 1984; Verlag Chemie: Weinheim, 1984; Vol. 5, p. 487.
57. M. Furuta, K. Sakata, M. Misono, Y. Yoneda, Chem. Lett. (1979) 31.
58. N. Mizuno, M. Misono, J. Phys. Chem. 93 (1989) 3334.
59. N. Mizuno, T. Watanabe, M. Misono, J. Phys. Chem. 89 (1985) 80.
60. Y. Izumi, K. Urabe, M. Onaka, Zeolite, Clay and Heteropoly Acid in Organic Reactions; Kodansha/VCH: Tokyo, 1992, p. 99.
61. W.-C. Cheng, N. P. Luthra, J. Catal. 109 (1988) 163.
62. K. Nowinska, R. Fiedorow, J. J. Adamiec, Chem. Soc., Faraday Trans. 87 (1991) 749.
63. K.M. Rao, R. Gobetto, A. Lannibello, A. Zecchina, J. Catal. 119 (1989) 512.
64. J.A.R. van Veer, P.A. J. M. Hendriks, R.R. Andrea, E.J.M. Romers, A. E. Wilson, J. Phys. Chem. 94 (1990) 1831.
65. V.M. Mastikhin, S.M. Kulikov, A.V. Nosov, I.V. Kozhevnikov, I.L. Mudrakovsky, M.N. Timofeeva, J. Mol. Catal. 60 (1990) 65.
66. F. Lefebvre, J. Chem. Soc., Chem. Commun. (1992) 756.
67. R. Thouvenot, C. Rocchiccioli-Delcheff, M. Fournier, J. Chem. Soc., Chem. Commun. (1991) 1252.
68. R. Thouvenot, M. Fournier. C. Rocchiccioli-Delcheff, J. Chem. Soc., Faraday Trans. 87 (1991) 2829.
69. C. Rocchicioli-Deltcheff, M. Amirouche, M. Fournier, J. Catal. 138 (1992) 445.
70. T. Baba, Y. Ono, Appl. Catal. 22 (1986) 321.
71. G.I. Kapustin, T.R. Brueva, A.L. Klyachko, M.N. Timofeeva, S.M. Kulikov, I.V. Kozhevnikov, Kinet. Katal. 31 (1990) 1017.
72. T. Okuhara, Chem. Rev. 102 (2002) 3641.
73. K.I. Matveev, Kinet. Katal. 18 (1977) 862.
74. K.I. Matveev, E.G. Zhizhina, N.B. Shitova, L.I. Kuznetsova,

Kinet. Katal. 18 (1977) 380.
75. C. Venturello, R. D'Aloisio, J.C.J. Bart, M. Ricci, J. Mol. Catal. 32, (1985) 107.
76. C. Venturello, E. Alneri, M. Ricci, J. Org. Chem. 48 (1983) 3831.
77. C. Venturello, M. Gambaro, Synthesis (1989) 295.
78. Y. Matoba, H. Inoue, J. Akagi, T. Okabayashi, Y. Ishii, M. Ogawa, Synth. Commun. 14 (1984) 865.
79. Y. Sakata, Y.J. Ishii, Org. Chem. 56 (1991) 6233.
80. Y. Ishii, Y. Sakata, J. Org. Chem. 55 (1990) 5545.
81. S. Sakaue, T. Tsubakino, Y. Nishiyama, Y. Ishii, J. Org. Chem. 58 (1993) 3633.
82. Y. Ishii, Y. Yamawaki, T. Ura, H. Yamada, T. Yoshida, M. Ogawa, J. Org. Chem. 53 (1988) 3587.
83. T. Oguchi, Y. Sakata, N. Takeuchi, K. Kaneda, Y. Ishii, M. Ogawa, Chem. Lett. (1989) 2053.
84. S. Sakaue, Y. Sakata, Y. Nishiyama, Y. Ishii, Chem. Lett. (1992) 289.
85. Y. Ishii, Y. Sakato, J. Org. Chem. 55, (1990) 5545.
86. S. Sakaguchi, S. Watase, Y. Katayama, Y. Sakata, Y. Nishiyama, Y. Ishii, J. Org. Chem. 59 (1994) 5681.
87. Y. Ishii, H. Tanaka, Y. Nishiyama, Chem. Lett. (1994) 1.
88. D. C. Duncan, R. C.Chambers, E. Hecht, C. L. Hill, J. Am. Chem. Soc. 117 (1995) 681.
89. T. Yamaguchi, Catal. Today 20 (1994) 199.
90. K. Tanabe, T. Yamaguchi, Catal. Today 20 (1994) 185.
91. V.C.F. Holm, G.C. Bailey, US patent 3,032,599, 1962.
92. M. Hino, K. Arata, J. Chem. Soc., Chem. Commun. (1979) 1148.
93. M. Hino, K. Arata, J. Chem. Soc., Chem. Commun. (1980) 851.
94. A. Corma, Chem. Rev. 95 (1995) 559.
95. F.R. Chen, G.Coudurier, J.F. Joly, J.C. Vedrine, J. Catal. 143 (1993) 616.
96. W. Stichert, F. Schüth, S. Kuba, H. Knözinger, J. Catal. 198 (2001) 277.
97. A. Clearfield, G.P.D. Serrette, A. H. Khazi-Syed, Catal. Today 20 (1994) 295.
98. T. Reimer, D. Spielbauer, M. Hunger, A.H. Mekhemer, H. Knozinger, J. Chem. Soc., Chem. Commun. (1994) 1181.
99. C. Morterra, G. Cerrato, S. Ardizzone, C.L. Bianchi, M. Signoretto, F. Pinna,

Phys. Chem. Chem. Phys. 4 (2002) 3136.
100. S.X. Song, R.A. Kydd, J. Chem. Soc., Faraday Trans. 94 (1998) 1333.
101. J.A. Navío, G. Colón, M. Macías, J.M. Camplelo, A.A. Romero, J. M. Marinas, J. Catal. 161 (1996) 605.
102. M. Benaïssa, J.G. Santiesteban, G. Díaz, C. D. Chang, M. José-Yacamán, J. Catal. 161 (1996) 694.
103. F. Babou, B. Bigot, P. Sautet, J. Phys. Chem. 97, (1993) 11501.
104. F. Haase, J. Sauer, J. Am. Chem. Soc. 120 (1998) 13503.
105. B.H. Davis, R.A. Keogh, R. Srinivasan, Catal. Today 20 (1994) 219.
106. X.M. Song, A. Sayari, Catal. ReV. Sci. Eng. 38 (1996) 320.
107. G.D. Yadav, N. Kirthivasan, Chem. Commun. (1995) 203.
108. G.D. Yadav, J.J. Nair, Microp. Mesop. Mater. 33 (1999) 1.
109. C.Y. Hsu, C.R. Heimbuch, C.T. Armes, B.C. Gates, J. Chem. Soc., Chem. Commun. (1992) 1645.
110. T.-K. Cheung, J. L. d'Itri, B. C. Gates, J. Catal. 151 (1995) 464.
111. T.-K. Cheung, B. C. Gates, Top. Catal. 6 (1998) 41.
112. B.-Q. Xu, W.M.H. Sachtler, J. Catal. 167 (1997) 224.
113. J. Sommer, R. Jost, M. Hachoumy, Catal. Today 38 (1997) 309.
114. R. Sreenivasan, R.A. Keogh, D.R. Milburn, B.H. Davis, J. Catal 153 (1995) 123.
115. G. Larsen, E. Lotero, R.D. Parra, L.M. Petkovic, H.S. Silva, S. Radhavan, Appl. Catal. A 130 (1995) 213.
116. M. Hino, K. Arata, J. Chem. Soc. Chem. Commun. 1259 (1988).
117. M. Scheithauer, T.K. Cheung, R.E. Jentoft, R.K. Grasselli, B.C. Gates, H. Knözinger, J. Catal. 180 (1998) 1.
118. M. Scheithauer, R.K. Grasselli, H. Knözinger, Langmuir 14 (1998) 3019.
119. D.G. Barton, S.L. Soled, G.D. Meitzner, G.A. Fuentes, E. Iglesia, J. Catal. 181 (1999) 57.
120. D.G. Barton, S.L. Soled, E. Iglesia, Topics Catal. 6 (1998) 87.
121. S. Kuba, P. Lukinskas, R.K. Grasselli, B.C. Gates, H. Knözinger, J. Catal. 216 (2003) 353 and references there in.

Chapter 2

Preparation and characterization of zirconia-supported heteropoly acid catalysts

2.1. Introduction

The successful heterogeneous catalysts should possess high catalytic activity for the desired reaction, high selectivity for the desired product and acceptable commercial life. The characterization of catalytic material is a very important step in the process of catalyst development, which gives insight into the relation between physical and chemical properties of the catalyst and its activity. If the structure and composition of the catalyst can be correlated with its activity and selectivity, the working of the catalyst can be understood.

In this work, the catalysts were prepared by impregnation method and characterized by various techniques such as surface area, X-ray diffraction, Raman spectroscopy, TG-DTA, XPS, FTIR pyridine adsorption, TPD of ammonia, DRUV-vis spectroscopy, NMR etc. The theory and experimental procedure of various characterization techniques used are briefly described in the following sections.

2.2. Catalyst preparation

The catalysts were prepared by suspending a known amount of dried zirconium oxyhydroxide powder in a methanol solution of heteropoly acids (HPAs). HPAs (Aldrich) under study include silicotungstic acid, phosphotungstic acid and phosphomolybdic acid. Zirconium oxyhydroxide was prepared by the hydrolysis of 0.5 M zirconyl chloride solution by the drop wise addition of aqueous ammonia (10 M) to a final pH of 10. The precipitate was filtered and washed with ammoniacal water (pH = 8) until free from chloride ions by the silver nitrate test. Zirconium oxyhydroxide thus obtained was dried at 120 ^{o}C for 12 h, powdered well and dried again for another 12 h. Each time, 4 ml of methanol per gram of solid support was used and the mixture was stirred in a rotary evaporator for 8-10 h. After stirring, the excess methanol was removed at ca. 50 ^{o}C under vacuum. The resulting solid materials were dried at 120 ^{o}C for 24 h and ground well. A series of catalysts with different HPA loading were prepared by changing the HPA concentration in methanol. The dried samples were then calcined in air. All samples were calcined in shallow quartz boats placed inside a 3 cm diameter quartz tube placed in a tubular furnace. The samples were heated at the rate of 5 ^{o}C min^{-1} to the specified temperature and held for 4 h under static conditions, and then cooled at the rate of 5 ^{o}C min^{-1} to room temperature.

2.3. Catalyst characterization – Theory and experimental procedure

2.3.1. Surface area measurement by BET method

The common method of measuring surface area of catalyst materials is based on the theory developed by Brunauer, Emmett and Teller in 1938 considering the concept of multilayer adsorption. The isotherm points are transformed into the linear version of BET equation [1]:

$$P/V(P_0-P) = 1/V_mC + [(C-1)/V_mC]\ (P/P_0) \quad (2.1)$$

Where, P is the adsorption equilibrium pressure, P_0 is the saturation vapor pressure of the adsorbate at the experimental temperature, V is the volume of gas adsorbed at pressure P, V_m is the volume of adsorbate required for monolayer coverage and C, a constant that is related to the heat of adsorption and liquefaction. A plot of $P/V(P_0-P)$ Vs (P/P_0) will yield a straight line usually in the range $0.05 \leq P/P_0 \leq 0.35$. The monolayer volume, V_m is given by 1/(S+I), where S is the slope, which is equal to $(C-1)/V_mC$ and I is the intercept, which is equal to $1/V_mC$. The surface area of the catalyst (S_{BET}) is related to V_m, by the equation,

$$S_{BET} = V_m/22414)\ N_a\ \sigma \quad (2.2)$$

where, N_a is the Avogadro number and σ is mean cross sectional area covered by one adsorbate molecule. The σ value generally used for N_2 is 0.162 nm^2.

The specific surface area of the catalysts were measured by N_2 physisorption at liquid nitrogen temperature using a Quantachrome Nova-1200 surface area analyzer and standard multi point BET analysis method. Zirconia-supported silicotungstic acid samples were dried in flowing N_2, while zirconia-supported phosphotungstic acid samples were dried under dynamic vacuum for 2 h at 300 ^oC before N_2 physisorption measurements.

2.3.2. X-ray diffraction

X-ray diffraction (XRD) is used to identify bulk phases, if desired under *in situ* conditions and to estimate particle sizes. In catalyst characterization, diffraction patterns

are mainly used to identify the crystallographic phases that are present in the catalyst [2]. This method involves the interaction between the incident monochromatized X-rays (like Cu Kα or Mo Kα source) with the atoms of a periodic lattice. X-rays scattered by atoms in an ordered lattice interfere constructively in directions given by Bragg's law:

$$n\lambda = 2\ d\ \sin\theta;\ n = 1, 2, 3,\ldots. \quad (2.3)$$

Where, λ is the wavelength of the X-rays, d is the distance between two lattice planes, θ is the angle between the incoming X-rays and the normal to the reflecting lattice plane and n is the integer called order of the reflection.

The Bragg peaks are measured by observing the intensity of the scattered radiation as a function of scattering angle 2θ. The angles of maximum intensity enable one to calculate the spacing between the lattice planes and allow phase identification. The width of diffraction peaks provides information on the dimensions of the reflecting planes. Diffraction lines from the perfect crystals are very narrow. For crystals with size below 100 nm, line broadening occurs due to incomplete destructive interference in scattering directions, where the X-rays are out of phase. The width of the diffraction lines can be used to estimate the crystal size by the relation, Debye-Scherrer formula [1],

$$D_{hkl} = 0.9\lambda/\beta\cos\theta \quad (2.4)$$

where, D_{hkl}, λ, β and θ are the volume averaged particle diameter, X-ray wavelength, full width at half maximum (FWHM), and diffraction angle respectively.

A major limitation of XRD is that this technique requires samples possessing sufficient long-range order. Amorphous phases and small particles give either broad and weak diffraction lines or no diffraction at all which makes them virtually invisible for XRD.

X-ray diffraction (XRD) measurements of the catalyst powder were recorded using a Rigaku Geigerflex diffractometer equipped with Ni filtered CuKα radiation (λ = 1.5418 Å). The volume percentage of the tetragonal phase (V_t) of the calcined samples was estimated using the formula proposed by Toraya et al. [3],

$$X_m = I_m\ (11\text{-}1) + I_m\ (111)/[I_m\ (11\text{-}1) + I_m\ (111) + I_t\ (111)] \quad (2.5)$$

$$V_m = 1.311\ X_m / [1 + 0.31\ X_m] \text{ and } V_t = 1\text{-}V_m \quad (2.6)$$

where, I_m (hkl) is the integral intensity of the (hkl) reflections of the monoclinic phase and I_t (111) the intensity of the (111) reflection of the tetragonal phase.

2.3.3. Raman spectroscopy

Raman spectroscopy is based on the inelastic scattering of photons, which loose energy by exciting vibrations in the sample. A vibration is Raman active if it changes the polarizability of the molecule. Raman and infrared spectroscopies complement each other, in particular for highly symmetrical molecules.

Raman spectroscopy can be used for investigations of oxides, supported and bulk metals, and has found increasing applications for the characterization of supported transition metal oxide catalysts since the work of Villa et al. in 1974 [4]. It is particularly powerful for investigations of the structure of supported oxide catalysts. All characteristic vibrational features of oxides of the transition metals like Mo, W, Cr, V and Re fall into the frequency range below 1100 cm^{-1}. These oxides have high Raman scattering cross-sections because of their relatively high covalent bond character. The usual support materials (particularly alumina and silica) have very low Raman scattering cross-sections and only show weak absorption bands in the 700-1100 cm^{-1} region. Hence, it has the advantage that the normal modes of the minority components, namely the transition metal oxides dispersed on the supports, can most frequently be detected by it with relative ease in the frequency region 500-1000 cm^{-1}. It should be also mentioned that titania and zirconia oxides possess strong Raman absorption bands in the region below 700 cm^{-1}. There are some major problems that may be encountered in it like the heating effects of the laser beam, low sensitivity of the technique and background fluorescence.

Raman spectra of the catalysts were recorded on powder samples at room temperature with a Bruker IFS 66 spectrometer connected to Raman module FRA 106. The 1.06 μm line of NdYAG laser was used for excitation and spectral resolution was 3 cm^{-1}.

2.3.4. Thermal analysis

Thermo analytical techniques involve the measurement of the response of the solid under study (energy or mass released or consumed) as a function of temperature (or time) dynamically by the application of a linear temperature program. Thermogravimetry (TG) is a technique, which measures the variation in mass of a sample when it undergoes temperature scanning in a controlled atmosphere. Differential thermal analysis (DTA) is a technique, which measures the difference in temperature between a sample and a reference (a thermally inert material) as a function of time or temperature, when they undergo temperature scanning in a controlled atmosphere. DTA method enables any

transformation to be detected for all the categories of materials, providing information on exothermic and endothermic reactions taking place in the sample, which include phase transitions, dehydration, decomposition, redox, or solid-state reactions. In catalysis, these techniques are used to study the genesis of catalytic materials via solid-state reactions.

Differential thermal analysis (DTA) measurements of zirconia-supported silicotungstic acid samples were performed on a Pyris Diamond TG-DTA apparatus from room temperature to 1000 ^{o}C in flowing dry oxygen (ca. 50 ml min^{-1}), using α-Al_2O_3 as reference. In each experiment, 5-8 mg of the sample was used with a heating rate of 20 ^{o}C min^{-1}.

Thermogravimetric and differential thermal analysis (TG-DTA) measurements of zirconia-supported phosphotungstic acid samples were performed on a Setaram TG-DTA 92 apparatus from room temperature to 1000 ^{o}C in flowing dry air (ca. 50 ml min^{-1}), using α-Al_2O_3 as reference. In each experiment, 25-30 mg of the sample was used with a heating rate of 10 ^{o}C min^{-1}. TGA curves are depicted as first derivative DTG of the direct weight loss traces.

2.3.5. X-ray photoelectron spectroscopy

X-ray photoelectron spectroscopy (XPS) is one of the most frequently used techniques in catalysis. It gives information on the elemental composition, the oxidation state of the elements and in some cases on the dispersion of one phase over another. XPS is based on the photoelectric effect [5-7] . In this technique, sample surface is irradiated with X rays and the emitted photoelectrons are measured. When an atom absorbs a photon of energy hν, a core or valence electron with binding energy E_b is ejected with kinetic energy E_k:

$$E_k = h\nu - E_b - \varphi \qquad (2.7)$$

where, h is Planck's constant, ν is the frequency of the exciting radiation, E_b is the binding energy of the photoelectron relative to the Fermi level of the sample and φ is the work function of the spectrometer.

XPS (also referred by the acronym ESCA, electron spectroscopy for chemical analysis) entails emission from both core and valence electrons of the solid, the stimulating X-ray sources being usually Al Kα (1486.6 eV) or Mg Kα (1253.6 eV). XPS spectrum is a plot of the intensity of photoelectrons Vs binding energy. Since, the electrons whose energies are analyzed in XPS arise from a depth of no greater than about 5 nm, the technique is highly surface specific. A set of binding energies is characteristic

for an element and hence XPS can be used to analyze the composition of samples, considering the area of the peak and cross section for photoemission. Binding energies are not only element specific but contain chemical information like oxidation state, because the energy levels of core electrons depend slightly on the chemical state of the atom.

An experimental problem in XPS is that electrically insulating samples may charge during measurement, as photoelectrons leave the sample. Due to the positive charge on the sample, all XPS peaks in the spectrum shift by the same amount to higher binding energies. Calibration for this effect can be done by using C 1s binding energy (284.9 eV) from carbon contamination, which is present in most of the catalysts.

X-ray photoelectron spectroscopy (XPS) measurements were performed on a VG Microtech Multilab ESCA 3000 specrometer with a non-monochromatized Mg-Kα X-ray source. Base pressure in the analysis chamber was maintained at 3-6 x 10^{-10} Torr range. Energy resolution of the spectrometer was set at 0.8 eV with Mg-Kα radiation at a pass energy of 50 eV.

2.3.6. Temperature programmed techniques: TPD of ammonia

Temperature programmed reduction (TPR), oxidation (TPO), desorption (TPD) and reaction spectroscopy (TPRS) typically involves monitoring surface or bulk processes between the solid catalyst and its gaseous environment via continuous analysis of the gas phase composition as the temperature is raised linearly with time. Instrumentation for temperature-programmed investigations consists of a reactor charged with catalyst in a furnace that can be temperature programmed and a thermal conductivity detector (TCD) to measure the concerned active gas of the gas mixture before and after interaction.

The acidity of the catalysts were measured by temperature programmed desorption of NH_3 (NH_3-TPD) using a micromeritics AutoChem-2910 instrument. It was carried out after ~ 0.5 g of the catalyst sample was dehydrated at 600 ^oC in helium flow (30 cm^3 min^{-1}) for 1 h. The temperature was decreased to 100 ^oC and NH_3 was adsorbed by exposing the samples treated in this manner to a stream containing 10 % NH_3 in helium for 1 h at 100 ^oC. It was then flushed with helium for another 1 h to remove physisorbed NH_3. The desorption of NH_3 was carried out in helium flow (30 cm^3 min^{-1}) by increasing the temperature to 600 ^oC at 10 ^oC min^{-1} measuring NH_3 desorption using TCD detector.

For zirconia-supported phosphotungstic acid catalysts, NH_3-TPD measurements were carried out after 0.1 g of the catalyst sample was dehydrated at 500 ^oC in dry air for

1 h and purged with helium for 0.5 h. The temperature was decreased to 125 ^{o}C under the flow of helium and then 0.5 ml NH_3 pulses were supplied to the samples until no further uptake of ammonia was observed. NH_3 was desorbed in helium flow by increasing the temperature to 540 ^{o}C at 10 ^{o}C min^{-1} measuring NH_3 desorption using a TCD detector.

2.3.7. Infrared adsorption studies - Pyridine adsorption

The most common application of IR in catalysis is to identify adsorbed species and to study the way in which these species are chemisorbed on the surface of the catalyst [8-10]. More specifically, IR spectroscopy has been used to study the adsorption of typical probe molecules like ammonia, pyridine and other bases, hydrocarbons, carbon dioxide which can monitor either the acidic or basic sites on oxide catalysts [11]. Investigation of adsorbed species in relation to their behavior in catalytic reactions is the main field of application of IR spectroscopy.

The pyridine adsorption studies were carried out in the DRIFT (diffuse reflectance infrared Fourier transform) mode using a Shimadzu SSU 8000 instrument. A calcined powder sample in a sample holder was placed in a specially designed cell. The samples were then heated *in-situ* from room temperature to 400 ^{o}C at a heating rate of 5 ^{o}C min^{-1} in a flowing stream (40 ml min^{-1}) of pure N_2. The samples were kept at 400 ^{o}C for 3 h and cooled to 100 ^{o}C and then pyridine vapor (20 µl) was introduced under N_2 flow and the IR spectra were recorded at different temperatures up to 400 ^{o}C. A resolution of 4 cm^{-1} was attained after averaging over 500 scans for all the IR spectra reported in this study.

For zirconia-supported phosphotungstic acid (PTA) catalysts with different PTA loading, pyridine adsorption studies were performed using NICOLET MODEL 60 SXB instrument by heating *in-situ* a self-supporting wafer (20 mg) of the sample from room temperature to 400 ^{o}C with a heating rate of 5 ^{o}C min^{-1} under vacuum (10^{-6} mbar). The samples were kept at 400 ^{o}C for 3 h followed by cooling to 100 ^{o}C. Pyridine vapor (10 mm Hg) was introduced into the cell and allowed to equilibrate for 45 minutes followed by evacuation at 100 ^{o}C for 30 minutes and the IR spectrum was recorded. Then the temperature was slowly increased and IR spectra were recorded at different temperatures up to 400 ^{o}C.

2.3.8. Diffuse reflectance UV-visible spectroscopy

Diffuse reflectance spectroscopy (DRS) is a spectroscopic technique based on the reflection of light in the ultraviolet (UV), visible (VIS) and near-infrared (NIR) region by a powdered sample. In a DRS spectrum, the ratio of the light scattered from an "infinitely thick" closely packed catalyst layer and the scattered light from an infinitely thick layer of an ideal non-absorbing (white) reference sample is measured as a function of the wavelength λ. The scattered radiation, emanating from the sample, is collected in an integration sphere and detected. The most popular continuum theory describing diffuse reflectance effect is Schuster-Kubelka-Munk (SKM) theory. If the sample is infinitely thick, the diffuse reflection of the sample (R_∞) is related to an apparent absorption (K) and apparent scattering coefficient (S) by the SKM equation [12, 13]:

$$F(R_\infty) = (1-R_\infty)^2 / 2R_\infty = K/S \qquad (2.8)$$

At low concentrations of supported transition metal ions (TMI), this equation is a good representation of the absorbing spectrum and allows a quantitative determination of the TMI.

$$F(R_\infty) = (1-R_\infty)^2 / 2R_\infty = K/S = \alpha C_{TMI} / S = k\, C_{TMI} \qquad (2.9)$$

At a given wavelength λ, S is constant, the above equation gives a linear relation between $F(R_\infty)$ and the TMI concentration, C_{TMI}. The coefficients α and k are proportionality constants.

DRS is a suitable technique for studying the speciation of supported TMIs because it measures both their d-d transitions and charge transfer bands. The obtained information is directly chemical since the outer shell electrons are probed. The DRS technique can be used under *in-situ* conditions and can be applied at different levels of sophistication, from detecting the presence of a certain oxidation state of a supported TMI to a detailed distribution of different oxidation states and coordination environments under catalytic conditions.

The disadvantage is that the DRS signals are usually broad and overlap with each other, leading to a biased spectral analysis. In addition, the origin of the specific electronic transition is sometimes difficult to isolate due to its dependence on the local coordination environment, the polymerization degree and the specific oxidation state.

Diffuse reflectance UV-vis (DRUV–vis) spectra of catalyst samples were obtained using a Shimadzu UV-2101 PC spectrometer equipped with a diffuse-reflectance attachment, with $BaSO_4$ as the reference. The reflectance spectra were converted into the Kubelka-Munk function, *F(R)*, which is proportional to the absorption coefficient for low values of *F(R)*. The spectra were measured in the range of 200-800 nm in air at room temperature.

2.3.9. ^{31}P solid-state nuclear magnetic resonance spectroscopy

Nuclear Magnetic Resonance (NMR) spectroscopy gives information on the interaction of a nucleus having a nuclear spin quantum number, I, greater than zero with an external magnetic field. The interaction of nuclear spins with the externally applied magnetic field, B_0, and their environment can be described by the spin Hamiltonian H:

$$H = H_Z + H_{CS} + H_Q + H_D + H_J \quad (2.10)$$

H_Z is a Hamiltonian, which describes the interaction of the nuclear spin with the external field B_0 (Zeeman interaction). The chemical shift Hamiltonian H_{CS} gives the information on the local environment of a nucleus. The chemical shift is measured relative to that of a reference compound and is expressed in Hertz or in ppm with respect to the resonance frequency of the reference compound. H_Q describes the quadrupolar interaction of the nucleus with the surrounding electric field gradient. H_D describes the dipolar interaction with other nuclei, while H_J describes the interaction with other nuclei through J-coupling.

In solid-state NMR, the line shape is determined by dipolar and quadrupolar interactions. The lines are usually broader because the rigid structure of the solid phase prevents the averaging of the dipolar interaction (H_D) by motions. Since, the first order quadrupolar and dipolar interactions are proportional to $(3\cos^2\theta - 1)$, where, θ is the angle between an internuclear vector and the magnetic field, these interactions can be removed, to a first order approximation, by spinning the sample around the so-called magic angle β with respect to the external magnetic field, for which $3\cos^2\beta - 1 = 0$, i.e. $\beta = 54.74^o$. This technique is known as Magic Angle Spinning (MAS) [14, 15].

Phosphorus contains only one isotope, ^{31}P, with a nuclear spin of $I = 1/2$. This and the high magnetic moment (which results in a high sensitivity) makes it an interesting nucleus for NMR spectroscopy. Solid state NMR gives insight into the structure of solids and enables us to probe the local environment of a nucleus. Unlike X-ray diffraction,

NMR spectroscopy is not restricted to materials with long-range order but can also be applied to amorphous substances.

The ^{31}P MAS NMR spectra were recorded using a Bruker DSX-300 spectrometer at 121.5 MHz with high power decoupling with a Bruker 4 mm probe head. The spinning rate was 10 KHz and the delay between two pulses was varied between 1 and 30 s to ensure the complete relaxation of the ^{31}P nuclei occurred. The chemical shifts are given relative to external 85 % H_3PO_4.

2.3. References

1. J. M. Thomas, W. J. Thomas, Principles and Practice of Heterogeneous catalysis, VCH, Weinheim, 1997.
2. J. W. Niemantsverdriet, Spectroscopic methods in Heterogeneous catalysis, VCH, Weinheim, 1993.
3. H. Toraya, M. Yoshimura, S. Somiya, J. Am. Ceram. Soc. 67, (1984) C 119.
4. P. L. Villa, F. Trifiro, I. Pasquon, React. Kinet. Catal. Lett., 1 (1974) 341.
5. T. A. Carlson, X-ray Photoelectron Spectroscopy, Dowden, Hutchinson & Ross: Stroudsburg, PA, 1978.
6. D. Briggs, M. P. Seah (Eds.), Practical Surface Analysis, Vol. 1: Auger and X-ray Photoelectron Spectroscopy (2nd ed.) Wiley, New York, 1990.
7. S. Hüfner, Photoelectron Spectroscopy, Springer-Verlag, Berlin, 1995.
8. M. D. Baker, Catal. Rev. Sci. & Eng., 29 (1987) 269.
9. J. A. Lercher, C. Grundling and G. Eder-Mirth, Catal. Today, 27 (1996) 353.
10. J. C. Lavalley, Catal. Today, 27 (1996) 377.
11. M. C. Kung and H. H. Kung, Catal. Rev. Sci. & Eng., 27 (1985) 425.
12. B. M. Weckhuysen, R. A. Schoonheydt, Catal. Today, 49 (1999) 441.
13. R. A. Schoonheydt, Diffuse Reflectance Spectroscopy, Chapter 4, in: Characterization of Heterogeneous Catalysts, F. Delannay (Ed.), Marcel Dekker, New York, 1984.
14. R. A. Wind, in A. I. Popov, K. Hallenga (Eds.), Modern NMR Techniques and Their Application in Chemistry, p. 156, Marcel Dekker, Inc., New York, 1991.
15. R. H. H. Smits, Ph. D. Thesis, Netherlands, 1994.

Chapter 3

Zirconia-supported silicotungstic acid

3.1. Introduction

This section deals with the characterization of zirconia-supported silicotungstic acid (STA) catalysts by techniques such as X-ray diffraction (XRD), Raman spectroscopy, differential thermal analysis (DTA), X-ray photoelectron spectroscopy (XPS), temperature programmed desorption of ammonia (NH_3-TPD), FTIR (Fourier transform infrared) pyridine adsorption, and diffuse reflectance ultraviolet-visible (DRUV-vis) spectroscopy. These catalysts were used in the liquid-phase benzoylation of veratrole (1,2-dimethoxy benzene) with benzoic anhydride and *tert*-butylation of phenol with *tert*-butanol.

3.2. Preparation

Zirconia-supported silicotungstic acid catalysts were prepared by the procedure given in section 2.2. These catalysts were represented by x SZ-T, where x represents wt. %, S represents STA, Z represents zirconia and T denotes calcination temperature (^oC).

For comparison, catalyst with 15 % STA on silica gel was prepared and calcined at 300 ^oC [1]. The silica gel support was prepared by the hydrolysis of tetraethyl orthosilicate, TEOS (Aldrich) in presence of HNO_3 followed by drying at 120 ^oC for 12 h, powdering and further drying for another 12 h. This catalyst was represented by 15 SS-300.

3.3. Characterization - Results and discussion

3.3.1. Surface area

Pure zirconium oxyhydroxide dried at 120 ^oC had a surface area 332 m^2g^{-1} and after calcination at 750 ^oC, the surface area was decreased to 16 $m^2\ g^{-1}$. Addition of STA to the support resulted in an increase of the surface area, which reached maximum at 15 % STA loading (Table 3.1). This could be explained as the strong interaction of STA with the support reduces the surface diffusion of zirconia and inhibits sintering and stabilizes the tetragonal phase of zirconia, which leads to an increase in surface area. Above 15 % STA

loading, surface area does not change appreciably, which could be due to the formation of crystalline WO_3 and this probably narrows or plug the pores of the samples.

The nominal WO_3 loading corresponding to different STA loading and surface area of the catalysts with different STA loading and calcination temperature were determined to calculate the nominal tungsten (W) surface density. The tungsten surface densities, expressed as the number of W atoms per nanometer square area (W atoms nm^{-2}), were obtained by the equation,

W surface density = {[WO_3 loading (wt. %)/100] x 6.023 x 10^{23}}/[231.8 (formula weight of WO_3) x BET surface area (m^2 g^{-1}) x 10^{18}] and are presented in Table 3.1. The values show that an increase of STA loading results in an increase of W surface density. The specific surface area of SZ catalyst also depends on the calcination temperature. The W surface density increased with the calcination temperature because of the concominant decrease in the ZrO_2 surface area (Table 3.1).

3.3.2. X-ray diffraction

The bulk structure of pure ZrO_2 and of supported-STA catalysts were determined by powder X-ray diffraction (Fig. 3.1). The support showed amorphous behavior up to 350 ^oC and crystallizes to a mixture of monoclinic and tetragonal phases and the intensity of monoclinic phase increased with the calcination temperature. The XRD pattern of the catalysts with different STA loading calcined at 750 ^oC showed the presence of STA strongly influences the crystallization of zirconium oxyhydroxide into zirconia. Pure zirconia calcined at 750 ^oC was mainly monoclinic with only small amount of tetragonal phase. For catalysts with low STA loading calcined at 750 ^oC, the XRD pattern could be described as the sum of the monoclinic and tetragonal phases of zirconia, this latter phase became dominant for catalyst with 15 % STA.

Table 3.1: Surface area, surface density and acidity of various catalysts.

Catalyst	Surface area ($m^2 g^{-1}$)	Surface density (W nm^{-2})	[a]Acidity (NH_3 nm^{-2})
Z-750	16	0	[b]n. e
5 SZ-750	43	3.1	2.63
10 SZ-750	50	5.4	2.77
15 SZ-750	55	7.4	2.81
20 SZ- 750	54	10	2.71
25 SZ-750	52	13.1	2.65
15 SZ-600	125	3.2	n. e.
15 SZ-650	108	3.7	1.93
15 SZ-700	80	5.0	2.43
15 SZ-800	46	8.7	2.61
15 SZ-850	36	11.4	n. e.

[a] Acidity values obtained from NH_3-TPD.

[b] not evaluated.

As shown in Fig. 3.1, 15 % catalyst was amorphous up to 450 ^oC and as the calcination temperature increased, zirconia crystallizes progressively to tetragonal phase and at 750 ^oC, the catalyst exists mainly in tetragonal phase. Above 750 ^oC, formation of monoclinic phase of zirconia was observed. The effectiveness of the surface species to stabilize ZrO_2 in tetragonal phase might lose at high temperatures because they diffuse into the bulk, decompose and desorbs, or "dewet" and agglomerate to form poorly interacting clusters as a separate phase [2]. Thus, the added STA stabilized the tetragonal phase of zirconia and such stabilization of tetragonal ZrO_2 in presence of HPAs has been reported in the literature [3, 4]. It could also be seen that up to a 15 % STA loading, for catalysts calcined at 750 ^oC and for 15 % catalyst, up to 750 ^oC calcination, no diffraction lines attributed to the polyacid or its decomposed products were observed, which indicated that STA is highly dispersed on the support. When the STA loading was higher

than 15 %, or when the calcination temperature exceeded 750 ^{o}C for 15 % loading, new diffraction lines appeared in the region 23-25°, characteristic of WO_3 [5].

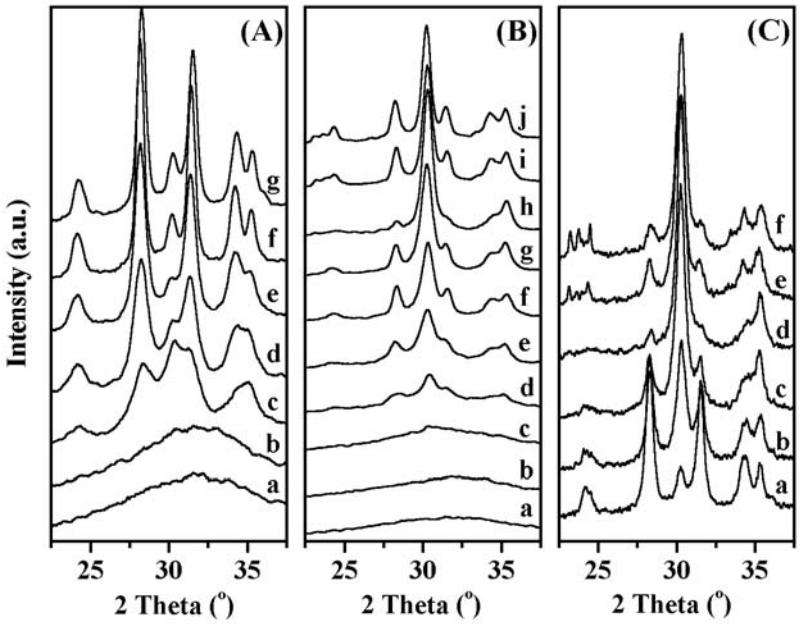

Fig. 3.1: X-ray diffractograms of (A) ZrO_2 calcined at a) 120, b) 250, c) 350, d) 450, e) 550, f) 650, g) 750 ^{o}C; (B) 15 SZ calcined at different temperatures a) 120, b) 250, c) 350, d) 450, e) 550, f) 650, g) 700, h) 750, i) 800, j) 850 ^{o}C; (C) catalysts with different STA loading calcined at 750 ^{o}C a) 0, b) 5, c) 10, d) 15, e) 20, f) 25 %.

3.3.3. Raman spectroscopy

Raman spectra of pure STA and 15 SZ catalyst calcined at different temperatures are shown in Fig. 3.2. The strong Raman bands of the support below 700 cm^{-1} interfere with the diagnostic Raman bands of tungstate species, while the range above 700 cm^{-1} is free from characteristic bands of ZrO_2 and hence, relevant to the determination of tungsten species structure. Pure STA shows a sharp band at 998 cm^{-1} with a distinct shoulder at 974 cm^{-1}. The bands at 998 and 974 cm^{-1} were attributed to $\nu_{(W=O)}$ symmetric and asymmetric stretching modes. In addition, another broad band observed at 893 cm^{-1} was assigned to the $\nu_{(W-O-W)}$ asymmetric stretching mode [6, 7]. Pure phosphotungstic acid (PTA) showed similar type of Raman spectrum as that of pure STA. The 15 SZ-120 catalyst showed a broad band with two components at 973 cm^{-1} and at 946 cm^{-1}. These bands appeared to be red-shifted in comparison with pure STA and it could be due to the partial weakening of W=O bonds, possibly due to the interaction of STA with the support

[8]. The position of $\nu_{(W=O)}$ band was shifted from 973 to 992 cm^{-1} with an increase in calcination temperature from 120 to 750 ^oC, indicating an increase in W=O bond order. The increase in $\nu_{(W=O)}$ wave number with calcination temperature could be due to an increase in the agglomeration of silicotungstate species [9]. This was also evidenced from the increase in tungsten surface density with calcination temperature (Table 3.1). At a calcination temperature of 650 ^oC and above, Raman spectra showed a new band centered near 825 cm^{-1} and Scheithauer et al. assigned this band to $\nu_{(W-O-W)}$ stretching mode [10]. Recently, Loridant et al. proved that this band originates from $\nu_{(W-O-Zr)}$ vibration and not from $\nu_{(W-O-W)}$ vibration [9]. In addition to the bands at 825 cm^{-1} and 992 cm^{-1}, the catalyst 15 SZ-750 showed an additional band at 910 cm^{-1} due to $\nu_{(W-O-W)}$ stretching mode [11]. However, the relative intensity of this band is very small in comparison with other bands indicating the formation of small amount of polyoxotungstate species [11, 12]. Raman spectra of 15 SZ catalyst did not show bands at 720 and 807 cm^{-1} that are characteristic of WO_3 up to calcination temperature of 750 ^oC. The 15 PZ-750 catalyst (15 % phosphotungstic acid on zirconia calcined at 750 ^oC) showed bands at 988 cm^{-1} and 822 cm^{-1} due to $\nu_{(W=O)}$ and $\nu_{(W-O-Zr)}$ vibrations, respectively.

3.3.4. Differential thermal analysis

The catalysts with different STA loading dried at 120 ^oC were characterized by differential thermal analysis (Fig. 3.3). The DTA of pure STA and zirconium oxyhydroxide (not shown) showed exothermic peaks at 548 ^oC and 452 ^oC and these are due to the decomposition of silicotungstic acid to its constituent oxides [13] and the crystallization of zirconium oxyhydroxide to zirconia. The 5 SZ catalyst showed an exothermic peak at 459 ^oC, while other catalysts showed an additional exothermic peak, which is slightly shifted from 573 ^oC for 10 SZ catalyst to 595 ^oC for 20 SZ catalyst. The 25 SZ catalyst exhibited a broad exothermic effect in the temperature range of 690 to 738 ^oC and this could be due to the crystallization of WO_3.

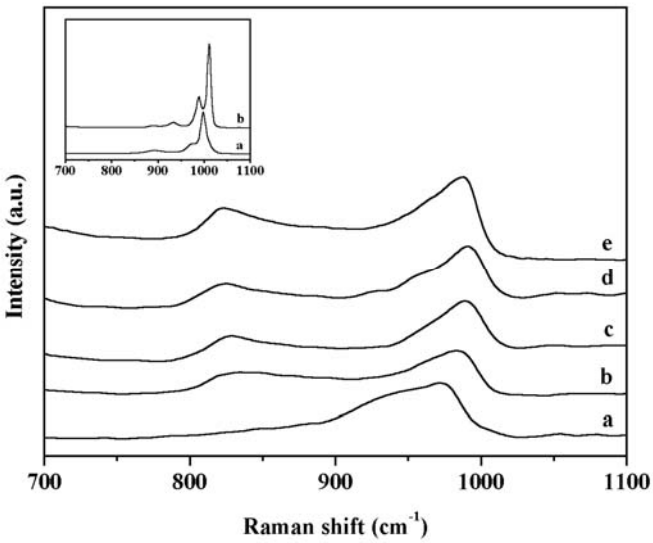

Fig. 3.2: Raman spectra of the catalysts a) 15 SZ-120, b) 15 SZ-650, c) 15 SZ-700, d) 15SZ-750, e) 15 PZ-750. Inset: a) STA, b) PTA.

Valigi et al. showed that zirconium oxyhydroxide is microporous (diameter <2 nm) in nature and it consists of aggregates of primary particles, which stick together to form large grains [14]. When the microporous zirconium oxyhydroxide is in contact with a solution of STA, the polyoxoanions can adsorb on the external surface of the grains, and diffuse into the pores together with the solvent molecules. As the micropores fill with the solvent, the driving force for diffusion is the concentration gradient along the pores. Since the size of the Keggin anion (12 Å) is of the order of pore size of the support, the rate of diffusion is controlled by the anion size and the large polyoxoanions should have a lower diffusion rate. Hence, the large polyanions fail to reach all the internal surface of zirconium oxyhydroxide.

When the samples are heated in an oxidizing atmosphere, the support undergoes dehydration, causing a surface shrinkage, and crystallizes, while the adsorbed species can decompose or can interact with the support to form anchored species. The unsupported zirconia crystallizes through an exothermic effect around 460 ^{o}C, while zirconia interacting with STA appears at higher temperature.

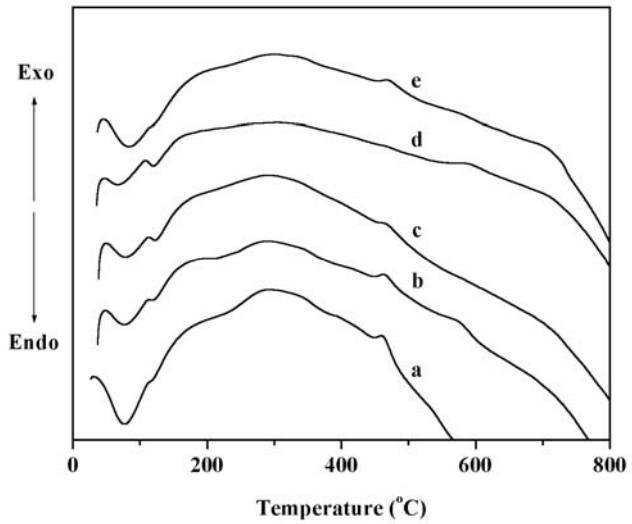

Fig. 3.3: DTA curves of catalysts with different STA loading dried at 120 °C a) 5, b) 10, c) 15, d) 20, e) 25 %.

3.3.5. X-ray photoelectron spectroscopy

The XPS spectra of the catalysts with different STA loading are shown in Fig. 3.4A. The peak at ca. 31 eV corresponds to Zr 4p level, while the peak at ca. 36 eV corresponds to W 4f level, which is characteristic of W(VI). The variation of I(W 4f/I(Zr 3d) intensity ratio with tungsten surface density (W nm^{-2}) was used for the estimation of monolayer coverage of STA on ZrO_2 [15, 16]. The I(W 4f/I(Zr 3d) intensity ratio increased linearly with surface density up to 7.4 W nm^{-2} (15 SZ-750 catalyst) and deviated from linearity with further increase in tungsten surface density (Fig. 3.4B). This suggests that the deposition of the tungstate species was not uniform with increase in tungsten surface density and deviation from linearity was observed at near-monolayer coverage. Further more, the theoretical surface coverage of STA on zirconia was calculated using the average surface area occupied per Keggin ion (144 $Å^2$) [17] and the nominal STA loading on ZrO_2 (calculated from the weight loss obtained in TG analysis) [2], which was found to be ~ 90 %, and was close to the monolayer coverage of STA on zirconia.

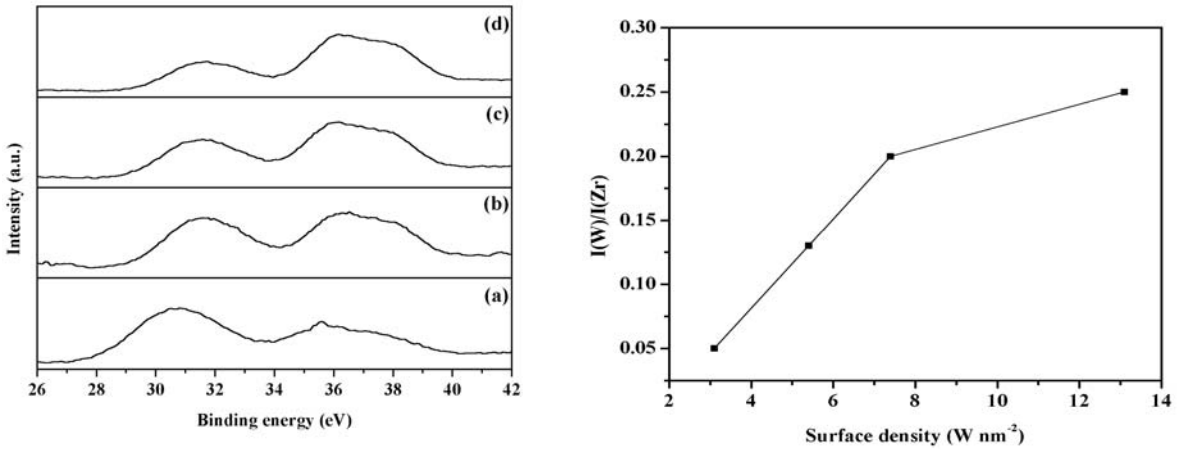

(A) **(B)**

Fig. 3.4: (A) XPS spectra of the catalysts a) 5 SZ-750, b) 10 SZ-750, c) 15 SZ-750, d) 25 SZ 750 and (B) change in XPS intensity ratio *I*(W)/*I*(Zr) with tungsten surface density.

3.3.6. TPD of NH_3

Ammonia adsorption-desorption technique is used for the determination of the strength of acid sites present on the catalyst surface together with total acidity. The NH_3-TPD profiles of the catalysts with different STA loading and of 15 SZ catalyst calcined at different temperatures are shown in Fig. 3.5 and the amount of NH_3 desorbed per nm^2 are presented in Table 3.1. All samples showed a broad TPD profile revealed that the surface acid strength has been widely distributed. It is seen from Table 3.1 that the acidity increased up to 15 % loading and thereafter decreased with further loading. For 15 SZ catalysts calcined at different temperatures, the amount of desorbed ammonia increased with calcination temperature and reached maximum at 750 ^oC.

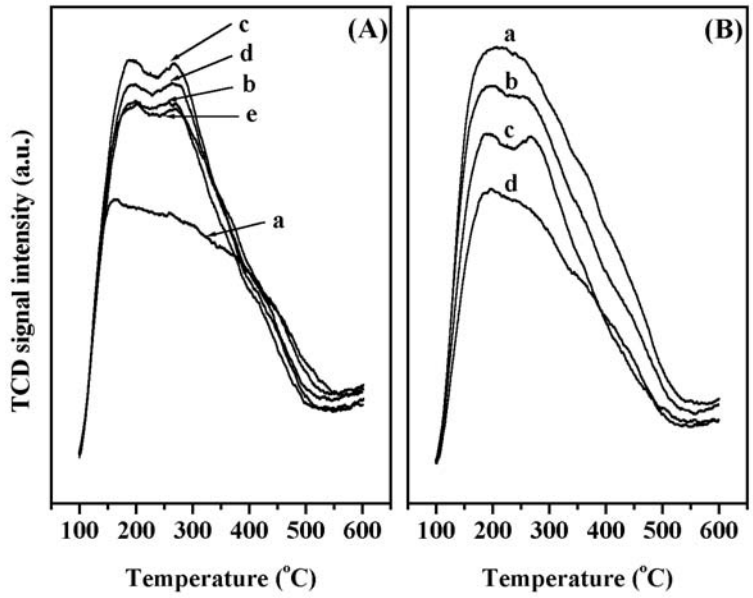

Fig. 3.5: NH_3-TPD profile of (A) catalyst with different STA loading calcined at 750 ^oC a) 5, b) 10, c) 15, d) 20, e) 25 % and (B) 15 SZ calcined at different temperatures a) 650, b) 700, c) 750, d) 800 ^oC.

3.3.7. FTIR pyridine adsorption

Adsorption of pyridine as a base on the surface of solid acids is one of the most frequently applied methods for the characterization of surface acidity. The use of IR spectroscopy to detect the adsorbed pyridine enables to distinguish different acid sites. The FTIR pyridine adsorption spectra of catalysts with different STA loading calcined at 750 ^oC and 15 SZ catalyst calcined at different temperatures are shown in Fig. 3.6. The spectra showed sharp pyridine absorption bands at 1604, 1485, 1444, 1636 and 1534cm^{-1}. Pyridine molecules bonded to Lewis acid sites absorbed at 1604 and 1444 cm^{-1}, while those responsible for Brönsted acid sites (pyridinium ion) absorbed at 1534 cm^{-1} and 1636 cm^{-1} [18]. The band at 1485 cm^{-1} is a combined band originating from pyridine bonded to both Brönsted and Lewis acid sites.

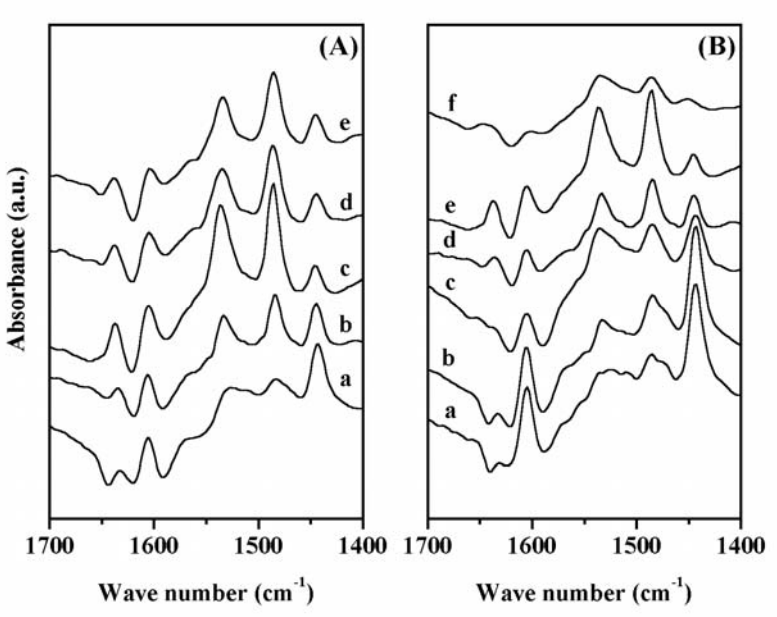

Fig. 3.6: FTIR pyridine adsorption spectra of (A) catalyst with different STA loading calcined at 750 ^{o}C a) 5, b) 10, c) 15, d) 20, e) 25 % and (B) 15 SZ calcined at different temperatures a) 450, b) 550, c) 650, d) 700, e) 750, f) 800 ^{o}C after *in-situ* activation at 300 ^{o}C.

The intensity of Brönsted (B) and Lewis (L) acid sites, obtained from the absorbance at 1534 cm^{-1} and at 1444 cm^{-1} [19] and the corresponding B/L ratio, I(B)/I(L) calculated are shown in Fig. 3.7. At low loading, the catalyst showed mainly Lewis acidity and with an increase in loading Brönsted acidity increases and reaches maximum at 15 % STA loading. An increase in STA loading above 15 %, decreased the Brönsted acidity keeping Lewis acidity similar to that of 15 % catalyst. The decrease in Brönsted acidity above 15 % could be due to the formation of crystalline WO_3, which prevents the accessibility of pyridine to the active sites. As in the case of catalysts with different loading, the nature of acidity depends also on calcination temperature. At low calcination temperature (450 ^{o}C), 15 SZ catalyst showed mainly Lewis acidity and Brönsted acidity increased with calcination temperature up to 750 ^{o}C. Thus, the Brönsted acidity of the catalyst increased with both loading and calcination temperature up to a monolayer of STA on ZrO_2.

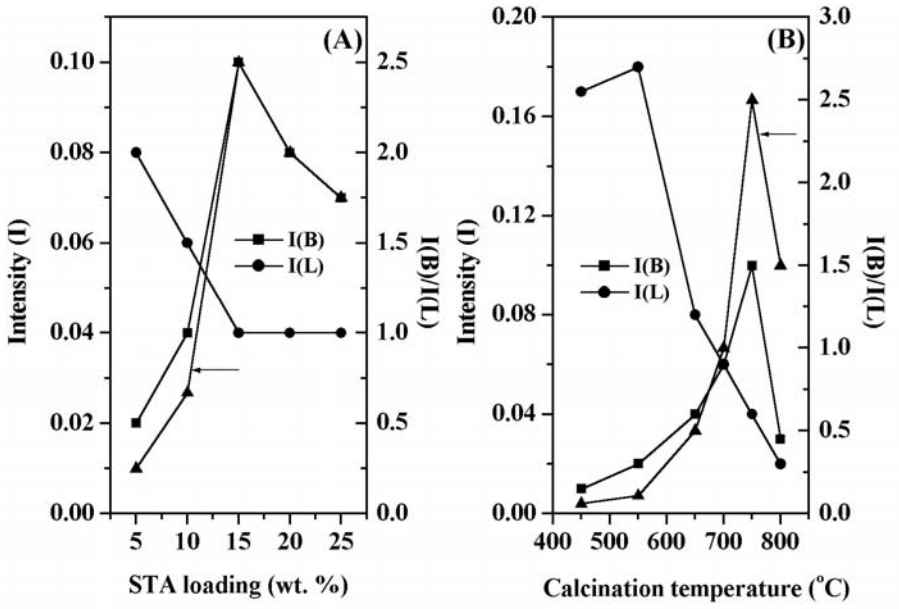

Fig. 3.7: Change in Brönsted acidity (B), Lewis acidity (L) and B/L ratio of (A) catalyst with different STA loading calcined at 750 °C and (B) 15 SZ calcined at different temperatures after *in-situ* activation at 300 °C.

3.3.8. Diffuse-reflectance UV-visible spectroscopy

Diffuse reflectance UV-vis spectra of pure STA, 15 SZ-750 and Z-750 are shown in Fig. 3.8. For pure STA bands are observed in the range of 3-5.5 eV arise from low-energy O^{2-} to W^{6+} charge transfer. The energy of an electronic transition can be characterized by the position of the energy of maximum absorption [20]. Since, the charge transfer bands are broad for zirconia-supported STA catalysts, charge-transfer transitions are more accurately characterized by energy at the absorption edge. The optical absorption edge energy is defined as the minimum photon energy required to excite an electron from the highest occupied molecular orbital (HOMO, at the top of the valence band in semiconductor domains) to the lowest unoccupied molecular orbital (LUMO, at the bottom of the conduction band. The fundamental optical absorption edge energy were determined following the procedure reported by Barton et al. [21] from the intercept of $[F(R)h\nu]^{1/2}$ Vs $h\nu$ plot, where, $F(R)$ is Kubelka-Munk function and $h\nu$ is the energy of the incident photon.

The absorption edge energies for the catalysts with different STA loading calcined at 750 °C and for 15 SZ catalyst calcined at different temperatures are shown in Fig. 3.9. Pure STA showed absorption edge energy of 3.19 eV, while pure ZrO_2 showed

absorption edge energy of 5.04 eV. After supporting STA on zirconium oxyhydroxide (15 %) followed by drying at 250 ^{o}C, the absorption edge energy increased to 3.84 eV. The increase in the edge energy compared to bulk STA is due to the effect of the support, which spreads silicotungstate and thus decreased the interaction between the polyanions [22]. There was no appreciable change in edge energy for 15 SZ catalyst up to 450 ^{o}C and with further increase in calcination temperature, the edge energy decreased up to 750 ^{o}C. For catalysts with different STA loading calcined at 750 ^{o}C, the edge energy decreased up to 15 % loading. Edge energy did not change appreciably with further increase in STA loading. Thus, the decrease in absorption edge energy with STA loading and calcination temperature up to a monolayer of silicotungstate on zirconia (15 SZ-750) could be explained on the basis of the interaction between polyanion. As the loading and calcination temperature increases, silicotungstate undergoes agglomeration resulting in an increase in interaction between polyanion and this could be considered as equivalent to the formation of a larger polyanion, which decreases the absorption edge energy [22, 23].

The increase in Brönsted acidity with loading and calcination temperature could be explained on the basis of the interaction between polyanion forming larger polyanion. Polyanion with larger size can effectively delocalize the negative charge required for the formation of Brönsted acid centers and this ultimately results in an increase in Brönsted acidity.

Thus, the results from different characterizations could be summarized as follows. The X-ray diffractograms of the catalysts with different STA loading and calcination temperature along with Raman spectra of 15 SZ catalyst showed the presence of zirconia-anchored mono-oxotungstate as the major tungsten species up to STA loading of ca. 15 % at 750 ^{o}C. The results from other characterization techniques such as NH_3-TPD and FTIR pyridine adsorption indicated that 15 SZ-750 catalyst had highest total and Brönsted acidity. Characterization of the catalysts by XPS showed that a monolayer of silicotungstate on zirconia was attained for 15 SZ-750 catalyst.

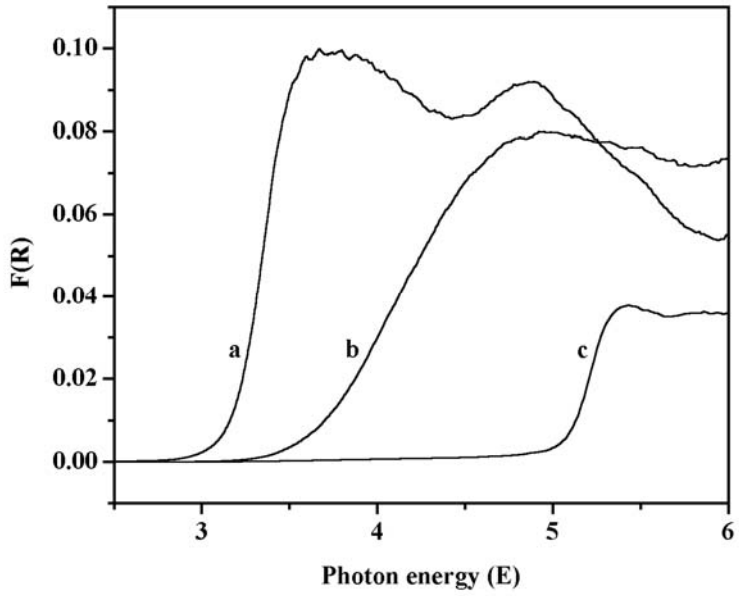

Fig. 3.8: DRUV-vis absorption spectra of a) pure STA, b) 15 SZ-750, c) ZrO_2-750.

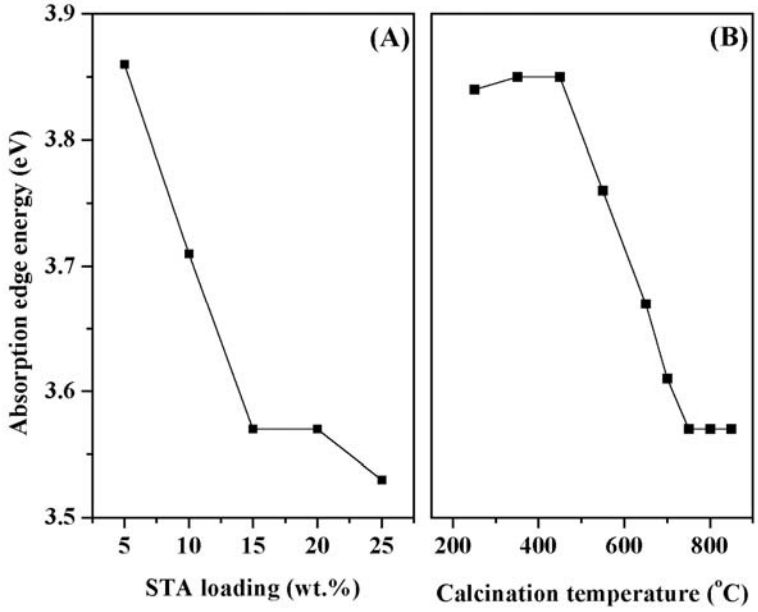

Fig. 3.9: Change in absorption edge energies of (A) catalyst with different STA loading calcined at 750 ^{o}C and (B) 15 SZ calcined at different temperatures.

So, the evolution of the catalysts could be explained as follows: until a STA loading of ca. 15 % at 750 ^{o}C, or for a 15 % catalyst up to a calcination temperature of 750 ^{o}C, i.e., up to a monolayer, the surface of the catalyst mainly occupied by mono-

oxotungstate and below this monolayer coverage, acidity of the catalyst increased with STA loading and calcination temperature. When the surface coverage exceeds monolayer, the formation of crystalline WO_3 was indicated, which was accompanied by a decrease in Brönsted acidity.

3.4. Veratrole benzoylation

3.4.1. Introduction

Friedel-Crafts acylation reactions are of great importance in the industrial manufacture of aryl ketones, and are used extensively in the production of pharmaceuticals, insecticides, dyes and other commercial products. Conventionally, these reactions are carried out in presence of aluminium chloride, using an acylating agent such as acid chloride in a volatile organic solvent [24]. Due to the complexation of the product ketone with aluminium chloride stoichiometric excess of the catalyst must be used, which is then destroyed in the hydrolysis step required for product isolation. The large quantities of metal salt waste formed, as well as the production of HCl, have aroused much research interest in the development of new cleaner technologies, which generate minimal waste. A major step towards waste minimization would be to develop a truly catalytic process, using an acid anhydride, where the catalyst does not form a strong complex with product and is recyclable. At present, considerable efforts are being made to find efficient, sustainable, recyclable and eco-friendly solid acid catalysts, as substitute for current homogeneous Brönsted and Lewis acids. Various catalysts such as zeolites [25-28], heteropoly acids [29-32], and sulfated metal oxides [33-35] were tested for this reaction.

3.4.2. Experimental procedure

The liquid-phase benzoylation reactions were carried out in a 50 ml glass batch reactor (slurry reactor) with anhydrous $CaCl_2$ guard tube. The reaction temperature was maintained by silicon oil bath equipped with a thermostat and magnetic stirrer. The catalyst freshly activated at 500 ^oC for 2 h, was weighed in the reactor and then veratrole (Aldrich, 99 %) was added according to the proportion desired. Finally benzoic anhydride, BA (E. Merck, 98 %) was added in order to obtain the desired molar ratio of veratrole to benzoic anhydride. For example, a typical reaction mixture consists of 3.77 g

(27.2 mmol) of veratrole, 1.23 g of benzoic anhydride (5.4 mmol) together with 0.15 g of catalyst. After 1 h, the reaction was stopped and the catalyst separated. The filtrate was analyzed using a Shimadzu 14B gas chromatograph fitted with HP-5 capillary column (cross linked 5 % ME silicone, 30 m x 0.53 x 1.5 μm film thickness) coupled with FID. The product identification was carried out using GC-MS and by comparing with authentic standards.

3.4.3. Results and discussion

The benzoylation of veratrole with benzoic anhydride over supported-HPA catalysts lead to the formation of 3,4-dimethoxy benzophenone as the benzoylated product as shown in Scheme 3.1. The conversion was expressed as the percentage of BA converted into the product and the conversion of BA on SZ catalysts with various STA loading and calcination temperature are shown in Fig. 3.10A. For catalysts with different STA loading calcined at 750 ^{o}C, the conversion of BA increased up to 15 % and decreased there onwards.

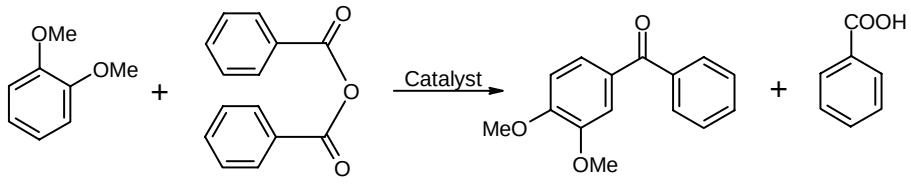

Scheme 3.1

Interestingly, the conversion of BA was found to depend strongly on calcination temperature of the catalyst. For instance, three catalyst samples with 10, 15, and 20 % STA loading calcined between 600 to 850 ^{o}C, were used in the reaction (Fig. 3.10A). The sample with higher STA loading (20 %) showed maximum conversion at lower calcination temperature (700 ^{o}C), while sample with lower STA loading (10 %) showed maximum conversion at higher calcination temperature (800 ^{o}C).

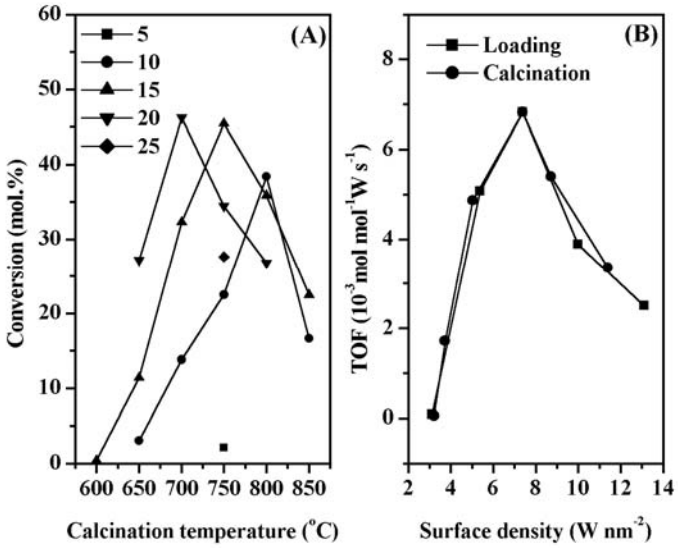

Fig. 3.10: Change in the conversion of BA with (A) STA loading and calcination temperature and (B) TOF versus surface density of catalysts with different STA loading calcined at 750 ^{o}C and 15 SZ calcined at different temperatures (conditions: total weight = 5 g, catalyst weight = 0.15g, veratrole/BA (molar ratio) = 5, time = 1 h).

In order to establish the relation between catalytic activity, STA loading and calcination temperature, the turn over frequency (TOF, mol mol^{-1}W s^{-1}) of catalysts with different STA loading (5-25 %) calcined at 750 ^{o}C and of 15 SZ calcined from 600-850 ^{o}C were determined (Fig. 3.10B). The 15 SZ-750 catalyst having the surface density 7.4 W nm^{-2} corresponding to monolayer coverage of STA on zirconia gave the highest TOF in the reaction. This result explicitly showed that irrespective of STA loading and calcination temperature, catalytic activity depends on STA coverage and the highest activity corresponds to monolayer of STA on zirconia. It is also interesting to note that acidity measurements of the catalysts by FTIR pyridine adsorption and NH_3-TPD showed that 15 SZ-750 catalyst possess the highest total acidity as well as Brönsted acidity. This clearly indicated that benzoylation of veratrole by benzoic anhydride is catalyzed by Brönsted acid sites present in the supported-catalyst.

The 15 SZ-750 catalyst was selected to compare its activity with that of 15 SS-300 catalyst (Fig. 3.11). The 15 SZ-750 and 15 SS-300 catalysts showed similar reaction profiles. Since, heteropoly acids are soluble in polar solvents, it is important to study the heterogeneity of the catalysts in the reaction. For this, the reaction is stopped after 15 min. and the catalyst is separated under hot conditions and the hot filtrate is monitored for further reaction up to 4 h (Fig. 3.11). It is apparent from Fig. 3.11 that no change in the

conversion of BA with time for filtrates obtained from 15 SZ-750 catalyst. However, for the filtrate obtained from 15 SS-300 catalyst, the conversion of BA increased from 14 % at 15 min. to 48 % after 4 h. The analysis of the filtrate by inductively coupled plasma-optical emission spectroscopy (ICP-OES) showed 70 % STA from 15 SS-300 catalyst leached into the reaction medium during reaction. This clearly showed that STA on zirconia act as heterogeneous catalyst, while STA on silica is not stable and leaches into the reaction medium during reaction.

Thus, 15 SZ-750 catalyst with highest activity was used to study the effect different reaction parameters. The influence of temperature on the conversion of BA was studied in the temperature range 60 to 120 ^{o}C for 2 h (Fig. 3.12A). At 60 ^{o}C, the conversion was 31 % and it increased to 99 % at 120 ^{o}C. The influence of veratrole/BA molar ratio (3 to 9) on the conversion of BA was studied keeping the total weight of the reaction mixture constant (Fig. 3.12B). At a molar ratio of 3, the conversion of BA was 35 % and as the molar ratio increased to 9, conversion increased to 83 %. This is probably due to the inhibiting effect of 3,4-dimethoxy benzophenone, which can be strongly adsorbed on the catalyst surface. This inhibiting effect would be less significant for mixtures richer in veratrole, because the excess of veratrole acts as a solvent for the ketone produced and product inhibition is reduced, and therefore the conversion of BA is higher at higher veratrole/BA molar ratio [27, 36]. The influence of catalyst weight on the conversion of BA showed that catalyst concentration of 2 wt. % (of the total mass of the reactants) gave conversion of BA 37 % and increased to 84 % with 5 wt. % catalyst (Fig. 3.12C), which could be due to the increase in the number of active sites of the catalyst.

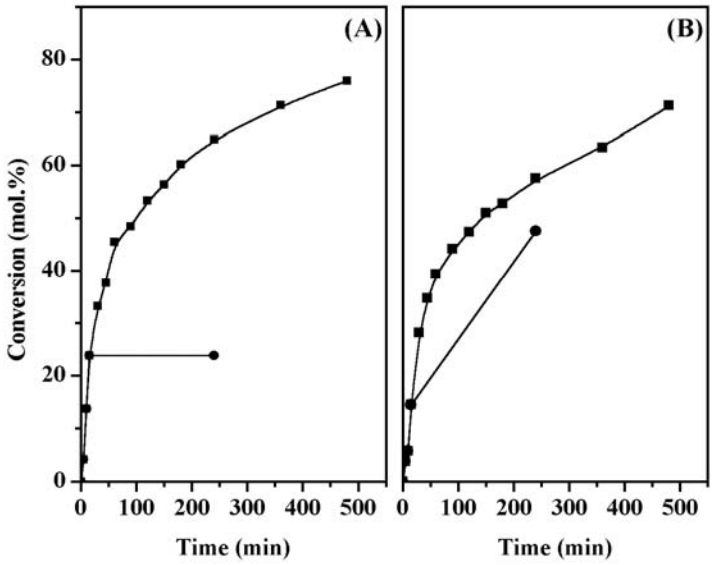

Fig. 3.11: Effect of time on the conversion of BA with the catalysts (A) 15 SZ-750, and (B) 15 SS-300, where ■ stands for reaction with fresh catalyst and • reaction after catalyst separation by hot filtration. (conditions: temperature = 80 ^{o}C, total weight = 5 g, veratrole/BA (molar ratio) = 5, catalyst weight = 0.15 g).

For supported heteropoly acid catalysts, it is important to study recycling of the catalyst, since the limited thermal stability of heteropoly acids usually prevents regeneration of the deactivated catalyst by thermal methods. In order to study the recycling, the catalyst after reaction (120 ^{o}C, 3 wt. % catalyst, 2 h and 5:1 molar reactants ratio) was separated, washed with dichloromethane, dried at 120 ^{o}C for 4 h and reused with fresh reaction mixture. After first use, the catalyst retained only 40 % of initial conversion. The lower activity of the separated catalyst could be due to the presence of surface bound benzoate species formed from the by-product benzoic acid, which is difficult to remove by washing [32, 37]. However, the catalytic activity is increased to 95 % of initial activity after regeneration of the catalyst by calcination at 500 ^{o}C for 4 h [38].

Table 3.2, compares the catalytic activity of 15 SZ-750 with those of H-Y zeolite under the reaction conditions reported in ref. [28]. Catalyst turnover frequencies (TOF) were expressed as the number of moles of veratrole converted per mole of protons in the catalyst per hour (mol mol^{-1} h^{-1}). For zeolite H-Y (Si/Al = 15), the number of active protons was taken to be equivalent to the Al content [6] and for the catalyst 15 SZ-750, the number of protons were calculated from the nominal $H_4SiW_{12}O_{40}$ loading on ZrO_2 (calculated from the weight loss obtained in TG analysis) [29]. The zeolite H-Y gave

more veratrole conversion, but 15 SZ-750 catalyst was more active and the TOF was nearly two times higher than that for H-Y zeolite.

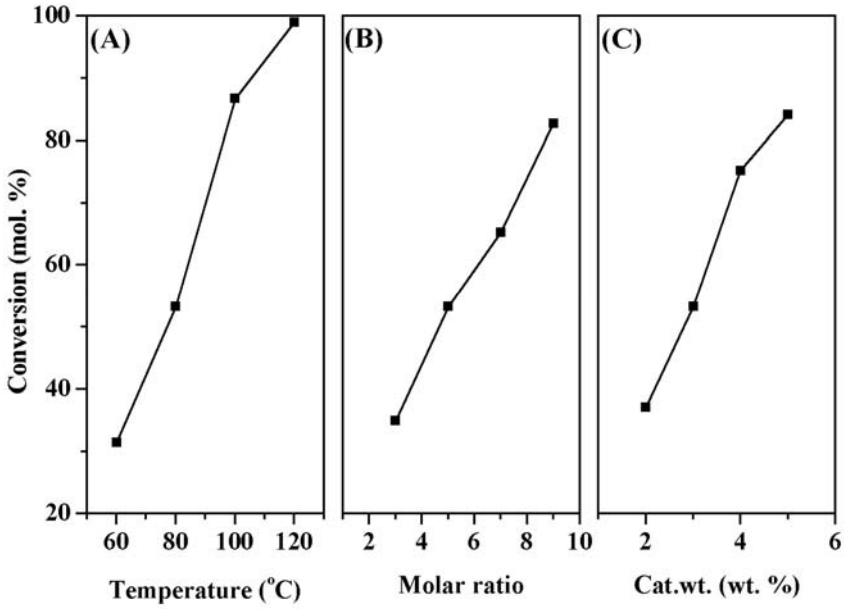

Fig. 3.12: Effect of reaction conditions on the conversion of BA.

(A) Effect of temperature (conditions: total weight = 5 g, veratrole/BA (molar ratio) = 5, catalyst weight = 0.15g, time = 2 h).

(B) Effect of molar ratio (conditions: temperature = 80 °C, total weight = 5 g, catalyst weight = 0.15 g, time = 2 h).

(C) Effect of catalyst weight (conditions: temperature = 80 °C, total weight = 5 g, veratrole/BA (molar ratio) = 5, time = 2 h).

Table 3.2: **Benzoylation of veratrole with benzoic anhydride: 15 SZ-750 catalyst Vs zeolite H-Y.**

Catalyst	**Veratrole conversion (mol. %)**	**TOF (mol mol^{-1}_{H+} h^{-1})**
H-Y [a]	75	14
15 SZ-750	40	27

Conditions: veratrole = 1.38 g (10 mmol), benzoic anhydride = 2.26g (10 mmol), chlorobenzene = 50 ml, catalyst weight = 0.5 g, temperature = 130 °C, time = 1 h.
[a] Si/Al = 15.

3.5. Phenol *tert*-butylation

3.5.1. Introduction

The alkylation of phenol with different alcohols is industrially important as it is used for the production of a variety of products [39]. Among these, alkylation of phenol with *tert*-butanol to *tert*-butylated phenols is important. For instance, 2-*tert*-butyl phenol (2-TBP) is a starting material for the synthesis of antioxidants and agrochemicals, whereas 4-*tert*-butyl phenol (4-TBP) is used to make fragrances and phosphate esters, 2,4-di-*tert*-butyl phenol (2,4-DTBP) is used in the synthesis of substituted triaryl phophites. Commercially *tert*-butyl phenols are produced by the reaction of phenol with isobutene in presence of homogeneous catalysts. The use of these catalysts possesses many problems concerning handling, safety, corrosion, and waste disposal. There fore, considerable efforts have been made for the development of suitable heterogeneous catalysts. The various catalysts reported for this reaction include metal oxides [40], zeolites [41-43], various microporous and mesoporous materials [44-48], clays and clay-based materials [49]. Both the formation of C- and O- alkylated products are possible depending on reaction conditions such as reaction temperature and type of catalyst. The catalyst with strong acidic sites or at high reaction temperature, the reaction results in the formation of C- alkylated products, while catalysts with weak acidic sites or at low reaction temperature leads to the formation of O-alkylated product [50, 51]. Even though many of the catalyst systems reported for this reactions show good activity, they do not provide sustainable catalytic activities and hence limits their successful application in large-scale production.

3.5.2. Experimental procedure

The alkylation of phenol with *tert*-butanol was carried out under atmospheric pressure using a fixed-bed down flow glass reactor (30 cm length and 1.3 cm OD). The catalyst (2 g, 30-40-mesh size) was loaded at the center of the reactor in such a way that the catalyst bed was sandwiched between inert porcelain beads. The reactor was placed in a double-zone furnace equipped with a thermocouple for sensing the reaction temperature. The catalyst was activated at 500 ^{o}C for 5 h in a flow of dry air and cooled to the reaction temperature in presence of dry nitrogen before the reactions were conducted. The feed containing a mixture of phenol (E. Merck, >99 %) and *tert*-butanol

(E. Merck, >99 %) of desired molar ratio was introduced into the reactor with a fixed space velocity using a syringe pump (Sage Instruments, Model 352, USA). Nitrogen was used as a carrier gas with a flow rate of 35 ml/min. Although fresh catalysts were used every time for different measurements, the reusability of the catalyst was also studied, by regenerating the catalyst calcination at 500 ^{o}C. The products were collected in a cold trap and analyzed by Shimadzu 14B gas chromatograph, equipped with a flame ionization detector and SE-52 packed column. The products were identified by GC-MS and by comparing with authentic samples. Conversion was defined as the percentage of phenol converted into products.

3.5.3. Results and discussion

The main products of the *tert*-butylation of phenol were 2-*tert*-butyl phenol (2-TBP), 4-*tert*-butyl phenol (4-TBP), 2,4-di-*tert*-butyl phenol (2,4-DTBP) and *tert*-butyl phenyl ether (TBPE). The products like 2,6-di-*tert*-butyl phenol and 2,4,6-tri-*tert*-butyl phenol were detected in trace amounts in some runs. C_8 and C_{12} olefins, formed by the oligomerization of isobutene were also observed in the reaction, where isobutene was formed by the acid catalyzed dehydration of *tert*-butanol. Scheme 3.2, represents the formation of different alkylated products during *tert*-butylation of phenol.

3.5.3.1. Effect of STA loading

In order to investigate the effect of STA loading, catalysts with 5-25 % STA on zirconia calcined at 750 ^{o}C were used in alkylation of phenol with *tert*-butanol at 120 ^{o}C with a space velocity of 6.7 h^{-1} (Fig. 3.13). Pure ZrO_2 calcined at 750 ^{o}C showed negligible activity. Out of the catalysts with different STA content, 5 SZ-750 catalyst showed the lowest conversion of phenol (29 %), while 15 SZ-750 catalyst gave the highest conversion (59 %) and further increase in STA loading decreased the conversion of phenol.

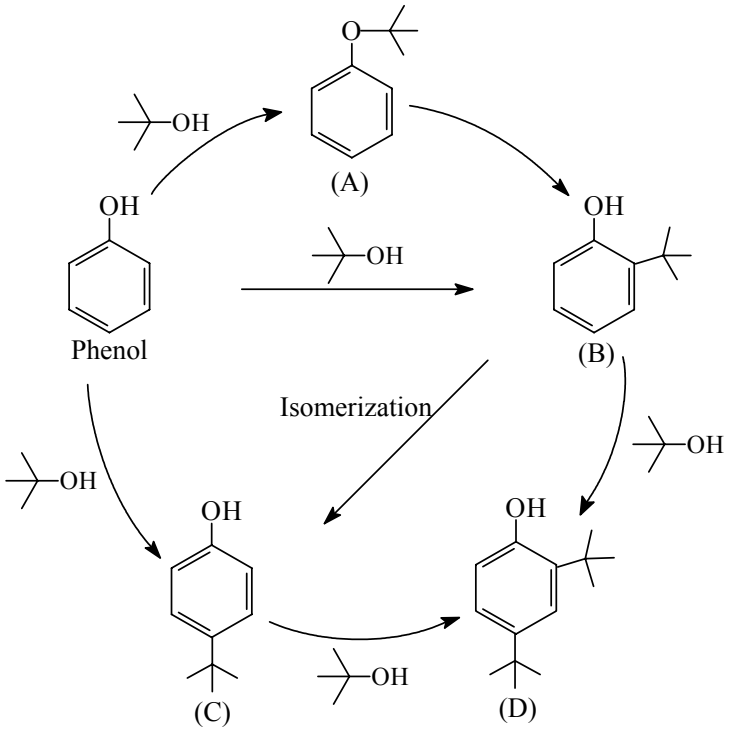

(A) *tert*-butyl phenyl ether, (B) 2-*tert*-butyl phenol, (C) 4-*tert*-butyl phenol and (D) 2,4-di-tert-butyl phenol

Scheme 3.2

The selectivity to different alkylated products depends on STA loading. The 5 SZ-750 catalyst showed the highest selectivity to TBPE. As the conversion of phenol increased from 29 to 59 % when the STA loading increased from 5 to 15 %, the selectivity to TBPE decreased from 32 to 1 %. The 5 SZ-750 catalyst showed of 26 % selectivity to 2-TBP and 28 % selectivity to 4-TBP. When STA content was increased to 10 %, the selectivity to 2-TBP was similar to that of 5 % STA catalyst (28 %), while selectivity to 4-TBP was increased to 31 %. The 15 SZ-750 catalyst showed the lowest 2-TBP selectivity (23 %), and the highest 4-TBP selectivity (33 %). The catalysts with still higher STA content gave products with similar selectivity to 2-TBP and 4-TBP. The selectivity to 2,4-DTBP increased up to 15 % STA loading (43 %) and further increase in STA content did not result in an appreciable change in its selectivity.

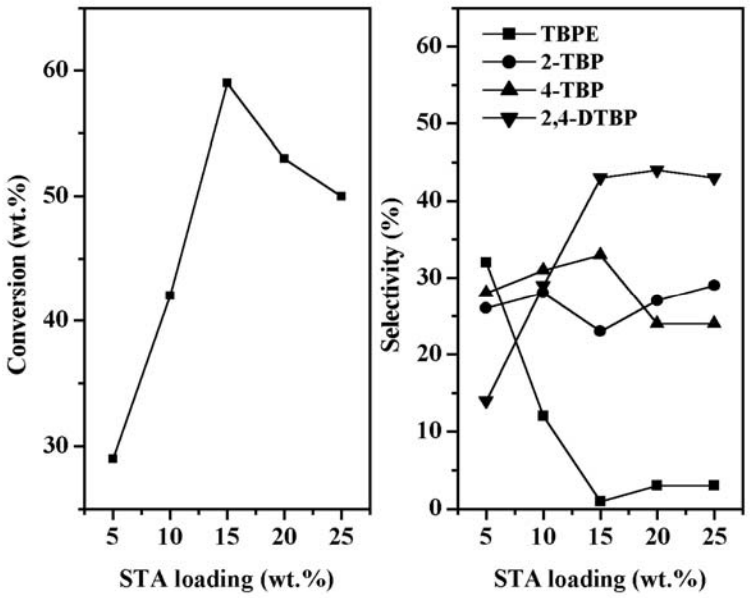

Fig. 3.13: Effect of STA loading on the conversion of phenol and product selectivity. (conditions: temperature = 120 ^{o}C, *tert*-butanol/phenol molar ratio = 1, LHSV = 6.7 h^{-1}, time = 2 h).

Subramanian *et al* have shown that 2-TBP can undergo isomerization to 4-TBP and alkylation to 2,4-DTBP [44]. Thus, the lower 2-TBP selectivity shown by 15 SZ-750 catalyst might be due to the isomerization of 2-TBP to 4-TBP and/or the successive alkylation of 2-TBP to 2,4-DTBP.

3.5.3.2. Effect of calcination temperature

The catalyst 15 SZ catalyst calcined between 350 to 850 ^{o}C has been used to study the effect of calcination temperature on catalytic activity (Fig. 3.14). It is clear from, Fig. 3.14 that calcination temperature has a profound effect on catalytic activity. The catalyst calcined at 350 ^{o}C, gave 13 % conversion of phenol and it increased to 60 % at a calcination temperature of 750 ^{o}C. Further increase in calcination temperature resulted in the decrease of conversion of phenol.

The selectivity to different alkylated products also varied with calcination temperature. As the conversion of phenol increased from 13 % for the catalyst calcined at 350 ^{o}C to 49 % for the one calcined at 650 ^{o}C, the selectivity to TBPE decreased from 89 to 8 %. The decrease in TBPE selectivity resulted in an increase in 2-TBP selectivity from 6 to 23 %. Further increase in calcination temperature to 750 ^{o}C resulted in the

decrease of TBPE selectivity to 1 %. On the other hand, the selectivity to 4-TBP increased continuously up to 750 ^{o}C. Further increase in calcination temperature did not change 4-TBP selectivity appreciably. The selectivity to 2,4-DTBP was increased up to 650 ^{o}C (44 %) and further increase in calcination temperature did not change its selectivity.

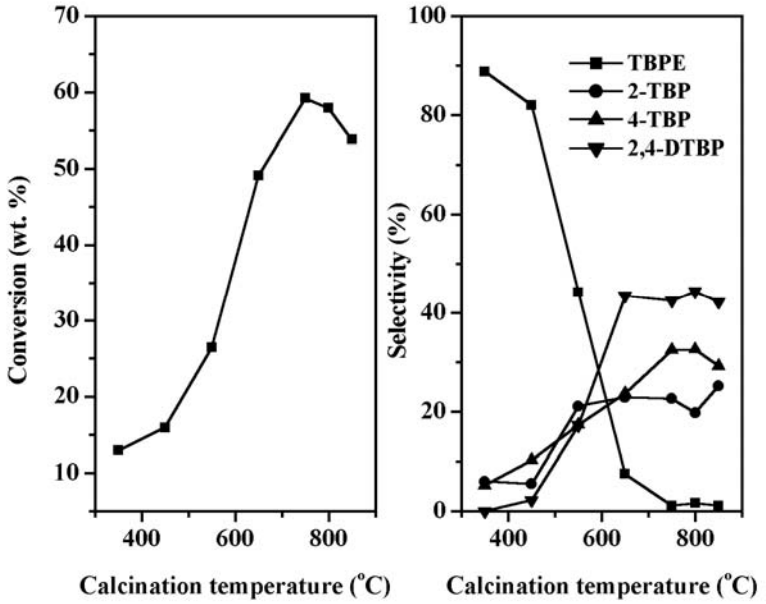

Fig. 3.14: Effect of calcination temperature on the conversion of phenol and product selectivity. (conditions: temperature = 120 ^{o}C, *tert*-butanol/phenol molar ratio = 1, LHSV = 6.7 h^{-1}, time = 2 h).

The variation of conversion of phenol and product selectivity with STA loading and calcination temperature depended on the acidity of the catalysts. The acidity measurement by NH_3-TPD and FTIR pyridine adsorption showed that 15 SZ-750 catalyst has the highest acidity and hence showed highest activity.

3.5.3.3. Effect of reaction temperature

The reaction was studied in the temperature range of 80 to 180 ^{o}C using the 15 SZ-750 catalyst. The changes in the conversion of phenol and selectivity to different products with temperature are shown in Fig. 3.15. At 80 ^{o}C, conversion of phenol was 16 % and it increased to 69 % at 140 ^{o}C. A further increase of reaction temperature decreased the conversion of phenol. The decrease in conversion could be due to the

dealkylation of *tert*-butyl phenol to phenol at high temperatures and also the diminishing availability of *tert*-butanol as it undergoes oligomerization rather than alkylation [44, 45].

At 80 ^{o}C, TBPE was obtained as the major product (86 %) and as the conversion of phenol increased, TBPE selectivity decreased and it was completely absent at 140 ^{o}C. The decrease in TBPE selectivity with temperature could be due to its rearrangement to C-alkylated product. Indeed, it has been shown that such rearrangements occurred on heating in presence of an acid catalyst [52]. The highest selectivity to 2-TBP was found to be at 100 ^{o}C (26 %), while the selectivity to 2,4-DTBP (43 %) was highest at 120 ^{o}C. The higher selectivity of 2,4-DTBP at this temperature could be due to the higher stability and the availability of *tert*-butyl cation at lower reaction temperature. The formation of 4-TBP was favored at high temperature as it is the thermodynamically stable product and hence an increase of temperature always resulted in an increase of its selectivity.

3.5.3.4. Effect of molar ratio

The effect of molar ratio on the conversion of phenol and product selectivity was studied at 140 ^{o}C with *tert*-butanol/phenol molar ratio of 0.5 to 4 using 15 SZ-750 catalyst (Fig. 3.16). Generally, the conversion of phenol was increased with an increase in the amount of *tert*-butanol. At a molar ratio of 0.5, conversion of phenol was 52 % and it increased to 89 % at a molar ratio of 2. An increase of molar ratio from 2 to 3 added an additional 5 % conversion of phenol. A further increase in molar ratio had no effect on the conversion of phenol. It was shown that the polar molecule, such as methanol and higher alcohols compete with phenol for adsorption sites and an increase in the molar excess of alkylating agent results in an increase in the conversion of phenol as observed in the present study [43].

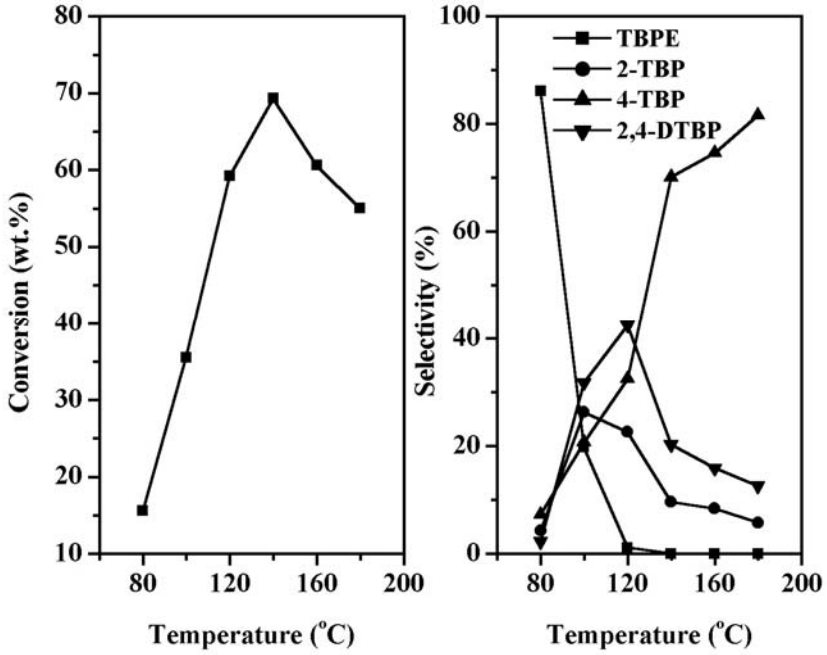

Fig. 3.15: Effect of reaction temperature on the conversion of phenol and product selectivity. (conditions: *tert*-butanol/phenol molar ratio = 1, LHSV = 6.7 h^{-1}, time = 2 h).

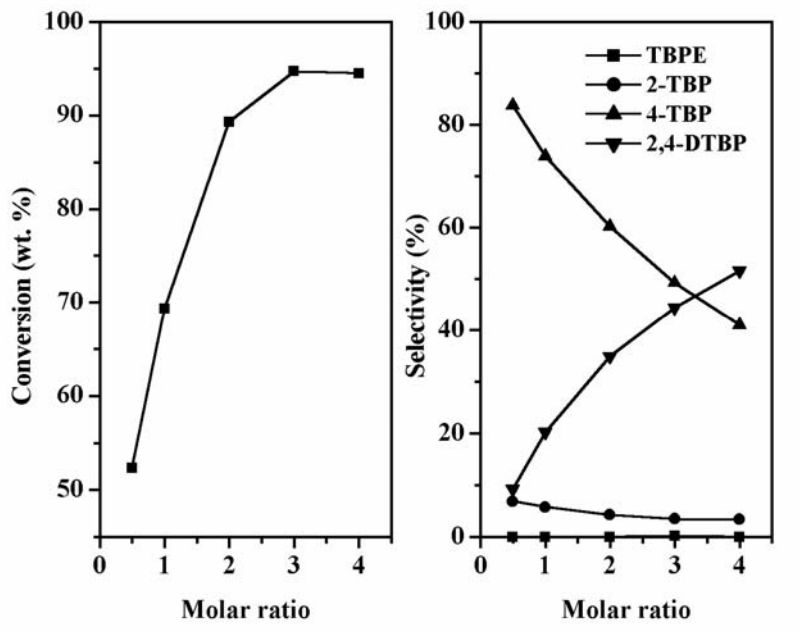

Fig. 3.16: Effect of molar ratio on the conversion of phenol and product selectivity. (conditions: temperature = 140 °C, LHSV = 6.7 h^{-1}, time = 2 h).

The selectivity to 2-TBP was low and it decreased from 7 to 3 % when the molar ratio increased from 0.5 to 4. With an increase in molar ratio from 0.5 to 4, the selectivity

to 4-TBP decreased from 84 to 41 %, while 2,4-DTBP selectivity increased from 9 to 52 %. This could be due to the higher availability of *tert*-butanol, which leads to the formation of the dialkylated product. The formation of TBPE was not observed under these conditions.

3.5.3.5. Effect of space velocity

The effect of space velocity on the conversion of phenol was studied at 140 ^{o}C using *tert*-butanol/phenol molar ratio of 2 from LHSV of 4 to 13.3 h^{-1} and the results are shown in Fig. 3.17. With an increase of space velocity from 4 to 13.3 h^{-1}, conversion of phenol was decreased 95 to 68 %. The decrease in conversion with an increase in space velocity is due to the lower contact time available for the reactants with the active sites of the catalyst.

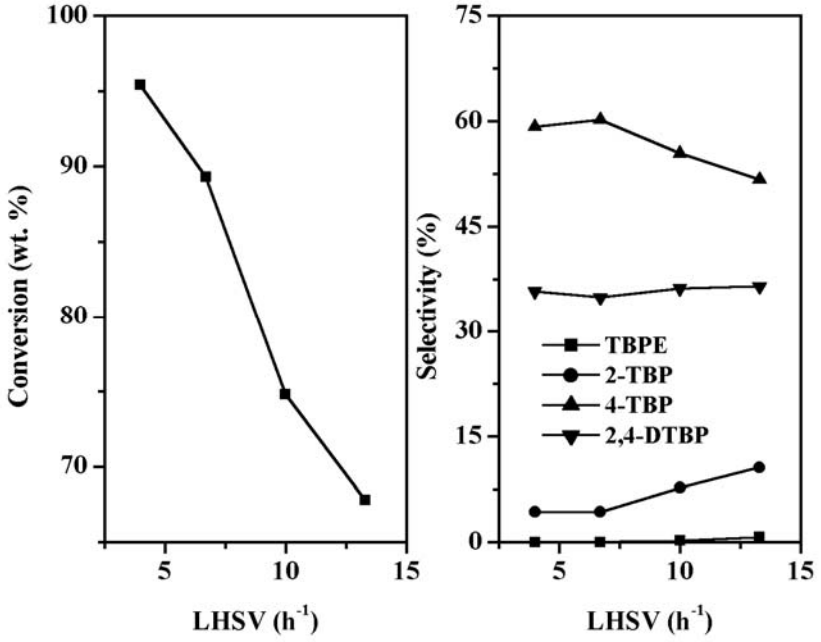

Fig. 3.17: Effect of space velocity on the conversion of phenol and product selectivity. (conditions: temperature = 140 ^{o}C, *tert*-butanol/phenol molar ratio = 2, time = 2 h).

The decrease in conversion of phenol resulted in marginal increase of 2-TBP from 4 to 11 % and decrease of 4-TBP selectivity from 59 to 52 %. The selectivity to 2,4-DTBP was similar under the reaction conditions and was found to be around 35 %.

3.5.3.6. Effect of time on stream

In order to study the deactivation behavior of the catalyst, the reaction was studied at 140 ^{o}C with LHSV of 4 h^{-1} using *tert*-butanol/phenol molar ratio of 2, for 50 h using 15 SZ-750 catalyst (Fig. 3.18 a). The conversion of phenol was found to be 95 % after 2 h with selectivity to 4-TBP 59 %, 2,4-DTBP 36 % and 2-TBP 4 %. Thus, the activity of this catalyst is found to be similar to that of large pore zeolites [42] and much higher than that of other microporous and mesoporous materials [44-48]. There was no change in the conversion of phenol and selectivity to different products after 50 h reaction.

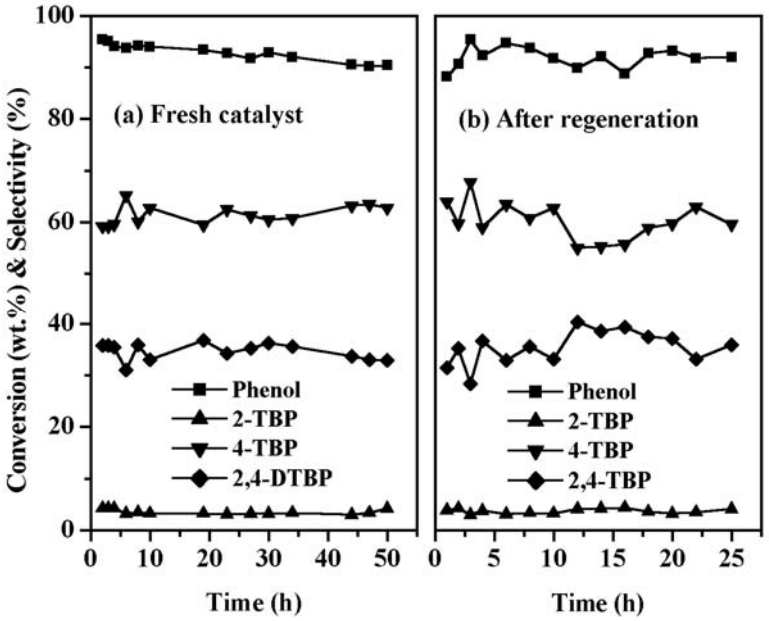

Fig. 3.18: Effect of time on the conversion of phenol and product selectivity.
(conditions: temperature = 140 ^{o}C, LHSV = 4 h^{-1}, *tert*-butanol/phenol molar ratio = 2).

The regenerability of the catalyst was also studied. Since, there was no appreciable change in the conversion of phenol after 50 h reaction, the catalyst was subjected to accelerated deactivation by performing the reaction at higher temperature. After 6 h reaction at 250 ^{o}C, the conversion of phenol was dropped to 20 %. At this point, the reaction was stopped and reactor was flushed with N_2 and the catalyst was regenerated with air at 500 ^{o}C for 6 h. The reaction was again studied with the regenerated catalyst for another 25 h (Fig. 3.18 b) and the catalyst showed similar performance as that of the fresh catalyst and no appreciable change in the conversion of phenol and product selectivity in the course of the reaction time.

3.6. References

1. Miyaji, T. Echizen, K. Nagata, Y. Yoshinaga, T. Okuhara, J. Mol. Catal. A 201(2003) 145.
2. D.G. Barton, S.L. Soled, G.D. Meitzner, G.A. Fuentes, E. Iglesia, J. Catal. 181 (1999) 57.
3. B.M. Devassy, S.B. Halligudi, S.G. Hegde, A.B. Halgeri, F. Lefebvre, Chem. Commun. (2002) 1074.
4. B.M. Devassy, F. Lefebvre, S.B. Halligudi, J. Catal. 231 (2005) 1.
5. JCPDS-International Center for diffraction data, 1990, Card 43-1035.
6. C. Rocchiccioli-Deltcheff, M. Fournier, R. Franck, R. Thouvenot, Inorg. Chem. 22 (1983) 207.
7. C.M. Teague, X. Li, M.E. Biggin, L. Lee, J. Kim, A.A. Gewirth, J. Phys. Chem. B 108 (2004) 1974.
8. E. Lopez-Salinas, J.G. Hermandez-Cortez, I. Schifter, E. Torres-Garcia, J. Navarrete, A. Gutierrez-Carrillo, T. Lopez, P.P. Lottici, D. Bersani, Appl. Catal. A 193 (2000) 215.
9. S. Loridant, C. Feche, N. Essayem, F. Figueras, J. Phys. Chem. B 109 (2005) 5631.
10. M. Scheithauer, R.K. Grasselli, H. Knözinger, Langmuir 14 (1998) 3019.
11. S. Kuba, P. Lukinskas, R.K. Grasselli, B.C. Gates, H. Knözinger, J. Catal. 216 (2003) 353.
12. M. Scheithauer, R.K. Grasselli, H. Knözinger, Langmuir 14 (1998) 3019.
13. I.V. Kozhevnikov, Catalysts for Fine Chenical Synthesis. Vol. 2. Catalysis by polyoxometalates, Wiley & Sons, Ltd., 2002. p. 15.
14. M. Valigi, D. Gazzoli, G. Ferraris, E. Bemporad, Phys. Chem. Chem. Phy. 5 (2003) 4974.
15. M. Valigi, D. Gazzoli, I. Pettiti, G. Mattei, S. Colonna, S.D. Rossi, G. Ferraris, Appl. Catal. A 231 (2002) 159.
16. F.J. Gil-Llambías, A.M. Escudey, J.L.G. Fierro, A.L. Agudo, J. Catal 95 (1985) 520.
17. M.S. Kaba, I.K. Song, D.C. Duncan, C.L. Hill, M.A. Barteau, Inorg. Chem. 37 (1998) 398.

18. G. Busca, Catal. Today 41 (1998) 191.
19. B.H. Davis, R.A. Keogh, S. Alerasool, D.J. Zalewski, D.E. Day, P.K. Doolin, J. Catal. 183 (1999) 45.
20. A. Khodakov, J. Yang, S. Su, E. Iglesia, A.T. Bell, J. Catal 177 (1998) 343.
21. D.G. Barton, M. Shtein, R.D. Wilson, S.L. Soled, E. Iglesia, J. Phys. Chem. B 103 (1999) 630.
22. M. Fournier, C. Louis, M. Che, P. Chaquin, D. Masure, J. Catal 119 (1989) 400.
23. D. Masure, P. Chaquin, C. Louis, M. Che, M. Fournier, J. Catal 119 (1989) 415.
24. G. Olah, Friedel-Crafts and related reactions, Wiley, New York, 1963-1964.
25. D. Rohan, C. Canaff, E. Fromentin, M. Guisnet, J. Catal. 177 (1998) 296.
26. E.G. Derouane, C.J. Dillon, D. Bethell, S.B. Derouane-Abd Hamid, J. Catal 187 (1999) 209.
27. E.G. Derouane, G. Crehan, C.J. Dillon, D. Bethell, H. He, S.B. Derouane-Abd Hamid, J. Catal. 194 (2000) 410.
28. T. Raja, A.P. Singh, A.V. Ramaswamy, A. Finiels, P. Moreau, Appl. Catal. A 211 (2001) 31.
29. J. Kaur, K. Griffin, B. Harrison, I.V. Kozhevnikov, J. Catal. 208 (2002) 448.
30. I.V. Kozhevnikov, Appl. Catal. A 256 (2003) 3.
31. L.A.M. Cardoso, W.A. Jr, A.R.E. Gonzaga, L.M.G. Aguiar, H.M.C. Andrade, J. Mol. Catal. A 209 (2004) 189.
32. B. Bachiller-Baeza, J.A. Anderson, J. Catal. 228 (2004) 225.
33. V. Quaschning, J. Deutsch, P. Druska, H.-J. Niclas, E. Kemnitz, J. Catal. 177 (1998) 164.
34. K. Arata, H. Nakamura, M. Shouji, Appl. Catal. A 197 (2000) 213.
35. J. Deutsch, H.A. Prescott, D. Müller, E. Kemnitz, H. Lieske, J. Catal. 231 (2005) 268.
36. P. Botella, A. Corma, J.M. López-Nieto, S. Valencia, R. Jacquot, J. Catal 195 (2000) 161.

37. A. Trunschke, J. Deutsch, D. Müller, H. Lieske, V. Quaschning, E. Kemnitz, Catal. Lett. 83 (2002) 271.
38. B.M. Devassy, G.V. Shanbhag, S.P. Mirajkar, W. Böhringer, J. Fletcher, S.B. Halligudi, J. Mol. Catal. A 233 (2005) 141.
39. H.-W. Voges, *in*: B. Elvers, S. Hawkins, G. Schulz (eds.), Ullmann's Encyclopedia of Industrial Chemistry, vol. A19, VHC, Weinheim, Germany, 1991, p. 328.
40. T. Mathew, B.S. Rao, C.S. Gopinath, J. Catal 222 (2004) 107.
41. A. Corma, H. Garcia, J. Primo, J. Chem. Res. 40 (1988).
42. K. Zhang, Ch. Huang, H. Zhang, S. Xiang, S. Liu, D. Xu, H. Li, Appl. Catal. A 166 (1998) 89.
43. R.F. Parton, J.M. Jacobs, D.R. Huybrechts, P.A. Jacobs, Stud. Surf. Sci. Catal. 46 (1989) 163.
44. S. Subramanian, A. Mitra, C.V.V. Satyanarayana, D.K. Chakrabarty, Appl. Catal. A. 159 (1997) 229.
45. A. Sakthivel, S. K. Badamali, P. Selvam, Micropor. Mesopor. Mater. 39 (2000) 457.
46. S.K. Badamali, A. Sakthivel, P. Selvam, Catal. Today 63 (2000) 291.
47. A. Vinu, K.U. Nandhini, V. Murugesan, W. Böhlmann, V. Umamaheswari, A. Pöppl, M. Hartmann, Appl. Catal. A 265 (2004) 1.
48. M. Karthik, A.K. Tripathi, N.M. Gupta, A. Vinu, M. Hartmann, M. Palanichamy, V. Murugesan, Appl. Catal. A 268 (2004) 139.
49. G.D. Yadav, N.S. Doshi, Appl. Catal. A 236 (2002) 129.
50. C. DeCastro, E. Sauvage, M.H. Valkenberg, W.F. Hoelderich, J. Catal196 (2000) 86.
51. Y. Ono, *in* "Catalysis by Zeolites" (B. Imelik, *etal*., Ed.), p. 19. Elsevier, Amsterdam 1980.
52. B.M. Devassy, S.B. Halligudi, S.P. Elangovan, S. Ernst, M. Hartmann, F. Lefebvre, J. Mol. Catal. A 210 (2004) 125.

Chapter 4

Zirconia-supported phosphotungstic acid

4.1. Introduction

This section deals with the characterization of zirconia-supported phosphotungstic acid (PTA) by the techniques such as X-ray diffraction (XRD), thermal analysis (DTG-DTA), temperature programmed desorption of ammonia (NH_3-TPD), FTIR (Fourier transform infrared) pyridine adsorption, and ^{31}P MAS NMR spectroscopy. These catalysts were used in the synthesis of linear alkyl benzenes by the alkylation of benzene with higher linear olefins such as 1-octene and 1-dodecene and acylation of 2-methoxynaphthalene (2-MN) with acetic anhydride (Ac_2O).

4.2. Preparation

The zirconia-supported phosphotungstic acid catalysts were prepared by the procedure given in section 2.2. These catalysts were represented by x PZ-T, where x represents wt. %, P represents PTA, Z represents zirconia and T denotes calcination temperature (^oC). In order to understand the role of the solvent used in the preparation, the catalyst with optimum PTA loading and calcination temperature (15 PZ-750) was prepared using different solvents. Additionally, 15 PZ-750 catalyst was also prepared simply by grinding a mixture of zirconium oxyhydroxide and PTA (neat) for 10 minutes followed by drying and calcination.

4.3. Characterization - Results and discussion

4.3.1. Surface area

The pure zirconium oxyhydroxide dried at 120 ^oC showed a surface area of 331.6 m^2g^{-1}. After calcination at 750 ^oC, the surface area decreased to 16 $m^2\ g^{-1}$. Addition of PTA to the support resulted in an increase of the surface area, which became maximum at ca. 53.2 $m^2\ g^{-1}$ for 15 % PTA loading (Table 4.1). Since this increase in surface area was affected by the change in weight of the catalyst by loading, the surface area per gram of the support indicated that the PTA loading gradually increased the surface area. This could be explained as the strong interaction of PTA with the support reduces the surface

diffusion of zirconia and inhibits sintering and stabilizes the tetragonal phase of zirconia, which leads to an increase in surface area.

The nominal WO_3 loading corresponding to different PTA loading and surface area of the catalysts with different PTA loading and calcination temperature were determined to calculate the nominal tungsten (W) surface density. The tungsten surface densities, expressed as the number of W atoms per nanometer square area (W atoms nm^{-2}), were obtained by the equation,

W surface density = {[WO_3 loading (wt. %)/100] x 6.023 x 10^{23}}/[231.8 (formula weight of WO_3) x BET surface area (m^2 g^{-1}) x 10^{18}] and are shown in Table 4.1. It is seen that an increase in PTA loading resulted in an increase in W surface density. The specific surface area of PZ catalysts also depends on the calcination temperature. The W surface density increased with the calcination temperature because of the concominant decrease in the ZrO_2 surface area (Table 4.1).

4.3.2. X-ray diffraction

The XRD pattern of the catalysts with different PTA loading calcined at 750 ^oC (Fig. 4.1) showed that, the presence of PTA strongly influenced the crystallization of zirconium oxyhydroxide into zirconia. Pure zirconia calcined at 750 ^oC was mainly monoclinic with only a small amount of the tetragonal phase (Table 4.1). For catalysts with low PTA loading calcined at 750 ^oC, the XRD pattern can be described as the sum of the monoclinic and tetragonal phases of zirconia, this latter phase becoming dominant for catalyst with 20 % PTA. The tetragonal content of zirconia at a fixed loading depends on the calcination temperature and for 15 % catalyst, zirconia exists mainly in the tetragonal form up to 750 ^oC and the tetragonal content decreased with further increase in calcination temperature (Table 4.1).

Table 4.1: Surface area, surface density and phase composition of various catalysts.

Sample	S_{BET} ($m^2 g^{-1}$ of sample)	S_{BET} ($m^2 g^{-1}$ of ZrO_2)	Surface density (W nm^{-2})	Vol. % *t*-ZrO_2
Z-750	16.0	16.0	0	5.6
5 PZ-750	40.2	42.3	3.18	21.9
10 PZ-750	46.3	51.5	5.53	75.7
15 PZ-750	53.2	62.5	7.23	84.2
20 PZ-750	52.3	65.4	9.75	94.6
15 PZ-650	105.4	124.0	3.64	95.4
15 PZ-700	78.0	91.6	4.93	93.8
15 PZ-750	53.2	62.5	7.23	84.2
15 PZ-800	40.7	47.8	9.46	79.3
15 PZ-850	30.4	35.7	12.66	58.9

Thus, the added PTA stabilizes the tetragonal phase of zirconia and such stabilization of tetragonal ZrO_2 in presence of PTA and other oxides has been reported in the literature [1, 2]. It could also be seen that up to a 15 % PTA loading, for catalysts calcined at 750 ^oC and for 15 % catalyst, up to 750 ^oC calcination, no diffraction lines which could be attributed to the polyacid or to its decomposition products were observed, indicating that PTA is highly dispersed on the support. When the PTA loading was higher than 15 %, or when the calcination temperature exceeded 750 ^oC for 15 % loading, new diffraction lines appeared in the region of 23-25°, characteristic of WO_3 [3]. This indicated that (i) PTA gets decomposed, at least partially and (ii) that tungsten oxide formed by this decomposition of PTA present as relatively large particles. Thus, when the PTA loading exceeded monolayer coverage (see latter), the excess PTA that does not interact with zirconia decomposed and the X-ray diffractogram showed the presence of bulk crystalline WO_3.

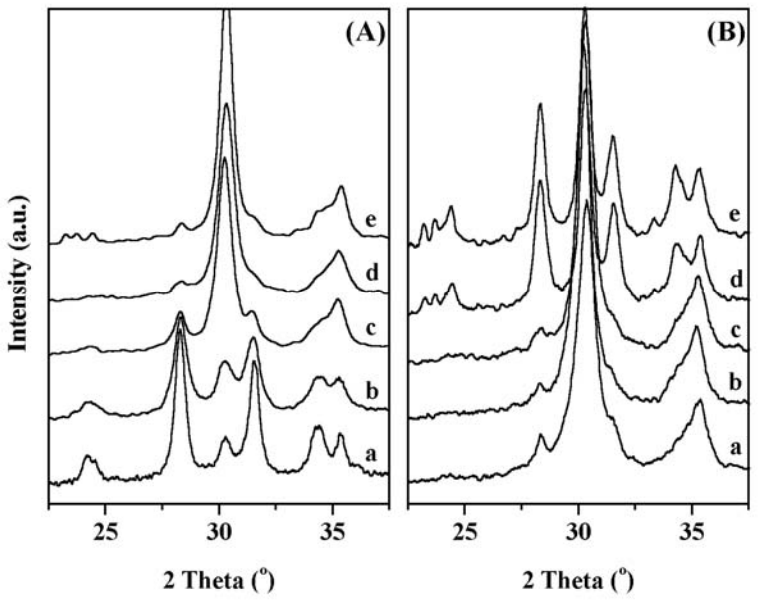

Fig. 4.2: X-ray diffractiograms of (A) catalysts with different PTA loading calcined at 750 °C a) 0, b) 5, c) 10, d) 15, e) 20 %; (B) 15 PZ calcined at different temperatures a) 650, b) 700, c) 750, d) 800, e) 850 °C.

4.3.3. Thermal analysis

The DTG and DTA traces of all the samples dried at 120 °C along with PTA hydrate are shown in Fig. 4.2. The DTG analysis of pure PTA hydrate ($H_3PW_{12}O_{40}$. x H_2O) showed three stages of weight loss (endothermic effects) [4]. The first weight loss occurred from room temperature to 125 °C due to the loss of physisorbed water. The second one from 130 to 305 °C accounts for the loss of crystallization water and the third one in the range of 370-550 °C for the loss of 1.5 molecules of H_2O originating from all acidic protons. The total weight loss of the sample corresponded to 21 H_2O molecules per Keggin unit (KU). The DTA showed an exothermic peak at 607 °C due to the complete decomposition of the Keggin structure to form a mixture of oxides followed by its crystallization.

The zirconium oxyhydroxide showed two endothermic and one exothermic peak. The first endothermic peak from room temperature to 180 °C due to the loss of physisorbed water, while the second peak from 182-335 °C ascribed to the dehydration and dehydroxylation of amorphous zirconium oxyhydroxide. The exothermic effect at 445 °C, termed "glow exotherm" is responsible for the crystallization of zirconium oxyhydroxide to metastable tetragonal ZrO_2. The DTG behavior of all the PZ samples was similar, but differed in DTA behavior. The DTA of the samples showed a broad exothermic peak from 273 to 360 °C with a peak maximum at 305 °C, assigned to the formation of Zr-O-W bonds between PTA's terminal W=O oxygen atoms and surface $\equiv Zr^+$ species or to the formation of water by the reaction of PTA protons with ≡ZrOH

hydroxyl groups [1, 5]. Along with the exothermic effect at 445 ^{o}C, another exothermic peak appeared in the temperature range 500-690 ^{o}C for samples with 5-20 % PTA and the peak position moved to higher temperature with increasing PTA content. The sample with 30 % PTA showed a sharp exothermic peak at 730 ^{o}C and was due to the crystallization of tungstate species formed by the decomposition of PTA.

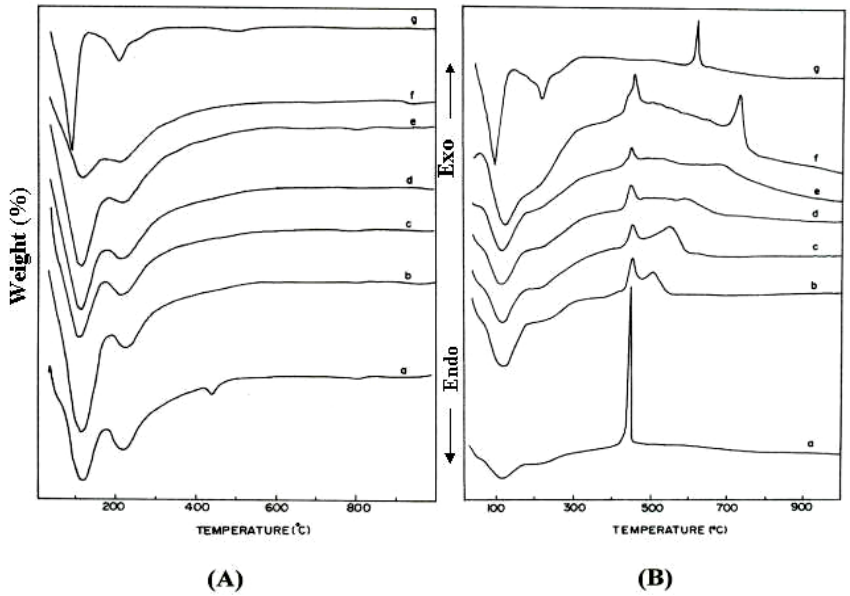

Fig. 4.3: DTG (A) and DTA (B) curves of a) hydrous ZrO_2, b) 5, c) 10, d) 15, e) 20, f) 30 % catalysts, and g) PTA hydrate.

4.3.4. FTIR pyridine adsorption

The FTIR pyridine adsorption spectra of catalyst with different PTA loading are shown in Fig. 4.3. The catalysts showed Brönsted (B) and Lewis (L) acidity at 1536 cm^{-1} and at 1442 cm^{-1} and the B/L ratio calculated from the IR absorbance intensities [6], are given in Table 4.2. The B/L ratio showed that the relative Brönsted acidity increased with PTA loading up to 15 % and decreased with further loading. For 15 % catalyst, the Brönsted character increased up to 750 ^{o}C calcination, while above an increase in Lewis acidic character was observed (Table 4.2). Thus, 15 PZ-750 catalyst shows the maximum relative Brönsted acidity and this corresponded to a monolayer of PTA on ZrO_2.

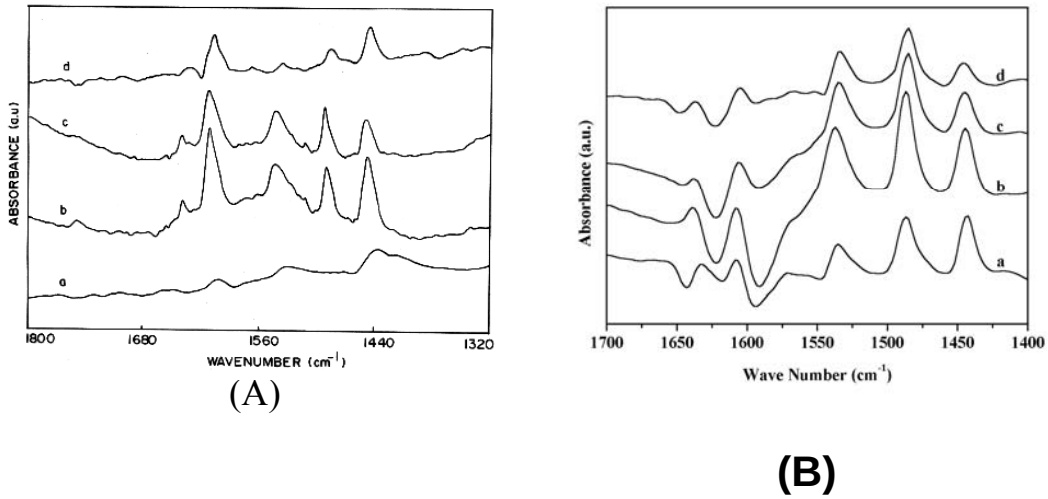

Fig. 4.4: FTIR pyridine adsorption spectra of (A) catalyst with different PTA loading calcined at 750 ^{o}C a) 5, b) 10, c) 15, d) 20 % and (B) 15 PZ calcined at different temperatures a) 650, b) 700, c) 750, d) 800 ^{o}C after *in-situ* activation at 300 ^{o}C.

4.3.5. TPD of NH_3

This adsorption-desorption technique enables the determination of the strength of acid sites present on the catalyst surface together with total acidity. The TPD profiles of the catalysts with different PTA loading are shown in Fig. 4.4 and the amount of sorbed NH_3 per nm^2 of the catalysts with different PTA loading and of catalyst with 15 % PTA calcined at different temperatures (650, 750 and 850 ^{o}C) are given in Table 4.2. All samples showed a broad TPD profile, which revealed that the surface acid strength has been widely distributed. It is evident from the data that there is an initial increase in the acidity until 15 % loading and thereafter gets decreased. For 15 PZ catalysts, calcined at different temperatures, the amount of adsorbed ammonia increased with calcination temperature and reached maximum at 750 ^{o}C.

Table 4.2: FTIR pyridine adsorption (after *in-situ* activation at 300 ^{o}C) and NH_3-TPD data on various catalyst samples.

Sample	B acidity *I* (B)	L acidity *I* (L)	[a]B/L ratio (*I*(B)/*I*(L)	[b]Acidity (NH_3 nm^{-2})
5 PZ-750	0.006	0.019	0.32	3.44
10 PZ-750	0.049	0.077	0.64	4.68
15 PZ-750	0.052	0.049	1.06	5.21
20 PZ-750	0.007	0.026	0.27	2.65
15 PZ-650	0.065	0.110	0.59	2.86
15 PZ-700	0.110	0.120	0.92	n. e.
15 PZ-750	0.090	0.060	1.50	
15 PZ-800	0.060	0.050	1.20	n. e.
15 PZ-850	0.01	-	n. e.	3.86

[a] For catalysts with different PTA loading, pyridine adsorption was carried out under vacuum and for 15 % catalyst with different calcination temperature, it was carried out under N_2 flow.
I is absorbance intensity
[b] Acidity values obtained from NH_3-TPD.
[c] not evaluated.

If we take into account the other characterizations, these results could be explained as at low PTA loadings, the polyoxometalate retains its structure and acidity, while for higher loadings, it decomposes at least partially into its oxides. Thus, the highest acidity corresponds to ca. one monolayer of polyoxometalate and was also evident from ^{31}P MAS NMR spectra. So, we could describe the evolution of the catalysts as follows: until a PTA loading of ca. 15 % at 750 ^{o}C, or for a 15 % catalyst up to a calcination temperature of 750 ^{o}C, i.e., up to a monolayer, the heteropolyanion is well dispersed on the zirconia surface and it retains its integrity. When the coverage exceeds monolayer, the polyanion is not stabilized by zirconia and decomposes to its oxides.

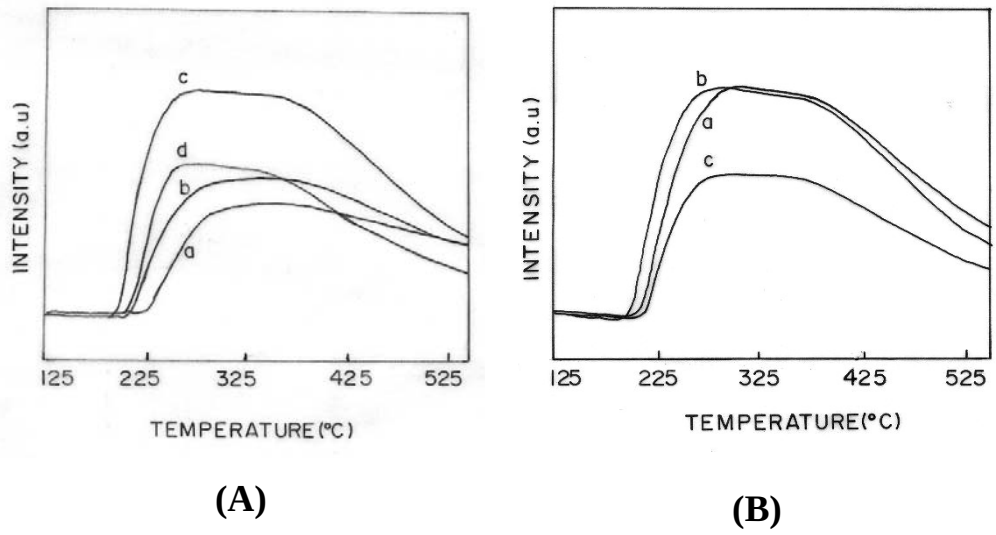

Fig. 4.5: NH_3-TPD profile of (A) catalyst with different PTA loading calcined at 750 ^oC a) 5, b) 10, c) 15, d) 20 % and (B) 15 PZ calcined at different temperature a) 650, b) 750, c) 850 ^oC.

4.3.6. ^{31}P MAS NMR spectroscopy

This is one of the most useful characterization techniques to study the state of phosphorous in heteropoly acids. The chemical shift depends upon the phosphorous environment and it depends on factors such as hydration number, addenda metal ion, and support, etc [7-11]. The ^{31}P MAS NMR spectra of the catalysts with 5 to 20 % PTA and 15 % catalyst calcined from 650 to 850 ^oC showed that the state of phosphorous in the catalyst depended on PTA loading and calcination temperature (Fig. 4.5). For low loadings and at calcination temperature of 750 ^oC, broad signal above –20 ppm was observed, is attributed to P-OH group associated with phosphotungstate, which is in interaction with zirconia [7, 11, 12]. While at higher loadings and at higher calcination temperatures, new signal appeared below –20 ppm, attributed to phosphorous oxide (P-O-P) resulting from the decomposition of the polyoxometalate [1]. This phosphorous oxide represents 20 and 45 % of the total phosphorous for 15 and 20 PZ-750 catalysts and 80 % for 15 PZ-850 catalyst, respectively.

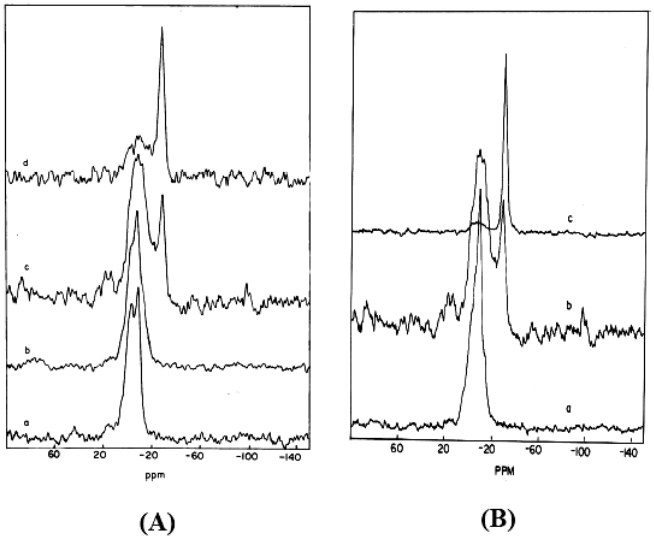

(A) **(B)**

Fig. 4.6: ^{31}P MAS NMR spectra of (A) catalysts with different PTA loading calcined at 750 ^{o}C a) 5, b) 10, c) 15, and d) 20 % and (B) 15 PZ calcined at different temperature a) 650, b) 750, and d) 850 ^{o}C.

The ^{31}P MAS NMR spectra of the catalysts with different PTA loading and calcination temperature showed that, PTA starts decomposing at a loading of ca. 15 % at 750 ^{o}C calcination. The results from different characterization techniques suggest that a geometric monolayer of PTA on zirconia was attained for 15 PZ-750 catalyst.

The 15 PZ-750 catalyst was selected to study the role of solvent used for the catalyst preparation. The NMR spectra of the catalysts prepared in different solvents showed two signals, one above –20 ppm and one below –20 ppm (Fig. 4.6). A careful examination of the spectra showed that the signal intensities depend upon the solvent used for the catalyst preparation, confirming the vital role played by the solvent in stabilizing heteropoly tungstate in the final catalyst. We have observed a direct relation between P-OH intensity and the dielectric constant of the solvent [13] used for the catalyst preparation (Table 4.3). It is evident from Table 4.3 that the P-OH intensity i.e., the amount of phosphotungstate present in the catalyst, increased with dielectric constant of the solvent except water.

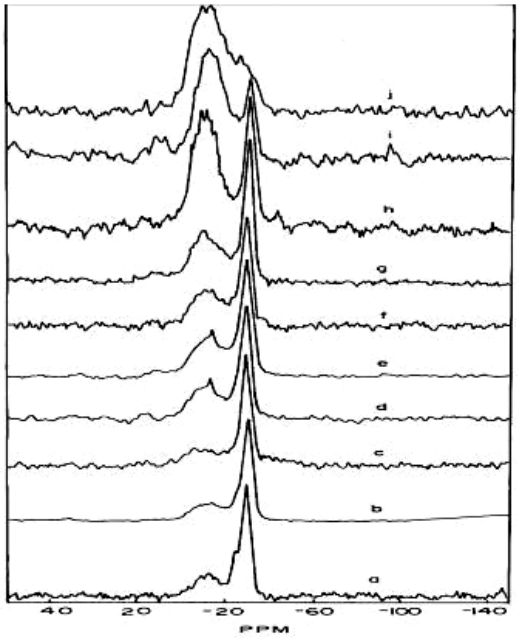

Fig. 4.7: ^{31}P MAS NMR spectra of 15 PZ-750 catalyst prepared in different solvents a) neat, b) ether, c) 1,4-dioxane, d) acetic acid, e) ethyl acetate, f) tetrahydrofuran, g) acetone, h) water, I) methanol, j) DMF.

From spectroscopic studies, Rocchiccioli-Deltcheff et al. showed the existence of anion-anion interaction in acid form of HPA both in solid and solution state [14, 15]. The present work showed that the interaction of HPA with solvents varies with the dielectric constant of the solvent. In solvents with high dielectric constant, for example solvents like dimethylformamide (DMF) and methanol, the anion-anion interaction seems to be absent or negligible and the catalyst prepared with these solvents retained maximum amount of phosphotungstate i.e., such catalysts showed the highest P-OH intensity. In the case of DMF solvent, DMF is protonated by PTA and the protonated DMF is interacting with the Keggin anion as in the case of tetraalkylammonium salts of HPA, explaining the lack of anion-anion interaction for the acid form in DMF [15, 16]. PTA in methanol forms protonated monomers as $CH_3OH_2^+$, and dimers, $(CH_3OH)_2H^+$ and these ions interact more with the Keggin ions rather than its direct interaction with the solvent [17]. PTA in other solvents under study shows varying degrees of anion-anion interaction arising from the formation of hydrogen-bonding networks in the solvent, resulting in solvent structure that holds the anion within interaction proximity [15]. Hence, we presume that as the dielectric constant of the solvent decreases, the ability of the solvent to form structured solvent and anion-anion interaction increases.

The hydroxyl group of the zirconium oxyhydroxide tends to be either positively or negatively charged below or above the isoelectric point, IEP (pH = 6-7) [18]. Above IEP, the hydroxyl groups tend to be negatively charged, so that it is relatively difficult for the anions to be adsorbed on the hydroxide surface, due to electrostatic repulsion. On the other hand, the adsorption of the anions is favored below the IEP of the support. Hence, the adsorption of phosphotungstate Keggin anions on the surface of zirconium oxyhydroxide is favorable when water is used as the solvent, which is not applicable in the case of non-aqueous solvents. The solvent water has the highest dielectric constant (79.7), but the catalyst prepared in water showed P-OH intensity lower than that prepared in methanol. In aqueous solution, heteropoly anions are not stable at pH > 1 as reported by McGarvey and Moffat and this has been observed in this study [19]. The low P-OH intensity of the catalyst prepared in water is attributed to the low stability of PTA in water [15].

The different behavior of the catalysts prepared in different solvents can also originate from diffusion limitation of PTA into the pores of the support. The size of the Keggin anion (12 Å) is of the order of pore size of the support (diameter < 2 nm) [20], the rate of diffusion is controlled by the anion size and the large polyoxoanions should have a lower diffusion rate. Since, the HPA anions are very weakly solvated in solvents, the solubility of heteropoly acids depend on the solvation of cations [21]. Thus, the effective size of the Keggin unit can vary from solvent to solvent and hence the diffusivity of the polyanion, which ultimately results in different dispersion of HPA on the support and hence the amount of phosphotungstate present on ZrO_2 surface. These results are in good agreement with the observations of Fournier et al. who suggest the use of DMF as solvent to achieve good dispersion during the preparation of supported heteropoly acid catalysts [15]. We have used methanol as the solvent due to its higher volatility and easiness in handling.

Table 4.3: ***P-OH intensity, dielectric constant, conversion of octene and product selectivity of 15 PZ-750 catalyst prepared in different solvents.***

Solvent	Dielectric constant	[a]P-OH intensity (%)	Octene conversion (mol. %)	MOB selectivity (%)	DOB selectivity (%)
Neat	-	32	12.1	100	0
Ether	2.21	33	14.2	100	0
1,4-Dioxane	4.30	36	14.3	100	0
Acetic acid	6.20	40	24.0	99.6	0.4
Ethyl acetate	6.02	44	27.0	99.4	0.6
THF	7.60	46	27.6	99.2	0.8
Acetone	20.60	52	32.8	99.4	0.6
Water	79.70	65	43.4	99.0	1.0
Methanol	32.60	80	53.4	95.5	4.5
DMF	36.70	82	55.5	95.4	4.6

(conditions: total weight = 25 g, catalyst weight = 0.125 g, temperature = 84 ^{o}C, benzene/1-octene (molar ratio) = 10, time = 1 h).

[a] relative amount of phosphotungstate present in the catalyst.

4.4. Alkylation of benzene

4.4.1. Introduction

The alkylation of aromatic hydrocarbons with olefins is applied on a large scale in the chemical industry. Alkylation of benzene with C_{10-14} linear alkenes is used for the synthesis of linear alkyl benzenes (LAB), which are the primary raw material for the production of LAB sulfonates, a surfactant detergent intermediate [22]. Traditionally this reaction is catalyzed by a homogeneous Lewis acid such as $AlCl_3$ or a strong Brönsted acid such as HF, which are highly toxic, generate a substantial amount of waste and cause severe corrosion problems. At present, considerable efforts are being made to find efficient, sustainable, recyclable and eco-friendly solid acid catalysts, which can successfully carry out above reaction [23, 24]. Various catalysts such as zeolites, clays, heteropoly acids, sulfated zirconia and immobilized ionic liquids were tested for this reaction [25-30]. The Detal process developed by UOP uses solid acid catalysts for alkylation of benzene with heavy olefins, under liquid-phase conditions [22].

4.4.2. Experimental procedure

The liquid-phase alkylation reactions were carried out using zirconia-supported PTA catalysts in a 50 ml glass batch reactor (slurry reactor) with anhydrous $CaCl_2$ guard tube. The reaction temperature was maintained by silicon oil bath equipped with a thermostat and magnetic stirrer; the temperature was measured at the reaction mixture. The catalyst freshly activated at 500 ^{o}C for 2 h, was weighed in the reactor and then benzene (E. Merck, >99 %) was added according to the proportion desired. Finally 1-alkene (Aldrich) [1-octene (98 %) and 1-dodecene (95 %)] was added in order to obtain the desired molar ratio of benzene to 1-alkene. For example, a typical reaction mixture consists of 21.86 g (280 mmol) of benzene, 3.14 g of 1-octene (28 mmol) together with 0.125 g of catalyst. The reaction carried out at the desired temperature was stopped after 1 h and the catalyst separated. The filtrate was analyzed using a Shimadzu 14B gas chromatograph using HP-5 capillary column (cross linked 5 % ME silicone, 30 m x 0.53 x 1.5 μm film thickness), coupled with FID. The product identification was carried out using GC-MS.

4.4.3. Results and discussion

The main reactions occurred with these catalysts were alkene double bond shift isomerization and benzene alkylation as shown in Scheme 4.1. Monoalkylbenzenes (MOB) was the main reaction product, whereas dialkylbenzenes (DOB) and alkene dimers (DIM) formed in low amount. The conversion was expressed as the percentage of alkene converted into products. The effect of PTA loading on the conversion of octene and product selectivity is presented in Table 4.4. The 5 PZ-750 catalyst gave 1.3 % conversion of octene and increased to 53.4 % at 15 % loading. The selectivity to mono and dialkylated products depended on PTA loading and the catalyst with 15 % PTA gave 95.5 % mono alkylation selectivity.

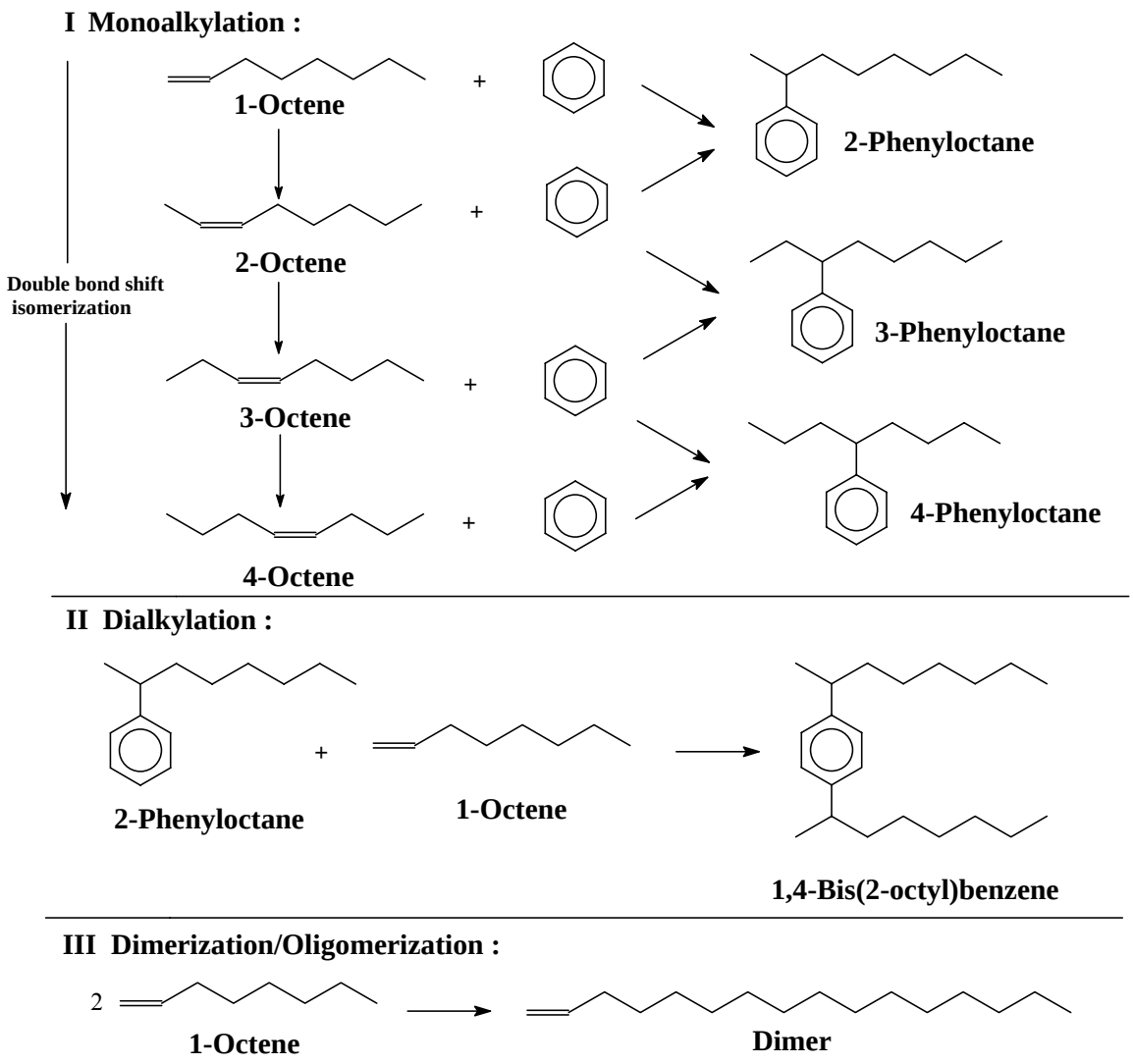

Scheme 4.1

To study the effect of calcination temperature on the conversion of octene and product selectivity, 15 PZ catalyst calcined between 650 and 850 ^{o}C were used. The catalyst calcined at 650 ^{o}C gave 8.7 % octene conversion, which increased to 53.4 % at 750 ^{o}C calcination (Table 4.4). With an increase in calcination temperature, selectivity to dialkylation increased up to 750 ^{o}C and then decreased. The highest activity of 15 PZ-750 catalyst was due to its higher Brönsted and total acidity.

Table 4.4: Conversion of octene and product selectivity over various catalysts.

Sample	**Octene conversion (mol. %)**	**TOF (10^{-3} mol mol^{-1} W s^{-1})**	**MOB selectivity (%)**	**DOB selectivity (%)**
5 PZ-750	1.3	3.7	100	0
10 PZ-750	14.9	20.8	100	0
15 PZ-750	53.4	50.0	95.5	4.5
20 PZ-750	47.6	33.6	97.9	2.1
25 PZ-750	41.1	23.1	98.7	1.3
15 PZ-650	8.7	8.1	100	0
15 PZ-700	34.6	32.5	97.8	2.2
15 PZ-800	24.0	22.5	99.0	1.0
15 PZ-850	5.4	5.0	100	0

(conditions: total weight = 25 g, catalyst weight = 0.125 g, temperature = 84 ^{o}C, benzene/1-octene (molar ratio) = 10, time = 1 h).

In order to establish the relation between catalytic activity, PTA loading and calcination temperature, the turn over frequency (TOF, mol mol^{-1} W s^{-1}) of different catalysts were (Table 4.4) calculated from the conversion of octene. The 15 PZ-750 catalyst showed highest TOF and the surface density of this catalyst is found to be 7.23 W nm^{-2} (Table 4.1), which corresponds to monolayer coverage of PTA on zirconia [12]. This clearly indicates that, irrespective of PTA loading and calcination temperature, catalytic activity depends on PTA coverage and the highest activity corresponds to monolayer of PTA on zirconia.

Therefore, the catalyst with optimum PTA loading (15 %) and calcination temperature (750 ^{o}C) was taken to study the role of the solvent used for catalyst preparation. The conversion and selectivity for 15 PZ-750 catalyst prepared in different solvents showed that, the conversion increased with an increase in P-OH intensity (Table 4.3). The catalyst prepared without solvent showed the lowest octene conversion of 12.1 %, while the catalyst prepared in DMF showed the highest conversion of 55.5 %. As the conversion increased, the selectivity to MOB decreased marginally from 100 to 95.4 %

for the catalyst prepared without solvent to the one prepared in DMF. It has to be noted that there was not much difference in the conversion of octene for the catalyst prepared in methanol and DMF as the solvents.

The 15 PZ-750 catalyst prepared with methanol as solvent was used to study the effect of temperature on the conversion of octene and product selectivity in the range 55 to 84 ^{o}C. The results indicated that temperature has a drastic effect on the conversion of octene (Fig. 4.7A). At 55 ^{o}C, the conversion was very small, which increased to 6.2 % at 75 ^{o}C. An increase of 47 % octene conversion was observed when the temperature was increased from 75 to 84 ^{o}C (boiling point of the reaction mixture).

The effect of benzene to octene molar ratio (4 to 10) on conversion and product selectivity was studied keeping the total weight of the reaction mixture constant under otherwise similar conditions (Fig. 4.7B). As the molar ratio increased from 4 to 10, the conversion of octene was increased from 29 to 53.4 %, while the selectivity to dialkylation decreased from 13.4 to 4.5 %. The dimerization of octene was also observed at low benzene-to-octene molar ratio and the dimer content decreased with an increase in the amount of benzene and was absent at a molar ratio of 10.

The effect of catalyst concentration on the conversion of octene showed that catalyst concentration of 0.5 wt. % (of the total mass of the reactants) gave an octene conversion of 53.4 % and increased to 98.1 % with 2 wt. % catalyst, having similar MOB selectivity (Fig. 4.7C). Thus, under the reaction conditions of 84 ^{o}C, 1 h and benzene to olefin molar ratio of 10; alkylation of benzene with 1-octene gave 98.1 % conversion of octene with 93.7 % MOB selectivity (isomer distribution 57.2 % 2-PO, 26 % 3-PO and 16.8 % 4-PO) and 6.3 % DOB selectivity.

Similarly, the alkylation of benzene with 1-dodecene was carried out under the reaction conditions optimized for 1-octene. The desired product monododecyl benzene (phenyl dodecane-PD) is the precursor to linear alkyl benzene sulfonate, which is the most widely used surfactant in the detergent industry. At 2 wt. % catalyst concentration the conversion of dodecene was 41 %, which increased to 99 % with 5 % catalyst. As the conversion increased from 41 to 99 %, the monododecyl benzene (MDB) selectivity slightly decreased from 98.8 to 95.3 % and didodecyl benzene selectivity slightly increased from 1.2 to 4.7 %. At dodecene conversion of 99 % the MDB isomer distribution was 49.4 % 2-PD, 17.3 % 3-PD, 11 % 4-PD and 22.3 % 5+6 PD. Sulfated

zirconia was shown to be more active [28], and zeolites as more selective catalyst (to 2-isomer but at low activity) [30] for this reaction.

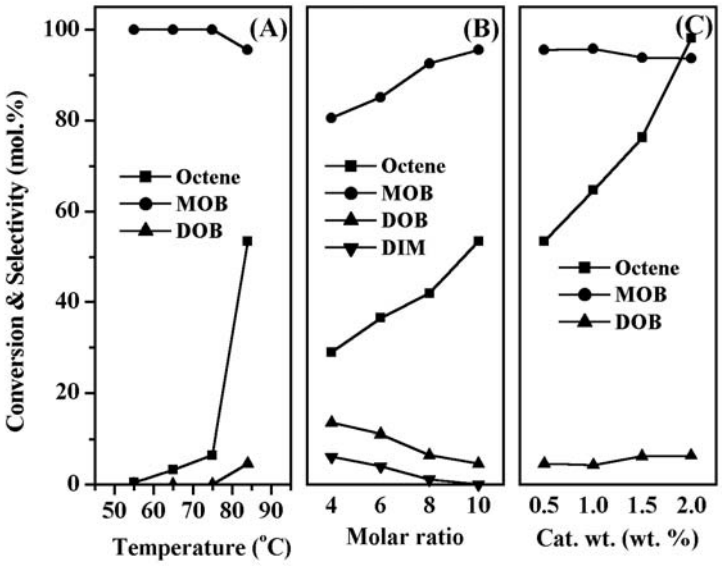

Fig. 4.7: Effect of reaction conditions on the conversion of octene and product selectivity.

(A) Effect of temperature (conditions: total weight = 25 g, catalyst weight = 0.125 g, benzene/1-octene (molar ratio) = 10, time = 1 h).

(B) Effect of molar ratio (conditions: total weight = 25 g, catalyst weight = 0.125 g, temperature = 84 ^{o}C, time = 1 h).

(C) Effect of catalyst weight (conditions: total weight = 25 g, temperature = 84 ^{o}C, benzene/1-octene (molar ratio) = 10, time = 1 h).

The recyclability of 15 TZ-750 catalyst was tested in the alkylation of benzene with 1-octene at 84 ^{o}C (2 wt. % catalyst, 1 h and benzene to octene molar ratio 10). In order to study the recycling, the catalyst after first cycle was separated (with out washing), dried in air at 80 ^{o}C for 4 h and reused with fresh reaction mixture. After first use, the catalyst retained only 30 % of initial conversion. Thermal analysis of the separated catalyst showed a continuous weight loss (3.8 %) in the temperature range of 230-580 ^{o}C, attributed to adsorbed products and alkene oligomers. This result suggests that the loss in catalytic activity is due the blockage of active sites of the catalyst by heavy aromatics and oligomerised octene [28]. The deactivated catalyst can be partially regenerated by refluxing with dichloromethane. The dried catalyst obtained after

refluxing with dichloromethane gave 60 % of initial conversion. After the first recycling, the catalyst was reused twice without appreciable loss in activity, after regeneration. The regeneration was achieved by catalyst separation followed by drying at 120 ^{o}C for 4 h and calcination at 600 ^{o}C for 4 h in presence of air. After 2nd regeneration, the catalyst gave more than 96 % initial conversion.

4.5. 2-Methoxynaphthalene acylation

4.5.1. Introduction

The Friedel–Crafts acylation is a key step in the production of aromatic ketones largely used as intermediates in the fine chemicals and pharmaceutical industry [31]. The conventional synthetic procedure is the Friedel–Crafts acylation in homogeneous phase with carboxylic acid derivatives and Lewis acid anhydrous metal halides like $AlCl_3$ as catalyst. The catalyst is used in more than stoichiometric amount and must be hydrolyzed after the reaction producing large amounts of waste products that cause serious technological and environmental problems. The use of recoverable and regenerable solid acid catalysts can overcome many of these problems [32].

The heterogeneously catalyzed acylation of 2-methoxynapthalene (2-MN) has been the object of several studies because the acylation in 6-position is of particular interest for the production of the anti-inflammatory drug Naproxen (2-(6-methoxy-2-naphthyl) propionic acid, Naproxyn, Syntex) [33]. The acylation of 2-methoxynaphthalene is actively catalyzed by zeolites [34-36], MCM-41 molecular sieves [37], sulfated zirconia [38, 39] and cation-exchanged clays [40]. In all the cases, 1-acetyl-2-methoxynaphthalene was obtained as the major product. The zeolite, H-beta with narrower 12-ring channels and no super cages is shown to be a selective catalyst for the synthesis of 6-acetyl-2-methoxynaohthalene [41-45].

4.5.2. Experimental procedure

The liquid-phase acylation reaction was carried out with zirconia supported-PTA catalyst in a 50 ml glass batch reactor (slurry reactor) with anhydrous $CaCl_2$ guard tube. The reaction temperature was maintained by silicon oil bath equipped with a thermostat and magnetic stirrer. The freshly activated catalyst at 500 ^oC for 2 h, was weighed in the reactor and then 2-MN (s.d. fine chemicals) was added according to the proportion desired. Finally, acetic anhydride (s.d. fine chemicals) was added in order to obtain the desired molar ratio of 2-MN to acetic anhydride. For example, a typical reaction mixture consists of 2 g (12.6 mmol) of 2-MN, 3.86 g of acetic anhydride (37.8 mmol) together with 0.2 g of catalyst. After 2 h, the reaction was stopped and the catalyst separated. The filtrate was analyzed using a Shimadzu 14B gas chromatograph using SE-52 packed column coupled with FID. The product identification was carried out using GC-MS and by comparing with authentic standards.

4.5.3. Results and discussion

The acylation of 2-MN with acetic anhydride (Ac_2O) over zirconia-supported PTA catalyst leads to the formation of 1-acetyl-2-methoxynaphthalene as the acylated product as shown in Scheme 4.2. The conversion was expressed as the percentage of 2-MN converted into the product and the conversion of 2-MN on PZ catalysts with various PTA loading calcined at 750 ^oC are shown in Fig. 4.8A. For catalysts with different PTA loading calcined at 750 ^oC, the conversion of 2-MN increased with loading and reached maximum at 15 % PTA and decreased further. Interestingly, the conversion of BA was found to depend strongly on the calcination temperature of the catalyst. For instance, catalyst with 15 % PTA loading calcined from 650 to 850 ^oC, were used in the reaction and the results are sown in Fig. 8B. The conversion increased with calcination temperature and reached maximum at 750 ^oC and decreased further. It is also interesting to note that acidity measurements of the catalysts by FTIR pyridine adsorption and NH_3-TPD showed that 15 PZ-750 catalyst possess the highest total acidity as well as Brönsted acidity and hence the acylation of 2-MN by acetic anhydride is catalyzed by Brönsted acid sites present in the supported catalyst.

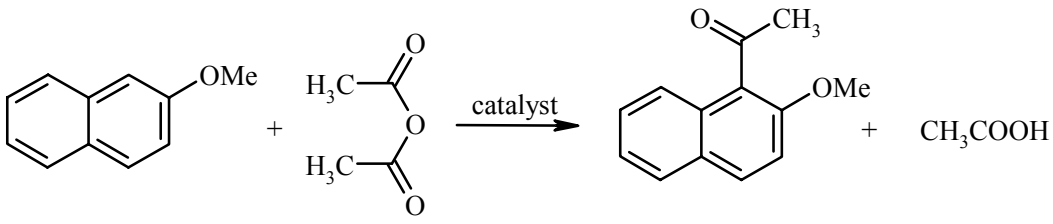

Scheme 4.2

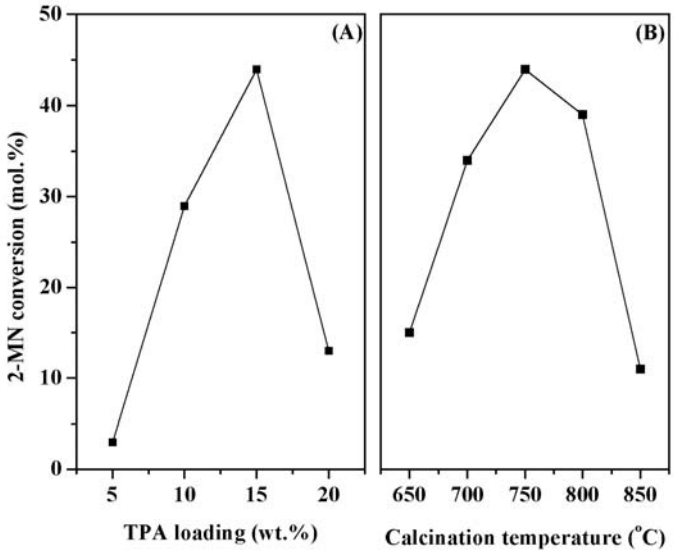

Fig. 4.8: **Change in the conversion of 2-MN for catalysts with (A) different PTA loading calcined at 750 ^{o}C and (B) 15 PZ calcined at different temperature (conditions: temperature = 120 ^{o}C, total weight = 5.86 g, Ac_2O/2-MN (molar ratio) = 3, catalyst weight = 0.2 g, time = 2 h).**

Thus, the catalyst with highest activity (15 PZ-750) was used to study different reaction parameters. The influence of temperature on the conversion of 2-MN was studied in the temperature range of 60 to 130 ^{o}C for 2 h (Fig. 4.9A). At 60 ^{o}C, the conversion was 26 %, which increased to 55 % at 130 ^{o}C. The influence of Ac_2O/2-MN molar ratio (1 to 10) on the conversion of 2-MN was studied keeping the total weight of the reaction mixture constant (Fig. 4.9B). At a molar ratio of 1, conversion of 2-MN was 37 %, which increased to 56 % at a molar ratio of 5. Further increase in molar ratio, decreased the conversion of 2-MN. This is probably due to the inhibiting effect of 1-acetyl-2-methoxynaphthalene, which can be strongly adsorbed on the catalyst surface. This inhibiting effect would be less significant for mixtures richer in Ac_2O, because the excess of Ac_2O acts as a solvent for the ketone produced, product inhibition is reduced,

and therefore the conversion of 2-MN is higher at higher Ac_2O/2-MN molar ratio [46]. The decrease in conversion above Ac_2O/2-MN molar ratio of 5 could be due to dilution effect. The influence of catalyst weight on the conversion of 2-MN showed that the conversion of 2-MN increased linearly with catalyst concentration up to 6.8 wt. % (of the total weight of the reactants), which could be due to increase in the number of active sites of the catalyst (Fig. 4.9C).

The effect of time on the conversion of 2-MN showed a clear deactivation by reaching a plateau between 120 and 540 min. before giving maximum conversion (Fig. 4.10), where the catalyst deactivation was mainly attributed to the strong adsorption of the acylation product on the catalyst surface which block the accessibility of the reactants to the active sites. Since, heteropoly acids are soluble in polar solvents, it is important to study the heterogeneity of the catalyst in the reaction. For this, the reaction was stopped at 10 min. and the catalyst was separated under hot conditions and the hot filtrate was monitored for further reaction up to 6 h. It is apparent from Fig. 4.10, that no change in the conversion of 2-MN with time for filtrates obtained from 15 PZ-750 catalyst, indicated the heterogeneous nature of the reaction.

In order to study the recycling, the catalyst after reaction (120 ^{o}C, 0.2 g catalyst, 2 h and 3:1 molar reactants ratio) was separated, washed with dichloromethane, dried at 120 ^{o}C for 4 h and reused with fresh reaction mixture. After first use, the catalyst retained only 50 % of initial conversion. The lower activity of the separated catalyst may be due to the presence of surface bound acetate species formed from the by-product acetic acid, which is difficult to remove by washing [47, 48]. However, the catalytic activity was increased to 97 % of initial activity after regeneration of the catalyst by calcination at 500 ^{o}C for 4 h.

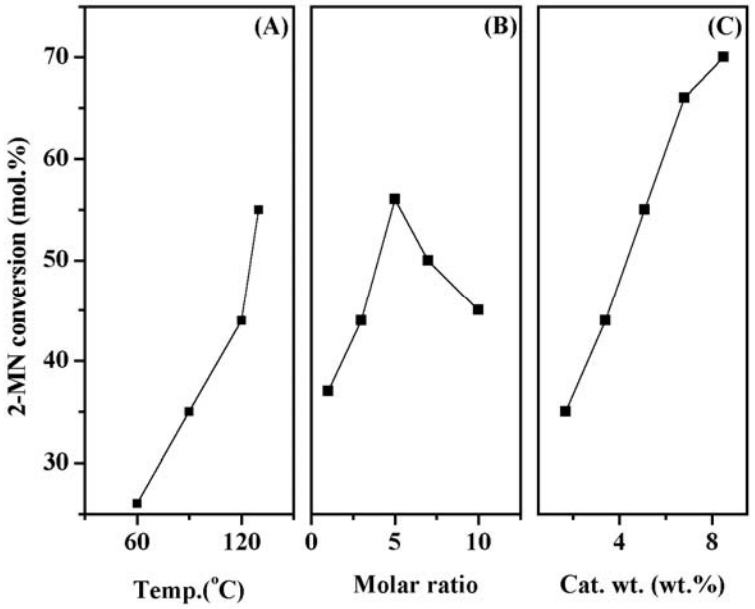

Fig. 4.9: Effect of reaction conditions on the conversion of 2-MN.

(A) Effect of temperature (conditions: total weight = 5.86 g, catalyst weight = 0.2 g, acetic anhydride/2-MN (molar ratio) = 3, time = 2 h).

(B) Effect of molar ratio (conditions: total weight = 5.86 g, catalyst weight = 0.2 g, temperature = 120 ^{o}C, time = 2 h).

(C) Effect of catalyst weight (conditions: total weight = 5.86 g, temperature = 120 ^{o}C, acetic anhydride/2-MN (molar ratio) = 3, time = 2 h).

4.6. Comparison of the activities of 15 SZ-750 and 15 PZ-750 catalysts

The activity of zirconia-supported STA and PTA catalysts having highest catalytic activities, 15 SZ-750 and 15 PZ-750 catalysts were compared in benzoylation of veratrole with benzoic anhydride (Fig. 4.11A) and alkylation of diphenyl ether with 1-dodecene (Fig. 4.11B). In veratrole benzoylation, 15 SZ-750 catalyst showed different reaction profile from that of 15 PZ-750 catalyst, where as in the alkylation diphenyl ether both catalysts showed similar reaction profile and 15 SZ-750 catalyst had higher activity than 15 PZ-750 catalyst. Since, heteropoly acids are soluble in polar solvents, it is important to study the heterogeneity of the catalysts in the reaction. For this, the reaction was stopped after 15 min. and the catalyst is separated under hot conditions and the hot filtrate is monitored for further reaction. From Fig. 4.11, it is apparent that no change in

conversion with time for filtrates obtained from 15 SZ-750 and 15 PZ-750 catalysts and this clearly indicate that STA and PTA on zirconia act as heterogeneous catalysts.

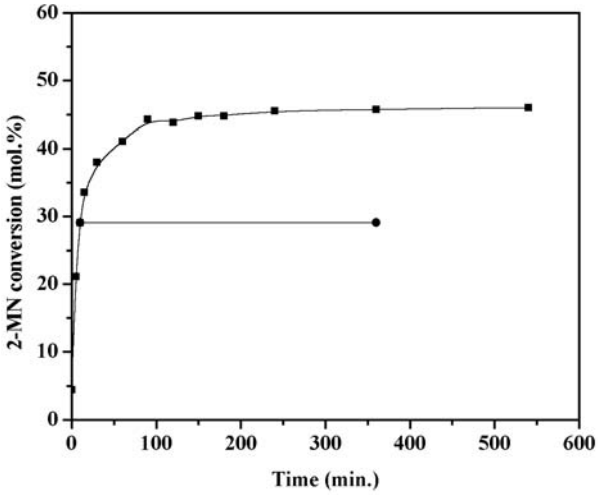

Fig. 4.10: Effect of time on the conversion of 2-MN over 15 PZ-750 catalyst where ■ stands for reaction with fresh catalyst and • reaction after catalyst separation by hot filtration (conditions: temperature = 120 ^{o}C, total weight = 5.86 g, acetic anhydride/2-MN (molar ratio) = 3, catalyst weight = 0.2 g).

However, it is interesting to note that both the heterogeneous catalysts, 15 SZ-750 and 15 PZ-750 showed different catalytic behavior in veratrole benzoylation. For the 15 SZ-750 catalyst, conversion of benzoic anhydride, BA increased continuously with time and reached 76 % after 480 min. while, for 15 PZ-750 catalyst, a clear deactivation occurred by reaching a plateau between 240 and 480 min. before giving maximum conversion. This reaction profile, particularly with 15 PZ-750 catalyst, is similar to that reported for zeolites [49-51] and heteropoly acids [47, 52-54] catalyzed acylation reactions, where the catalyst deactivation is mainly attributed to the strong adsorption of the acylation product on the catalyst surface which block the accessibility of the reactants to the active sites. The kinetic profile of the reaction with 15 SZ-750 and 15 PZ-750 catalysts indicated that product inhibition is more prominent with 15 PZ-750 catalyst [Fig. 4.11A].

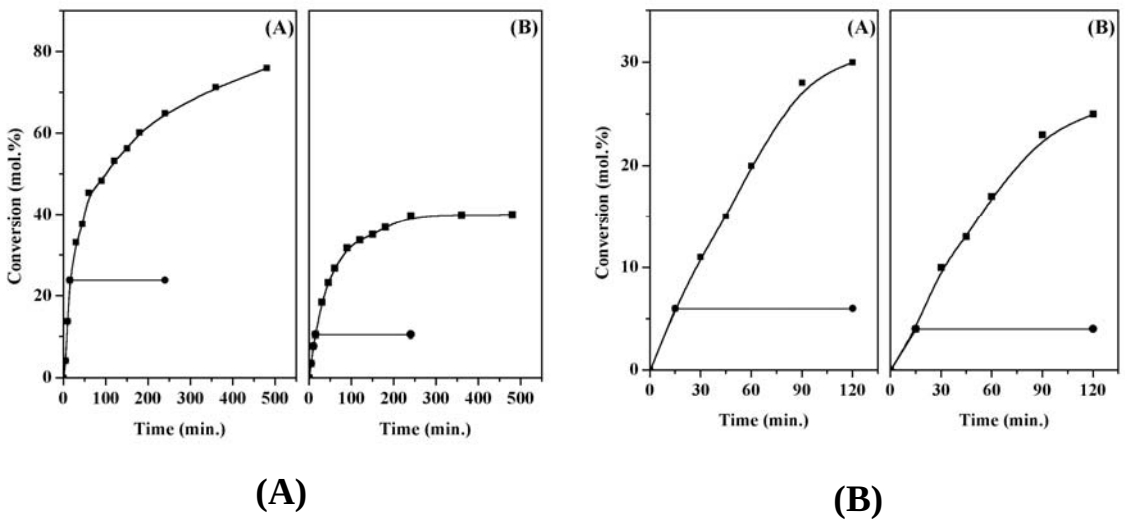

Fig. 4.11: (A) Effect of time on the conversion of BA over the catalysts (A) 15 SZ-750, (B) 15 PZ-750 (conditions: temperature = 80 ^{o}C, total weight = 5 g, veratrole/BA (molar ratio) = 5, catalyst weight = 0.15 g) and **(B)** Effect of time on the conversion of dodecene over the catalysts (A) 15 SZ-750, (B) 15 PZ-750 (conditions: temperature = 90 ^{o}C, total weight = 10 g, diphenyl ether/1-dodecene (molar ratio) = 10, catalyst weight = 0.30 g) where ■ stands for reaction with fresh catalyst and • reaction after catalyst separation by hot filtration.

In order to explain the difference in the catalytic behavior, the catalysts were characterized by different methods. The surface area, tungsten surface density, XRD and Raman spectra of the catalysts were found to be similar for both the catalysts. Absorption edge energy of 15 PZ-750 catalyst (3.7 eV) was found to be slightly higher than that of 15 SZ-750 catalyst (3.57 eV). NH_3-TPD showed that 15 PZ-750 catalyst has slightly higher acidity than that of 15 SZ-750. However, FTIR pyridine adsorption revealed that the Lewis acidity of 15 PZ-750 catalyst was higher than 15 SZ-750 (Table 4.5). Anderson et al. have reported that the catalyst with higher Lewis acidity is more susceptible for deactivation by product inhibition [47]. Thus, the higher conversion and greater deactivation resistance of 15 SZ-750 catalyst in veratrole benzoylation could be due to the presence of higher amount of strong Brönsted acid sites. Similarly, the higher activity of 15 SZ-750 catalyst in diphenyl ether alkylation (30 % dodecene conversion) in comparison with 15 PZ-750 (25 % dodecene conversion) also could be explained on the basis of its higher Brönsted acidity.

[a]**Table 4.5:** Pyridine adsorption data for 15 SZ-750 and 15 PZ-750 catalysts at different activation temperatures.

Activation temperature (^{o}C)	**B acidity *I*(B)**	**L acidity *I*(L)**	**B/L ratio *I*(B)/*I*(L)**
100	0.19	0.14	1.36
	(0.15)	(0.17)	(0.88)
200	0.16	0.09	1.78
	(0.16)	(0.12)	(1.33)
300	0.10	0.04	2.50
	(0.09)	(0.06)	(1.5)
400	0.05	0	[b]n. e.
	(0.08)	(0.03)	(2.67)

[a] For 15 PZ-750 catalyst, B, L and B/L values are indicated in bracket
I is absorbance intensity
[b] not evaluated.

4.7. References

1. E. Lopez-Salinas, J.G. Hermandez-Cortez, I. Schifter, E. Torres-Garcia, J. Navarrete, A. Gutierrez-Carrillo, T. Lopez, P.P. Lottici, D. Bersani, Appl. Catal. A 193 (2000) 215.
2. A. Khodakov, J. Yang, S. Su, E. Iglesia, J. Catal. 177 (1998) 343.
3. JCPDS-International Center for diffraction data, 1990, Card 43-1035.
4. I.V. Kozhevnikov, Catalysts for Fine Chenical Synthesis. Vol. 2. Catalysis by polyoxometalates, Wiley & Sons, Ltd., 2002. p. 15.
5. J.B. Moffat, Catalysis by Acids and Bases, Elsevier, Amsterdam, 1985, p. 157.
6. B.H. Davis, R.A. Keogh, S. Alerasool, D.J. Zalewski, D.E. Day, P.K. Doolin, J. Catal. 183 (1999) 45.
7. M. Misono, Chem. Commun. (2001) 1141.
8. C.J. Dillon, J.H. Holles, R.J. Davis, J. A. Labinger, M.E. Davis, J. Catal. 218 (2003) 54.
9. A. Ghanbari-Siahkali, A. Philippou, J. Dwyer, M.W. Anderson. Appl. Catal. A 192 (2000) 57.
10. A. Molnar, T. Beregszaszi, A. Fudala, P. Lentz, J.B. Nagy, Z. Konya, I. Kiricsi J. Catal. 202 (2001) 379.
11. S. Uchida, K. Inumaru, M. Misono, J. Phys. Chem. B 104 (2000) 8108.
12. B.M. Devassy, S.B. Halligudi, S.G. Hegde, A.B. Halgeri, F. Lefebvre, Chem. Commun. (2002) 1074.
13. I.M. Smallwood, Handbook of organic solvent properties, Arnold, London NW1 3BH, 1996.
14. C. Rocchiccioli-Deltcheff, M. Fournier, R. Franck, R. Thouvenot Inorg. Chem. 22 (1983) 207.
15. M. Fournier, R. Thouvenot, C. Rocchiccioli-Deltcheff, J. Chem. Soc. Faraday Trans. 87 (1991) 349.
16. G. Zukowska, J.R. Stevens, K.R. Jeffrey, Electrochem. Acta. 48 (2003) 2157.
17. Y. Hirano, K. Inumaru, T. Okuhara, M. Misono, Chem Lett. (1996) 1111.
18. A.A. Parks, Chem. Rev. 65 (1965) 177.
19. G.B. McGarvey, J.B. Moffat, J. Mol. Catal.69 (1991) 137.

20. M. Valigi, D. Gazzoli, G. Ferraris, E. Bemporad,
Phys. Chem. Chem. Phy. 5 (2003) 4974.
21. L.C.W. Baker, D. Glick, Chem. Rev. 98 (1998) 3.
22. J.A. Kocal, B.V. Vora, T. Imai, Appl. Catal. A 221 (2001) 295.
23. A. Corma, Chem. Rev. 95 (1995) 559.
24. A. Corma, H. Garcia, Chem. Rev. 103 (2003) 4307.
25. S. Sivasankar, A. Thangaraj, J. Catal.138 (1992) 386.
26. J.L.B. Tejero, A.M. Danvila, US Patent 5 146 026 (1992) to Petroquimica Espanola, S.A. Petresa.
27. R.T. Sebulsky, A.M. Henke, Ind. Eng. Chem. Process Res. Dev. 10 (1971) 272.
28. J.H. Clark, G.L. Monks, D.J. Nightingale, P.M. Price, J.F. White,
J. Catal. 193 (2000) 348.
29. C. DeCastro, E. Sauvage, M.H. Valkenberg, W.F. Hölderich,
J. Catal. 196 (2000) 86.
30. J.LG. de Almeida, M. Dufaux, Y. Ben Tarrit, C. Naccache,
J. Am. Oil Chem. Soc. 71, 7 (1994) 675.
31. G.A. Olah, Friedel-Crafts and Related Reactions, Vol. III, Interscience,
New York, 1964.
32. K. Tanabe, W.E. Hölderich, Appl. Catal. A 181 (1999) 399.
33. P.J. Harrington, E. Lodewijk, Org. Proc. Res. Dev. 1 (1997) 72.
34. G. Harvey, G. Mäder, Collect. Czech. Chem. Commun. 57 (1992) 862.
35. G. Harvey, G. Binder, R. Prins, in: H.K. Beyer et al. (Eds.),
Stud. Surf. Sci. Catal.94 (1995) 397.
36. G.D. Yadav, M.S. Krishnan, in: T.S.R.P. Rao et al. (Eds.),
Stud. Surf. Sci. Catal. 113 (1998) 259.
37. E.A. Gunnewegh, S.S. Gopie, H. van Bekkum, J. Mol. Catal. A 106 (1996) 151.
38. G.D. Yadav, M.S. Krishnan, Chemical Engineering Sciene 54 (1999) 4189.
39. J. Deutsch, H.A. Prescot, D. Müller, E. Kemnitz, H. Lieske,
J. Catal. 231 (2005) 269.
40. B.M. Choudary, M. Sateesh, M.L. Kantam, K.V.R. Prasad,
Appl. Catal. A 171 (1998) 155.
41. P. Andy, J. Garcia-Martinez, G. Lee, H. Gonzalez, C. W. Jones, M. E. Davis,

J. Catal. 192 (2000) 215.
42. D. Das, S. Cheng, Appl. Catal. A 201 (2000) 159.
43. M. Casagrande, L. Storaro, M. Lenarda, R. Ganzerla,
Appl. Catal. A 201 (2000) 263.
44. S.D. Kim, K.H. Lee, J.S. Lee, Y.G. Kim, K.E. Yoon
J. Mol. Catal. A 152 (2000) 33.
45. H.K. Heinichen and W. F. H olderich, J. Catal. 185 (1999) 408.
46. E.G. Derouane, G. Crehan, C.J. Dillon, D. Bethell, H. He,
S.B. Derouane-Abd Hamid, J. Catal. 194 (2000) 410.
47. B. Bachiller-Baeza, J.A. Anderson, J. Catal. 228 (2004) 225.
48. A. Trunschke, J. Deutsch, D. Müller, H. Lieske, V. Quaschning,
E. Kemnitz, Catal. Lett. 83 (2002) 271.
49. D. Rohan, C. Canaff, E. Fromentin, M. Guisnet, J. Catal. 177 (1998) 296.
50. E.G. Derouane, C.J. Dillon, D. Bethell, S.B. Derouane-Abd Hamid,
J. Catal 187 (1999) 209.
51. E.G. Derouane, G. Crehan, C.J. Dillon, D. Bethell, H. He,
S.B. Derouane-Abd Hamid, J. Catal. 194 (2000) 410.
52. J. Kaur, K. Griffin, B. Harrison, I.V. Kozhevnikov,
J. Catal. 208 (2002) 448.
53. I.V. Kozhevnikov, Appl. Catal. A 256 (2003) 3.
54. L.A.M. Cardoso, W.A. Jr, A.R.E. Gonzaga, L.M.G. Aguiar,
H.M.C. Andrade, J. Mol. Catal. A 209 (2004) 189.

Chapter 5

Zirconia-supported phosphomolybdic acid

5.1. Introduction

This section deals with the characterization of zirconia-supported phosphomolybdic acid (PMA) catalysts by X-ray diffraction, and ^{31}P MAS NMR spectroscopy and the nature of acidic sites present in the most active catalyst by FTIR pyridine adsorption spectroscopy. These catalysts were used in the synthesis of linear alkyl benzenes by alkylation of benzene with higher linear alkenes such as 1-octene and 1-dodecene and alkylation of phenol with *tert*-butanol.

5.2. Preparation

The zirconia-supported phosphomolybdic acid catalysts were prepared by the procedure given in Section 2.2. These catalysts were represented by x MZ-T, where x represents wt. %, M represents PMA, Z represents zirconia and T denotes calcination temperature (^oC).

For comparison, a catalyst with 15 % MoO_3 on ZrO_2 calcined at 700 ^oC (15 Mo-700) was prepared by wet impregnation of zirconium oxyhydroxide with an aqueous solution of ammonium heptamolybdate (s.d. fine chemicals), followed by drying and calcination.

5.3. Catalyst characterization - Results and discussion

5.3.1. X-ray diffraction

The XRD pattern of the catalysts with different PMA loading calcined at 700 ^oC (Fig. 5.1A) showed the presence of PMA strongly influences the crystallization of zirconium oxyhydroxide into zirconia. Pure zirconia calcined at 700 ^oC is mainly monoclinic with small amount of the tetragonal phase. For catalysts with low PMA loading calcined at 700 ^oC, the XRD pattern could be described as the sum of the monoclinic and tetragonal phases of zirconia, this latter phase becoming dominant for catalyst with 15 % PMA. This can be explained as the strong interaction of PMA with the support reduces the surface diffusion of zirconia, inhibits sintering and stabilizes the tetragonal phase of zirconia. It could be seen that up to a 15 % PMA loading, no diffraction lines, which could be attributed to the polyacid or to its decomposition products, were observed. The 20 MZ-700 catalyst showed the presence of new diffraction

lines characteristic of MoO_3 and for 25 % catalyst, formation of $ZrMo_2O_8$ was observed. This indicated that, PMA decomposed to molybdenum oxide, forming relatively large particles and also reacting with the support forms $ZrMo_2O_8$.

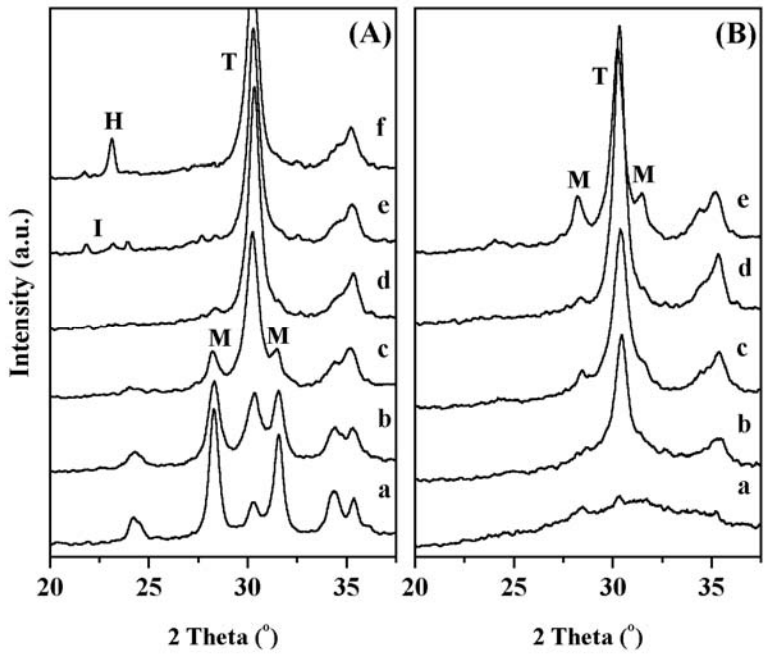

Fig. 5.8: X-ray diffractograms (A) a) ZrO_2, b) 5, c) 10, d) 15, e) 20, f) 25 MZ-700 catalysts; (B) 15 MZ catalyst calcined at a) 400, b) 500, c) 600, d) 700, e) 750 ^oC and f)15 Mo-700 catalyst. T = tetragonal ZrO_2, M = monoclinic ZrO_2, I = MoO_3, H = $ZrMo_2O_8$.

As shown in Fig. 5.1B, 15 % catalyst was amorphous, when it was calcined below 400 ^oC and the crystalline nature of zirconia increased with calcination temperature. As the calcination temperature increased from 500 to 700 ^oC, zirconia crystallized to tetragonal phase and at 750 ^oC, the formation of monoclinic phase was indicated. Such stabilization of tetragonal ZrO_2 in presence of other heteropoly acids has been known in literature [1, 2]. For comparison, the XRD of 15 % molybdenum oxide supported on zirconia calcined at 700 ^oC (15 Mo-700) was recorded and it showed the stabilization of ZrO_2 in tetragonal phase together with the formation of small amount of $ZrMo_2O_8$ [3].

5.3.2. ^{31}P MAS NMR spectroscopy

This is one of the most important characterization techniques to study the state of phosphorous in heteropoly acids. The bulk PMA showed a sharp intense peak at –3.5 ppm in the ^{31}P MAS NMR spectrum, due to the uniform phosphorous environment in highly hydrated structure of the PMA. The small peak observed nearer to the main peak at 6.3 ppm might be due to the part of the sample containing different degrees of

hydration [4]. The ^{31}P MAS NMR spectra of catalysts with 5 to 25 % PMA calcined at 700 ^{o}C and 15 % PMA calcined between 600 to 750 ^{o}C shows that the state of phosphorous in catalysts depend on PMA loading and calcination temperatures. The spectra of catalysts with different PMA loading are shown in Fig. 5.2A. For 5 % PMA catalyst, NMR showed a peak at –8.6 ppm assigned to the presence of phosphomolybdate, which is in interaction with zirconia [5, 6]. However, when the PMA loading increased to 10 %, NMR showed peaks at –3.5 ppm, -8.2 ppm and 18 ppm, respectively. The peak at –3.5 ppm is assigned to microcrystalline PMA, similar to the unsupported PMA [6, 7] and the chemical shift at –8.2 ppm is due to PMA interacting strongly with the zirconia surface. The origin of the peak at 18 ppm is not clear at present. For catalysts with 15 % PMA loading and above, an additional peak at –30 ppm was observed, which is attributed to phosphorous oxide (P-O-P) resulting from the decomposition of the polyoxometalate [8]. However, 15 MZ-700 catalyst gave the highest conversion of octene and the ^{31}P CPMAS NMR spectrum of this catalyst showed the peak at –8.5 ppm due to the presence of PMA strongly interacting with zirconia surface (Fig. 5.2C).

The ^{31}P MAS NMR spectra of 15 MZ catalyst calcined between 500-750 ^{o}C are shown in Fig. 5.2B. At a calcination temperature of 500 ^{o}C, NMR spectrum showed two peaks, one at –8 ppm and the other at 17.2 ppm. As the calcination temperature was increased to 600 ^{o}C, NMR spectrum showed peaks at –3.5 ppm, –8.2 ppm and 18 ppm, similar to the NMR spectrum of 10 MZ-700 catalyst and 15 MZ-750 catalyst showed a sharp peak at –30 ppm.

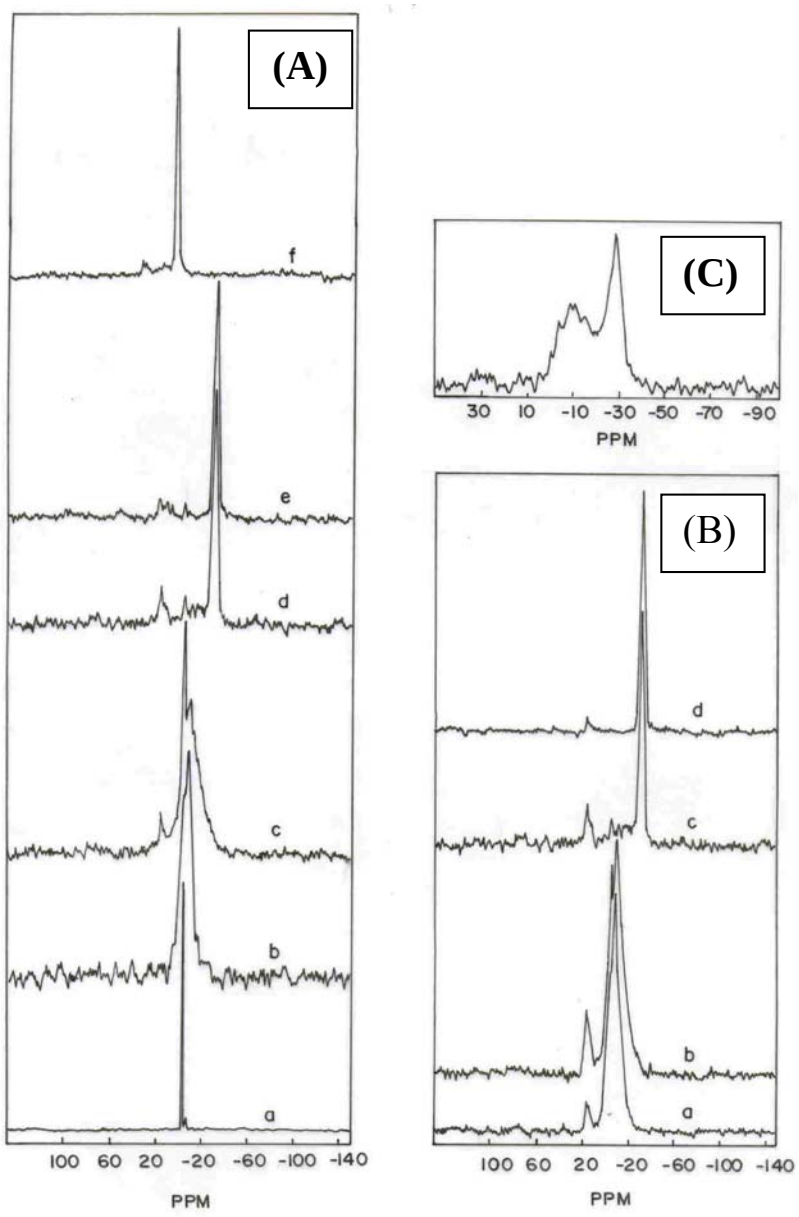

Fig. 5.9: ^{31}P MAS NMR spectra of (A) catalysts with different PMA loading a) pure PMA, b) 5 MZ-700, c) 10 MZ-700, d) 15 MZ-700, e) 20 MZ-700, f) 25 MZ-700; (B) 15 MZ catalyst calcined at different temperature a) 500, b) 600, c) 700, d) 750 ^{o}C; (C) ^{31}P CP MAS NMR spectrum of 15 MZ-700 catalyst.

5.3.3. FTIR pyridine adsorption

FTIR spectra of pyridine adsorbed on 15 MZ-700 catalyst recorded from 100 to 400 ^{o}C are shown in Fig. 5.3A. At 100 ^{o}C, important pyridine ring modes occur at approximately 1609, 1579, 1487 and 1443 cm^{-1} termed 8a, 8b, 19a and 19b, respectively [9, 10]. In addition to these modes of vibrations, spectra showed two peaks at 1637 and 1535 cm^{-1}. The peak at 1579 cm^{-1} was found to be very labile and its stability on the surface was temperature dependant. When the temperature was increased to 200 ^{o}C, this peak almost disappeared, confirming its labile nature and hence, it is concluded that these species are bound to the surface OH groups *via* H-bonding. Pyridine molecules bonded to Lewis acid sites absorbed at 1609 and 1443 cm^{-1} (ascribed to the 8a and 19b-ring mode of pyridine), while those responsible for Brönsted acid sites (pyridinium ion) showed absorbance at 1535 cm^{-1} and at 1637 cm^{-1} [11]. The band at 1487 cm^{-1} (19a-ring mode of pyridine) is a combined band originating from pyridine bonded to both Brönsted and Lewis acid sites. The Brönsted/Lewis (B/L) site ratio was calculated from the IR absorbance intensities of bands at 1536 and 1442 cm^{-1} [12], respectively and is shown in Fig. 5.3B. The results indicated that an increase of activation temperature decreased both Brönsted and Lewis acidity but an overall increase in Brönsted character of the catalyst up to an activation temperature of 300 ^{o}C. This clearly indicates the presence of strong Brönsted acid sites in the catalyst.

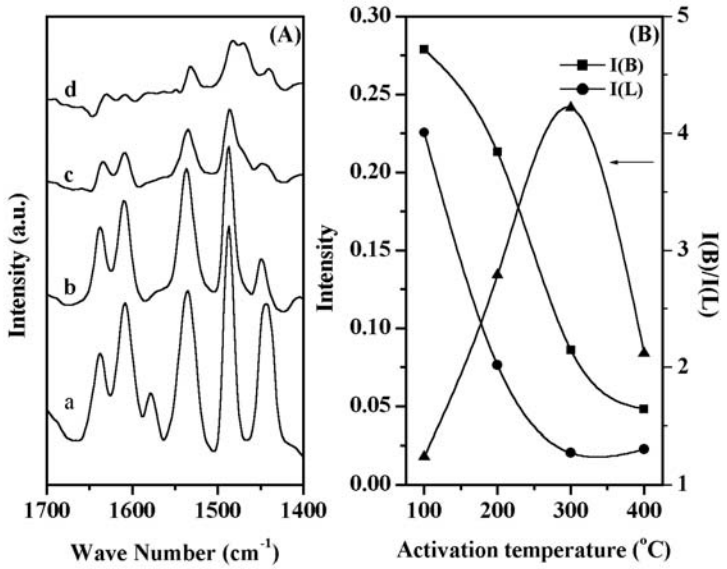

Fig. 5.10: The IR spectra of pyridine adsorbed on 15 % catalyst after *in-situ* activation at a) 100, b) 200, c) 300, and d) 400 ^{o}C.

5.4. Alkylation of benzene

General introduction to linear alkyl benzenes (LAB) and the procedure to carry out alkylation of benzene with higher linear olefins are given in section 4.4.1, 4.4.2 respectively and the formation of different reaction products are shown in Scheme 4.1.

5.4.1. Results and discussion

Zirconia-supported PMA catalysts were used in alkylation of benzene with 1-octene. The main reactions occurred with these catalysts were double bond shift isomerization of alkene and alkylation of benzene. Monooctyl benzene (MOB) was the major product of alkylation, whereas dioctyl benzene (DOB) appeared as minor product. The conversion is expressed as the percentage of alkene converted into alkylated products. The effect of PMA loading on conversion of octene and product selectivity is shown in Fig. 5.4A. The 5 MZ-700 catalyst showed 3 % conversion and the conversion increased to a maximum of 53 % with 15 MZ-700 catalyst under the reaction conditions studied.

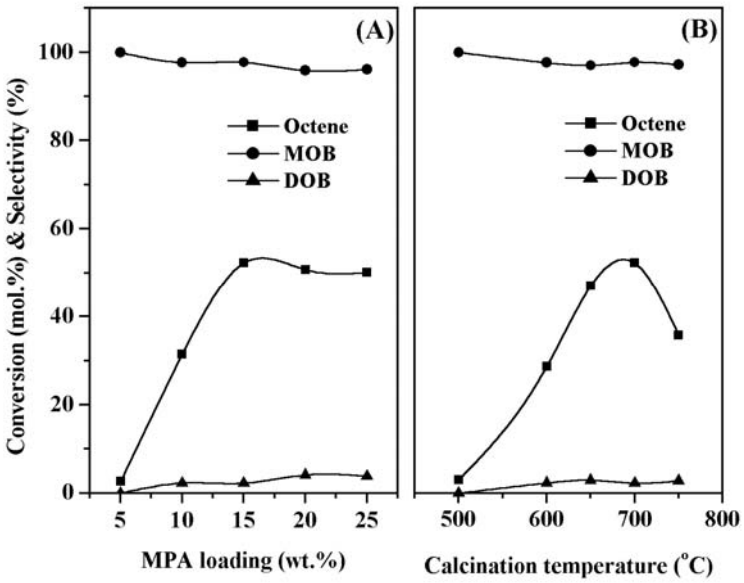

Fig. 5.11: The conversion of octene and product selectivity over various catalysts. (conditions: total weight = 25 g, catalyst weight = 0.125 g, temperature = 83 ^{o}C, benzene/1-octene (molar ratio) = 10, time = 1 h).

To study the effect of calcination temperature on conversion of octene and product selectivity, 15 MZ catalyst calcined between 500 and 750 ^{o}C were used. The catalyst calcined at 500 ^{o}C showed 3 % conversion of octene and conversion increased to 52 % at a calcination temperature of 700 ^{o}C (Fig. 5.4B). The selectivity to mono and dialkylated products was found to be independent on PMA loading and calcination temperature and all the catalysts gave more than 95 % mono-alkylation selectivity. For comparison, alkylation of benzene with 1-octene was also carried out using 15 Mo-700 catalyst and it showed an octene conversion of 30 % with 96 % MOB selectivity and 4 % DOB selectivity under the same reaction conditions. Thus, 15 MZ-700 catalyst was nearly two times more active than 15 Mo-700 catalyst. This clearly indicates that the higher activity of 15 MP-700 catalyst compared to 15 Mo-700 is due to the presence of PMA in the catalyst.

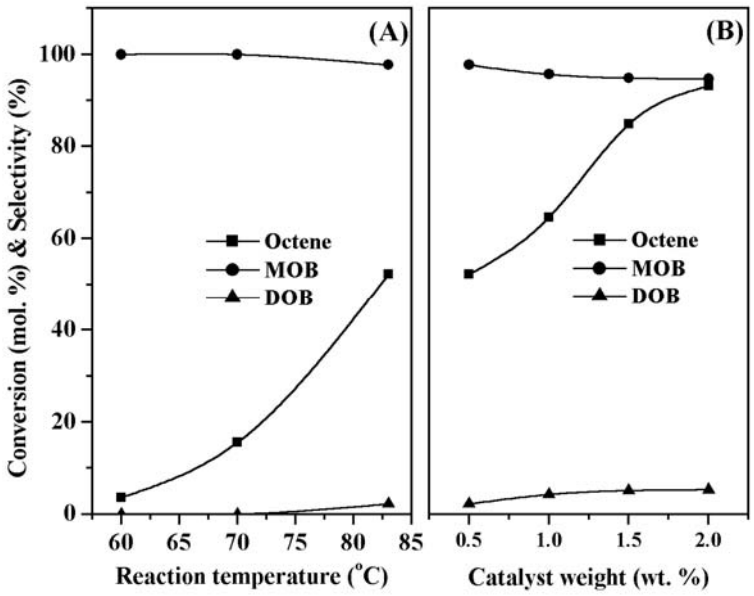

Fig. 5.12: Effect of reaction conditions on the conversion of octene and product selectivity.
(A) Effect of temperature (conditions: total weight = 25 g, catalyst weight = 0.125g, benzene/1-octene (molar ratio) = 10, time = 1 h).
(B) Effect of catalyst weight (conditions: total weight = 25 g, temperature = 83 ^{o}C, benzene/1-octene (molar ratio) = 10, time = 1 h).

Therefore, the catalyst with optimum PMA loading (15 %) and calcination temperature (700 ^{o}C) was taken to study the influence of different reaction parameters on

the conversion of octene of and products selectivity. The influence of temperature was studied in the range 60 to 83 ^{o}C, keeping other conditions similar. The results indicated that the temperature has a profound effect on the conversion of octene (Fig. 5.5A). At 60 ^{o}C, the conversion was 4 % and it increased to 16 % at 70 ^{o}C. An increase of 37 % conversion of octene was observed when the temperature was increased from 70 to 83 ^{o}C (boiling point of the reaction mixture, 83-84 ^{o}C).

The effect of catalyst concentration on the conversion of octene showed that 0.5 wt. % (of the total mass of the reactants) of catalyst gave 53 % conversion of octene and increased to 93 % with 2 wt. % catalyst, with similar MOB selectivity (Fig. 5.5B). The increase in conversion with increasing catalyst concentration is due to the proportional increase in the number of active sites.

Thus, under the reaction conditions of 83 ^{o}C, 1 h and benzene/olefin molar ratio of 10, alkylation of benzene with 1-octene gave 93 % conversion of octene with 95 % MOB selectivity (isomer distribution 55 % 2-PO, 25 % 3-PO and 20 % 4-PO) and 5 % DOB selectivity.

Similarly, alkylation of benzene with 1-dodecene was carried under the reaction conditions of 83 ^{o}C, 1 h and benzene/ olefin molar ratio of 10. The 5 wt. % catalyst of the total reaction mixture gave 91 % conversion of dodecene, with the MDB isomer distribution of 45 % 2-PD, 20 % 3-PD, 12 % 4-PD and 23 % 5+6 PD.

The recyclability of 15 MZ-700 catalyst was tested in the alkylation of benzene with 1-octene at 83 ^{o}C (2 wt. % catalyst, 1 h and 10:1 molar reactants ratio). In order to study recycling, the separated catalyst after first cycle was refluxed with dichloromethane to remove adsorbed products and alkene oligomers [2] and dried in air at 120 ^{o}C for 4 h. This catalyst was reused with fresh reaction **mixture and was found to be completely inactive after first use. The loss in catalytic activity is due the reduction of PMA during reaction as indicated by the color change of the catalyst from light yellow to dark blue after reaction [13]. However, the deactivated catalyst could be regenerated by thermal methods and the regeneration was achieved by calcination of the separated catalyst at 500 ^{o}C for 3 h in air. After the first use, the regenerated catalyst was reused twice without appreciable loss in activity.**

5.5. Phenol *tert*-butylation

General introduction to phenol *tert*-butylation and the procedure to carry out alkylation of phenol with *tert*-butanol are given in section 3.5.1, 3.5.2 respectively and the formation of different reaction products are shown in Scheme 3.2.

5.5.1. Results and discussion

The main products of the *tert*-butylation of phenol were 2-*tert*-butyl phenol (2-TBP), 4-*tert*-butyl phenol (4-TBP), 2,4-di-*tert*-butyl phenol (2,4-DTBP) and *tert*-butyl phenyl ether (TBPE). The products like 2,6-di-*tert*-butyl phenol and 2,4,6-tri-*tert*-butyl phenol (TTBP) were formed in small amount. C_8 and C_{12} olefins, formed by the olegomerization of isobutene were also observed in the reaction, where isobutene was formed by the acid catalyzed dehydration of *tert*-butanol.

5.5.1.1. Effect of PMA loading

In order to investigate the effect of PMA loading, catalysts with 5-25 % PMA on zirconia calcined at 700 ^{o}C were used in alkylation of phenol with *tert*-butanol at 120 ^{o}C with a space velocity of 4 h^{-1} (Fig. 5.6). The 5 MZ-700 catalyst showed the lowest conversion of phenol 41.9 %, while 15 MZ-700 catalyst gave the highest conversion 64.6 %. Further increase in PMA loading decreased the conversion of phenol and for 25 % catalyst it was 60.8 %.

The selectivity to different alkylated products also depended on PMA loading. The 5 MZ-700 catalyst showed the highest selectivity to TBPE. As the conversion of phenol increased from 51.9 % for 5 % catalyst to 64.6 % for 15 % catalyst, the selectivity to TBPE decreased from 10.3 to 1.6 %. The 5 % catalyst showed 2-TBP selectivity of 25 % and 4-TBP selectivity of 21.1 %. When PMA content was increased to 10 %, the selectivity to 2-TBP was decreased to 20.2 %, while selectivity to 4-TBP was similar to that of 5 % catalyst. The catalysts with higher PMA content gave products with similar selectivity to 2-TBP and 4-TBP as that of 10 % catalyst. The selectivity to 2,4-DTBP increased up to 15 % PMA loading (52.2 %) and further increases in PMA loading decreased its selectivity.

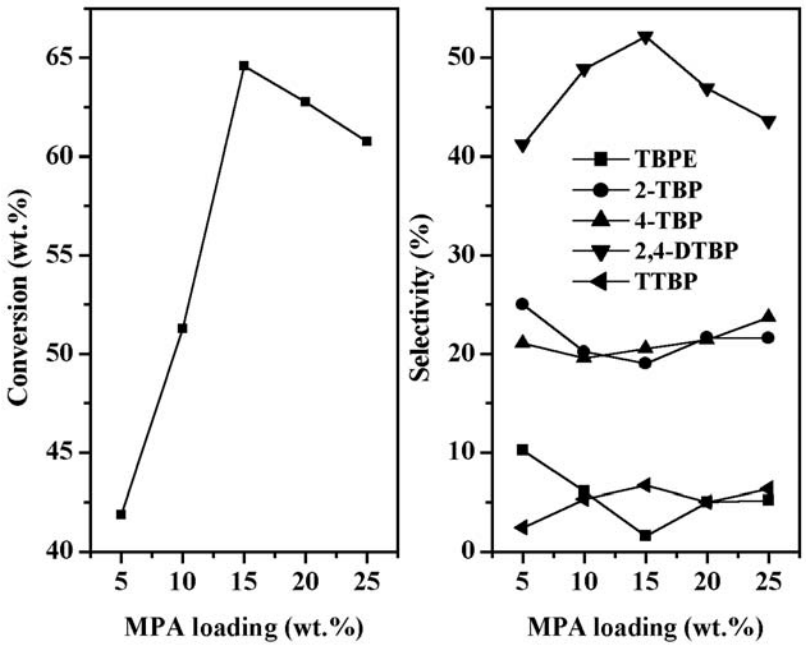

Fig. 5.13: Effect of PMA loading on the conversion of phenol and product selectivity. (conditions: temperature = 120 ^{o}C, *tert*-butanol/phenol molar ratio = 2, LHSV = 4 h^{-1}, time = 2 h).

5.5.1.2. Effect of calcination temperature

The 15 MZ catalyst calcined between 500 ^{o}C to 750 ^{o}C were used to study the change in catalytic activity with calcination temperature (Fig. 5.7). It is clear from Fig. 5.7, that calcination temperature has a profound effect on catalytic activity. The catalyst calcined at 500 ^{o}C, gave 40 % conversion of phenol and increased to 64.6 % at a calcination temperature of 700 ^{o}C. Further increase in calcination temperature decreased the conversion of phenol.

The selectivity to different alkylated products also varied with catalyst calcination temperature. As the conversion of phenol increased from 40 % for the catalyst calcined at 500 ^{o}C to 64.6 % for the one calcined at 700 ^{o}C, the selectivity to TBPE decreased from 12.5 to 1.6 %, 2-TBP from 26.5 to 19 % and 4-TBP from 25.8 to 20.5 %. However, the selectivity to 2,4-DTBP was increased with calcination temperature up to 700 ^{o}C (52.2 %) and further increase in calcination temperature decreased its selectivity.

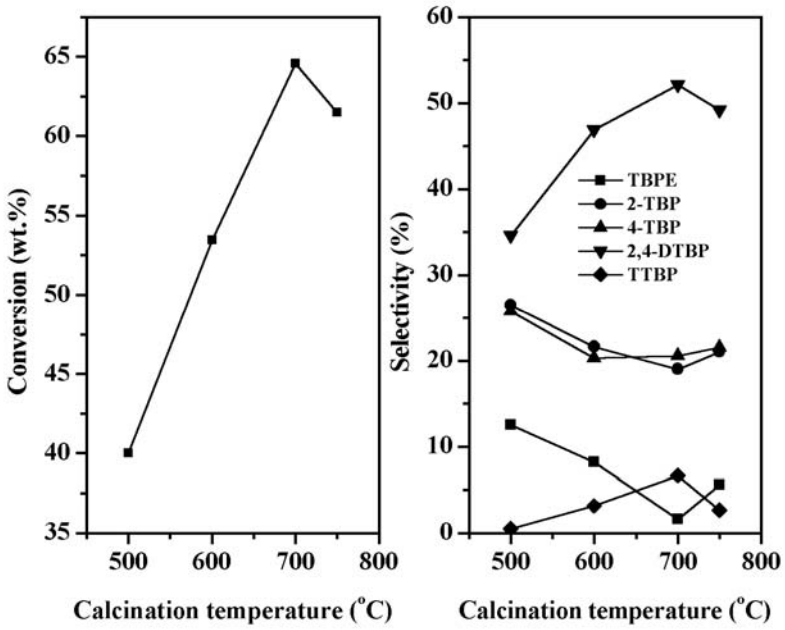

Fig. 5.14: Effect of calcination temperature on the conversion of phenol and product selectivity. (conditions: temperature = 120 ^{o}C, *tert*-butanol/phenol molar ratio = 2, LHSV = 4 h^{-1}, time = 2 h).

5.5.1.3. Effect of reaction temperature

The reaction was studied in the temperature range of 80 to 180 ^{o}C using 15 MZ-700 catalyst. The changes in the conversion of phenol and selectivity to different products as a function of temperature are shown in Fig. 5.8. At 80 ^{o}C, the conversion of phenol was 21.3 % and increased to 76.5 % at 140 ^{o}C. An increase in temperature above 140 ^{o}C decreased of the conversion of phenol. The decrease in conversion of phenol could be due to the dealkylation of *tert*-butyl phenol to phenol at high temperature and also the diminishing availability of *tert*-butanol as it undergoes oligomerization rather than alkylation [14, 15].

At 80 ^{o}C, TBPE obtained as the major product (53.5 %) and as the conversion of phenol increased, TBPE selectivity decreased and it was completely absent at 140 ^{o}C. The decrease in TBPE selectivity with temperature might be due to its rearrangement to C-alkylated product. Indeed, it has been shown that such rearrangement occurred on heating by contact with an acid catalyst [16]. The highest selectivity to 2-TBP was found to be at 100-120 ^{o}C (21 %), while, selectivity to 2,4-DTBP (45 %) was highest at 140 ^{o}C. The higher selectivity of 2,4-DTBP at this temperature might be due to the higher stability and the availability of *tert*-butyl cation at this reaction temperature. The

formation of 4-TBP is favored at high temperature as it is the thermodynamically stable product and hence an increase in temperature always increased its selectivity.

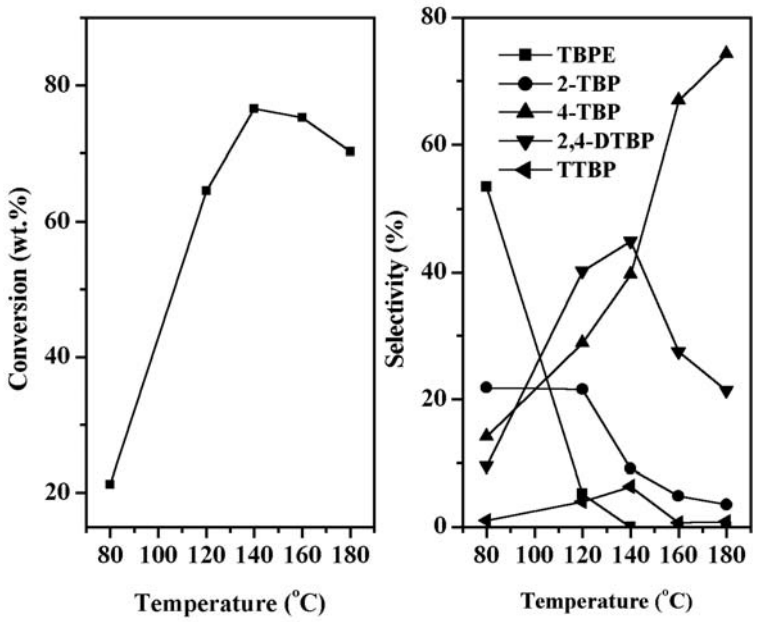

Fig. 5.15: Effect of reaction temperature on the conversion of phenol and product selectivity. (conditions: *tert*-butanol/phenol molar ratio = 2, LHSV = 4 h^{-1}, time = 2 h).

5.5.1.4. Effect of molar ratio

The effect of molar ratio on the conversion of phenol and product selectivity was studied at 120 ^{o}C by varying *tert*-butanol/phenol molar ratio from 1 to 4 (Fig. 5.9). Generally, the conversion of phenol was increased with an increase in the amount of *tert*-butanol. At a molar ratio of 1, conversion of phenol was 58.1 %, which increased to 80.6 % at a molar ratio of 3. A further increase in molar ratio had no appreciable effect on the conversion of phenol. It was shown that the polar molecule, such as methanol and higher alcohols compete with phenol for adsorption sites and an increase in the molar excess of alkylating agent results in an increase in the conversion of phenol as observed in the present study [17].

The formation of TBPE was observed in small amounts under these conditions. The selectivity to 2-TBP was low and it decreased from 17.3 to 9.8 %, when the molar ratio increased from 1 to 4. With an increase in molar ratio from 1 to 4, the selectivity to 4-TBP decreased from 41.3 to 21.3 %, while 2,4-DTBP selectivity increased from 38 to

64.6 %. This could be due to the higher availability of *tert*-butanol, which leads to the formation of the dialkylated product.

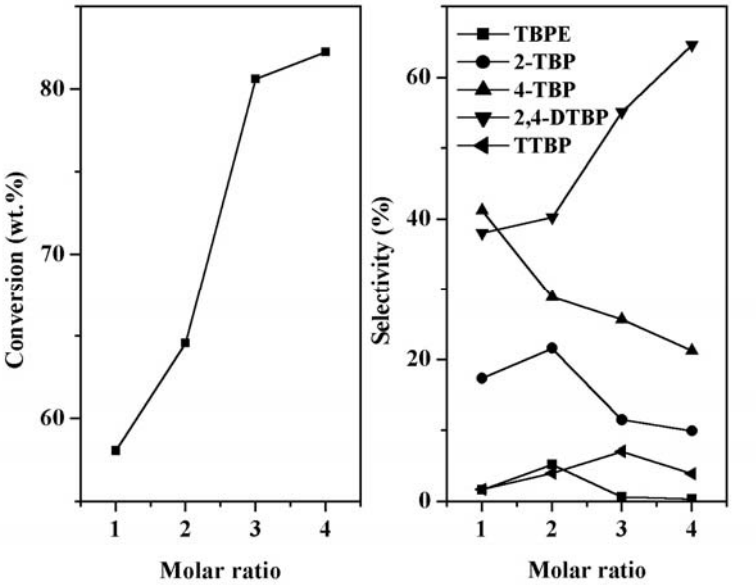

Fig. 5.16: Effect of molar ratio on the conversion of phenol and product selectivity. (conditions: temperature = 120 ^{o}C, LHSV = 4 h^{-1}, time = 2 h).

5.5.1.5. Effect of space velocity

The effect of space velocity was studied at 140 ^{o}C using *tert*-butanol/phenol molar ratio of 3 from LHSV of 2 to 10 h^{-1} and the results are shown in Fig. 5.10. With an increase of space velocity from 2 to 10 h^{-1}, the conversion of phenol was changed from 82 to 62.4 %. The decrease in conversion with an increase in space velocity is due to the lower contact time available for the reactants to be in contact with the active sites of the catalyst. With decrease in the conversion of phenol, the selectivity to 2,4-DTBP decreased from 60.5 to 44.6 %. However, change in space velocity had no appreciable effect on the selectivity to other products.

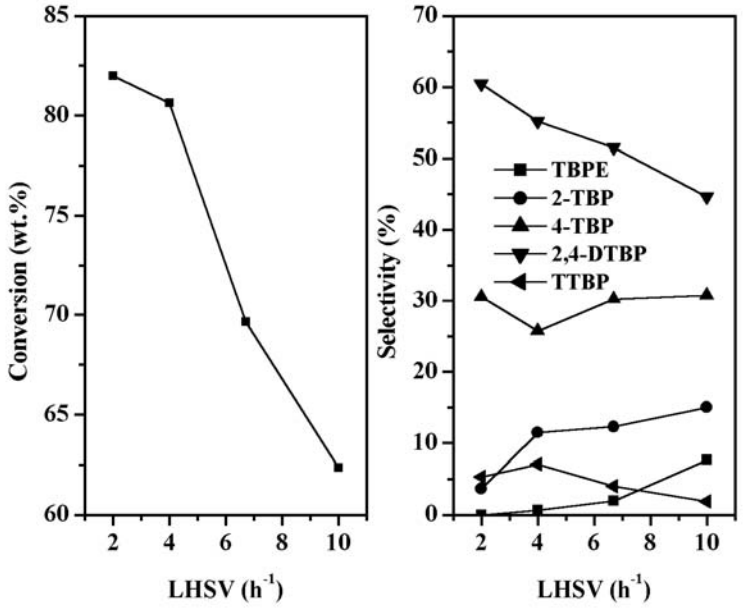

Fig. 5.17: Effect of space velocity on the conversion of phenol and product selectivity. (conditions: temperature = 140 ^{o}C, *tert*-butanol/phenol molar ratio = 3, time = 2 h).

5.5.1.6. Effect of time on stream

In order to study the deactivation behavior of the catalyst, the reaction was studied at 140 ^{o}C with LHSV of 4 h^{-1} using *tert*-butanol/phenol molar ratio of 3, for 31 h (Fig. 5.11). The conversion of phenol was found to be 80.6 % after 2 h with selectivity to 2-TBP 11.5 %, 2,4-DTBP 55.2 %, and 4-TBP 25.7 %, and after 31 h, the conversion of phenol was decreased to be 58.5 % with selectivity to 2-TBP 15.2 %, 2,4-DTBP 41.6 %, and 4-TBP 38.4 %. However, the major drawback of PMA/ZrO_2 catalyst is its deactivation, which is in sharp contrast with the catalytic behavior of zirconia-supported silicotungstic acid catalyst, where the catalyst is found to be stable and regenerable [16]. The color of the product mixture obtained from 15 MZ-700 catalyst was found to be dark blue and it indicated the major reason for the catalyst deactivation is due to the reduction and leaching of PMA from the catalyst surface [14].

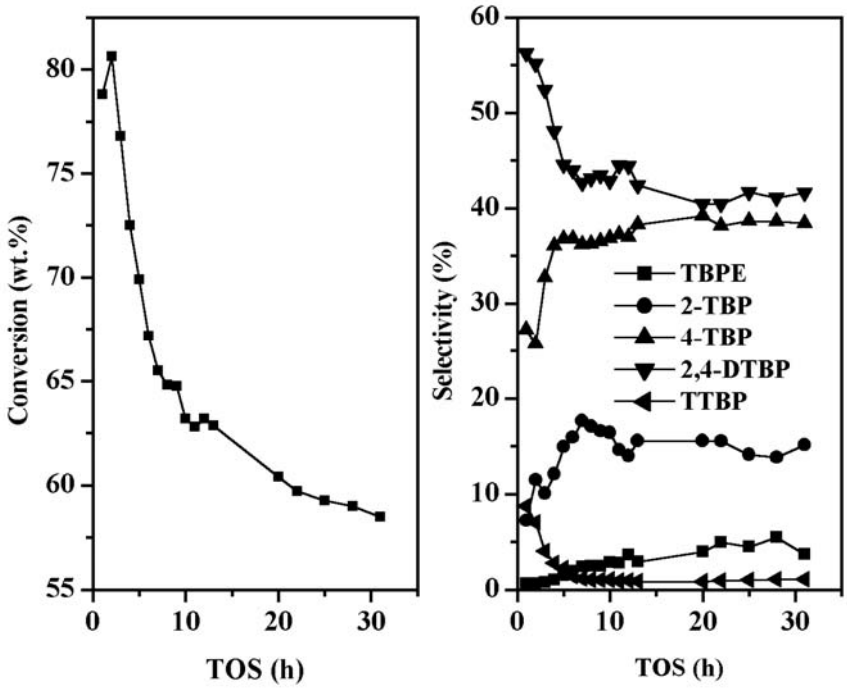

Fig. 5.18: Effect of time on stream (TOS) on the conversion of phenol and product selectivity. (conditions: temperature = 140 ^{o}C, LHSV = 4 h^{-1}, *tert*-butanol/phenol molar ratio = 3).

5.6. References

1. B.M. Devassy, S.B. Halligudi, S.G. Hegde, A.B. Halgeri, F. Lefebvre, Chem. Commun. (2002) 1074.
2. B.M. Devassy, F. Lefebvre, S.B. Halligudi, J. Catal. 229 (2005) 576.
3. L. Li, Y. Y. Yoshinaga, T. Okuhara, Phys. Chem. Chem. Phys. 1 (1999) 4913.
4. S. Damyanova, J.L.G. Fierro, I. Sobrados, J. Sanz, Langmuir 15 (1999) 469.
5. S. Kasztelan, E. Payen, J.B. Moffat, J. Catal. 125 (1990) 45.
6. Patricia G. Vázquez, Mirta N. Blanco, Carmen V. Cáceres, Catal. Lett. 60 (1999) 205.
7. C. Rocchiccioli-Deltcheff, A. Aouissi, S. Launay, M. Fournier, J. Mol. Catal. A 114 (1996) 331.
8. E. Lopez-Salinas, J.G. Hermandez-Cortez, I. Schifter, E. Torres-Garcia, J. Navarrete, A. Gutierrez-Carrillo, T. Lopez, P.P. Lottici, D. Bersani, Appl. Catal. A 193 (2000) 215.
9. C.H. Cline, J. Turkevich, J. Chem. Phys. 12 (1944) 300.
10. C. Morterra, A. Chiorino, G. Ghiotti and E. Garrone, J. Chem. Soc. Faraday Trans. 75 (1), (1979) 271.
11. G. Busca, Catal. Today 41 (1998) 191.
12. B.H. Davis, R.A. Keogh, S. Alerasool, D.J. Zalewski, D.E. Day, P.K. Doolin, J. Catal. 183 (1999) 45.
13. M.T. Pope, Heteropoly and Isopoly Oxometalates, Springer-Verlag, Berlin, 1983.
14. S. Subramanian, A. Mitra, C.V.V. Satyanarayana, D.K. Chakrabarty, Appl. Catal. A. 159 (1997) 229.
15. A. Sakthivel, S. K. Badamali, P. Selvam, Micropor. Mesopor. Mater. 39 (2000) 457.
16. B.M. Devassy, G.V. Shanbhag, S.P. Mirajkar, W. Böhringer, J. Fletcher, S.B. Halligudi, J. Mol. Catal. A. 233 (2005) 141.
17. R.F. Parton, J.M. Jacobs, D.R. Huybrechts, P.A. Jacobs, Stud. Surf. Sci. Catal. 46 (1989) 163.

Chapter 6

Summary and conclusions

This thesis describes the preparation, characterization and catalytic evaluation of zirconia-supported Keggin heteropoly acids such as silicotungstic acid, phosphotungstic acid and phosphomolybdic acid. This chapter present a brief summary of the work described in previous chapters and general conclusions arrived from the work.

Chapter 1 gives a general introduction about heteropoly acids (HPAs), its structure, classification, and catalytic properties. It also gives an introduction to supported-heteropoly acids and the conventional supports used for the preparation of supported-heteropoly acids. Further, this chapter gives an introduction to zirconia, its properties, and zirconia based solid acids. Finally the aim of the thesis is given: to explore the possibility of the preparation of stable supported heteropolyacid catalysts.

Chapter 2 describes the procedure for the preparation of zirconia-supported heteropoly acids. The catalysts were characterized by different techniques such as surface area, X-ray diffraction, Raman spectroscopy, TG-DTA, XPS, FTIR pyridine adsorption, TPD of ammonia, DRUV-vis spectroscopy, ^{31}P MAS NMR etc. Theory and experimental procedure employed for each technique is discussed in this section.

Chapter 3 describe the preparation of zirconia-supported silicotungstic acid catalyst with different STA loading (5-25 wt. %) and calcination temperature (600-850 ^{o}C), characterization by different techniques such as surface area, XRD, Raman spectroscopy, DTA, XPS, NH_3-TPD, FTIR pyridine adsorption, and DRUV-vis spectroscopy and application in veratrole benzoylation with benzoic anhydride and *tert*-butylation of phenol with *tert*-butanol. XRD results indicate that the presence of STA retards the crystallization of zirconia and stabilizes ZrO_2 in tetragonal phase. Characterization of the catalyst with optimum STA loading (15 %) by Raman spectroscopy showed the presence of zirconia-anchored mono-oxotungstate as the major tungsten species up to 750 ^{o}C. The catalysts showed both Brönsted as well as Lewis acidity and the catalyst 15 SZ-750 had the highest Brönsted acidity and total acidity.

Characterization of the catalysts by XPS shows that a monolayer of silicotungstate on zirconia was attained for the catalyst 15 SZ-750

The activity of these catalysts depends on STA coverage and the catalyst with monolayer of silicotungstate on zirconia (15 SZ-750) shows the highest activity. Comparison of the catalytic activity of 15 SZ-750 with 15 SS-300 in veratrole benzoylation showed that STA supported on zirconia act as efficient and stable solid acid catalysts, while STA supported on silica gets leached into the reaction medium and catalyze the reaction homogeneously. These catalysts were also found to be efficient for *tert*-butylation of phenol. The deactivated catalyst could be regenerated by calcination with out appreciable lose in activity and selectivity.

Chapter 4 describes the preparation of zirconia-supported phosphotungstic acid catalysts with different PTA loading (5-20 %) and calcination temperature (650 to 850 ^{o}C), characterization by different techniques such as surface area, XRD, DTG-DTA, FTIR pyridine adsorption, NH_3-TPD and ^{31}P MAS NMR spectroscopy measurements and application in the synthesis of linear alkyl benzenes by the alkylation of benzene with 1-octene and 1-dodecene and acylation of 2-MN with acetic anhydride. The catalyst with optimum PTA loading and calcination temperature (15 PZ-750) was prepared in different solvents and characterized by ^{31}P MAS NMR spectroscopy. The XRD results indicate that PTA stabilizes the tetragonal phase of zirconia. The catalysts show both Brönsted and Lewis acidity and the catalyst 15 PZ-750 shows the highest acidity. ^{31}P MAS NMR spectra show two types of phosphorous species, one is phosphotungstate which is in interaction with zirconia and the other is the decomposition product of PTA and the relative amount of each depend on PTA loading, calcination temperature and the solvent used for the catalyst preparation.

The activity of the catalyst in alkylation of benzene with 1-octene was found to depend on the solvent used for the catalyst preparation and solvents like methanol and DMF are the best for catalyst preparation. The catalyst with monolayer of PTA on zirconia (15 PZ-750) prepared in methanol showed the highest activity. In acylation of 2-MN, 15 PZ-750 catalyst showed deactivation due to product inhibition. The deactivated catalyst could be regenerated by calcination without appreciable loss in its activity and product selectivity.

Thus, 15 SZ-750 and 15 PZ-750 catalysts were found to be the most active catalysts and the activities of these catalysts were compared in benzoylation of veratrole with benzoic anhydride and alkylation of diphenyl ether with 1-dodecene. In benzoylation of veratrole, 15 SZ-750 catalyst showed different reaction profile compared to 15 PZ-750 catalyst, while in alkylation of diphenyl ether, both catalysts showed similar reaction profiles and 15 SZ-750 catalyst has higher activity than 15 PZ-750 catalyst. The kinetic profile of the reaction with 15 SZ-750 and 15 PZ-750 catalysts in veratrole benzoylation indicated that product inhibition was more prominent with 15 PZ-750 catalyst. Thus, the higher conversion and greater deactivation resistance of 15 SZ-750 catalyst in benzoylation of veratrole and also its higher activity in alkylation of diphenyl ether could be due to the presence of higher amount of strong Brönsted acid sites.

Chapter 5 describes the preparation of zirconia-supported phosphomolybdic acid catalysts with different PMA loading (5-25 %) and calcination temperature (500 to 750 ^{o}C), characterization by XRD and ^{31}P MAS NMR spectroscopy measurements and application in the synthesis of linear alkyl benzenes by the reaction of benzene with 1-octene and 1-dodecene and *tert*-butylation of phenol with *tert*-butanol. The XRD results indicated that MPA stabilizes the tetragonal phase of zirconia. ^{31}P MAS NMR spectra showed the presence of three types of phosphorous species, phosphomolybdate in interaction with zirconia, decomposition product of PMA and an unidentified species. FTIR pyridine adsorption on 15 MZ-700 catalyst showed the presence both the Brönsted and Lewis acidity.

The 15 MZ-700 catalyst showed the highest activity in alkylation of benzene with 1-octene and phenol with *tert*-butanol. In benzene alkylation, these catalysts deactivated mainly due to the formation of carbonaceous deposits on catalyst surface and phosphomolybdate reduction and the deactivated catalysts could be regenerated without appreciable loss in its activity and product selectivity. These catalysts were also highly active in *tert*-butylation of phenol but deactivated with time. In *tert*-butylation of phenol, catalyst deactivation was mainly due to the reduction of phosphomolybdate and leaching of PMA from the catalyst surface to the reaction medium.

Chapter 6 summarizes the conclusions made in this thesis.

Thus, the present work showed that heteropoly tungstic acids such as silicotungstic acid and phosphotungstic acid supported on zirconia acts as efficient and stable solid acid catalysts, while heteropoly molybdic acid such as phosphomolybdic acid supported on zirconia leaches to the reaction medium in presence of polar reactants.

List of publications

1. 12-tungstophosphoric acid/zirconia-a highly active stable solid acid-comparison with a tungstated zirconia catalyst
   B.M. Devassy, S.B. Halligudi, S.G. Hegde, A.B. Halgeri, F. Lefebvre,
   Chem. Commun. (2002) 1074.

2. Zirconia-supported 12-tungstophosphoric acid as a solid catalyst for the synthesis of linear alkyl benzenes
   B.M. Devassy, F. Lefebvre, S.B. Halligudi, J. Catal. 231 (2005) 1.

3. Alkylation of *p*-cresol with *tert*-butanol catalyzed by heteropoly acid supported on zirconia catalyst
   B.M. Devassy, G.V. Shanbag, F. Lefebvre, S.B. Halligudi,
   J. Mol. Catal. A 210 (2004) 125.

4. Zirconia supported phosphotungstic acid as an efficient catalyst for resorcinol *tert*-butylation and *n*-heptane hydroisomerization
   B.M. Devassy, S.B. Halligudi, S.P. Elangovan, S. Ernst, M. Hartmann,
   F. Lefebvre, J. Mol. Catal. A 221 (2004) 113.

5. Zirconia-supported phosphotungstic acid as catalyst for alkylation of phenol with benzyl alcohol
   B.M. Devassy, G.V. Shanbhag, F. Lefebvre, W. Böhringer, J. Fletcher,
   S.B. Halligudi, J. Mol. Catal. A 230 (2005) 113.

6. Silicotungstate-modified zirconia as an efficient catalyst for phenol *tert*-butylation
   B.M. Devassy, G.V. Shanbhag, S.P. Mirajkar, W. Böhringer, J. Fletcher,
   S.B. Halligudi, J. Mol. Catal. A 233 (2005) 141.

7. Kinetic study of vapor phase hydrodechlorination of halons by Pd supported catalysts
   S.B. Halligudi, **B.M. Devassy**, A. Ghosh, V. Ravikumar,
   J. Mol. Catal. A 184 (2002) 175.

8. Liquid phase allylation of anisole using TPA/ZrO_2 catalyst
   G.V. Shanbhag, **B.M. Devassy**, S.B. Halligudi, J. Mol. Catal. A 218 (2004) 67.

9. Friedel–Crafts benzoylation of diphenyl oxide over zirconia supported 12-tungstophosphoric acid
   D.P. Sawant, **B.M. Devassy**, S.B. Halligudi, J. Mol. Catal. A 217 (2004) 211.

10. Metal schiff-base compex catalyzed oxidation of *p*-xylene and methyl 4-methyl benzoate to carboxylic acids
    S.B. Halligudi, **B.M. Devassy**, K. Raj N.K, M.P. Degaonkar, S. Gopinathan,
    React. Kinet. Catal. Lett. 71, 2, (2000) 289.

11. Highly active and selective AlSBA-15 catalysts for the vapor phase *tert*-butylation of phenol

A. Vinu, **B. M. Devassy**, S.B. Halligudi, W. Böhlmann, M. Hartmann,
Appl. Catal. A 281 (2005) 207.

12. Selective production of orthoalkyl phenols on $Cu_{0.5}Co_{0.5}Fe_2O_4$: a study of catalysis and characterization
T. Mathew, S. Shylesh, **B.M. Devassy**, M. Vijayaraj, C.V.V. Satyanarayana, B.S. Rao, C.S. Gopinath, Appl. Catal. A 273 (2004) 35.

13. Vapor-phase methylation of pyridine with methanol to 3-picoline over $Zn_{1-x}Co_xFe_2O_4$ (x = 0, 0.2, 0.5, 0.8, 1.0) - type ternary spinels prepared via low temperature method
K. Sreekumar, T. Mathew, **M.D. Biju**, R. Rajgopal, R. Vetrivel, B. S. Rao, Appl. Catal. A 205 (2001) 11.

14. Oxidative dehydrogenation of ethylbenzene over $Zn_{1-x}Ni_xFe_2O_4$ (x = 0, 0.2, 0.5, 0.8 and 1.0) type systems: Effect of composition on surface properties and catalytic activities.
K. Sreekumar, M. Thomas, T.M. Jyothi, **M.D. Biju**, S. Sugunan, B.S. Rao, Polish J. Chem. 74, (2000) 509.

15. Synthesis of linear alkyl benzenes over zirconia-supported 12-molybdophosphoric acid catalysts.
B.M. Devassy, F. Lefebvre, W. Böhringer, J. Fletcher, S.B. Halligudi
J. Mol. Catal. A 236 (2005) 162.

16. *Tert*-butylation of *p*-cresol over WO_x/ZrO_2 solid acid catalysts.
S. Sarish, **B.M. Devassy**, S.B. Halligudi, J. Mol. Catal. A 235 (2005) 44.

17. Alkylation of phenol with long-chain olefins over WO_x/ZrO_2 solid acid catalysts
S. Sarish, **B.M. Devassy**, W. Böhringer, J. Fletcher, S.B. Halligudi,
J. Mol. Catal. A 240 (2005) 123.

18. Zirconia-supported heteropoly acids: Characterization and catalytic behavior in liquid-phase veratrole benzoylation
B.M. Devassy, G.V. Shanbhag, S.B. Halligudi, J. Catal (2005) In press.